The Role of the Unfolded Protein Response and Alternatively Activated Macrophages in Pulmonary Fibrosis.

BY

KARUN TANDON
B.Sc.

Thesis Submitted in Partial Fulfillment of the Requirements for the Degree Master of Science

McMaster University

THE UNFOLDED PROTEIN RESPONSE, ALTERNATIVELY ACTIVATED MACROPHAGES, AND IPF

Descriptive Note

MASTER OF SCIENCE (2017)
(Medical Sciences)

McMaster University
Hamilton, Ontario

TITLE: The Role of the Unfolded Protein Response and Alternatively Activated Macrophages in Pulmonary Fibrosis.

AUTHOR: Karun Tandon, B.Sc. (McMaster University)

SUPERVISOR: Dr. Kjetil Ask

NUMBER OF PAGES: 120

Abstract

Idiopathic pulmonary fibrosis is is characterized by the irreversible deposition of irreversible deposition of extracellular matrix (ECM) proteins. The pathogenesis of IPF is not entirely understood, but myofibroblasts that accumulate at the site of injury are thought to be the key drivers of ECM deposition and are often associated in the disease. Although it is poorly understood how these immune cells differentiate in the lung, one hypothesis suggests a major role of alternatively activated profibrotic macrophages in this process.

There are different classifications of macrophages, which vary in phenotype and function, depending on their activation profile and polarization process. A crucial component of the macrophage polarization process involves the internal membrane expansion program of the endoplasmic reticulum. An essential mediator in this ER expansion process is the IRE1-XBP1 pathway. Here, it was investigated whether unfolded protein response (UPR) proteins and alternatively activated macrophages were present in patients with IPF. By accessing lung biopsies of IPF patients, a tissue microarray was created to compare the presence of both UPR and alternatively activated macrophages proteins in IPF patients.

Next, to determine whether the IRE1-XBP1 pathway was crucial for the polarization of naive macrophages to alternatively activated macrophages, the THP-1 macrophage cell line was treated with STF-080310 and 4μ8C inhibitors of this pathway. These results indicate that the inhibition of the IRE1-XBP1 pathway may have resulted in an attenuation of ER expansion and cytokine secretion. Preliminary data also shows that

standard alternatively activated cocktail IL-4/IL-13 stimulation with the addition of IL-6 resulted in enhanced XBP1 splicing and ER expansion, coupled with a dramatic increase in cytokine secretion.

To further elucidate the links between macrophages and fibrosis, the role of alternatively activated and hyperpolarized macrophages on the transition of fibroblasts to myofibroblasts was examined using a novel co-culture system. Fibroblast to myofibroblast transition was quantified through αSMA and collagen staining. The results demonstrate that hyperpolarized alternatively activated macrophages may have affected the transition of healthy primary lung fibroblasts to myofibroblasts and STF-080310 prevented this process.

Finally, Nintedanib, a specific tyrosine kinase inhibitor approved for the treatment of IPF, was investigated to determine its effect on the polarization of alternatively activated macrophages and on experimental bleomycin-induced lung fibrosis in mice. This work provided evidence that Nintedanib prevented IL-4/IL-13- and IL-4/IL-13/IL-6-mediated polarization of profibrotic macrophages *in vitro*. In THP-1 cells, Nintedanib treatment prevented phosphorylation of tyrosine residues in the CSF1 receptor suggesting a possible mechanism of action. Nintedanib also prevented the secretion of collagen in IPF-derived fibroblasts.

These findings suggest that IL-6 addition enhances the ER expansion and cytokine secretion of IL-4/IL-13 macrophages. It also identifies profibrotic-mediated ER expansion of macrophages plays a role in the fibrotic process, and may be a viable therapeutic target in the context of fibrotic disease.

Acknowledgements

I would first like to thank my family for their unconditional love and support. My parent's kindness and encouragement throughout my education has allowed me to achieve accomplishments beyond my dreams. To my brother, I thank you for being so patient with me and for being a role model. Finally, I wish to thank my late grandmother, my love for you will live forever.

To the friends I have made over the last two years, thank you for all the great memories, I am forever indebted to you. I am immensely grateful to the members of the Ask Lab, and all the individuals at McMaster Immunology Research Centre and St. Joesph's Research Centre.

To my thesis supervisor and mentor; Dr. Kjetil Ask for whom I express my greatest appreciation. I feel fortunate to have been able to learn from his professional guidance, patience and support through the last two years. He has enabled me to grown both in science and in life with his constant encouragement and motivation.

I also appreciate the effort, and constructive feedback put forth by my committee members, Dr. Nathan Hambly, Dr. J.C. Cutz, and Dr. Mark Inman. They have been role models in the pursuit of science and understanding, and valuable advice has allowed my scientific career to progress. Additionally, I would like to thank Dr. Naqvi for taking the time to mentor and teach me.

Table of Contents

List of Abbreviations

αSMA= Alpha Smooth Muscle Actin
AAM= Alternatively Activated Macrophage
ATF6=Activating Transcription Factor 6
AE= Acute Exacerbation
ANOVA = Analysis of Variance
BALF= Broncheoalveolar Lavage Fluid
BSA= Bovine Serum Albumin
BMDM= Bone-Marrow Derived Precursor Murine ells
CCL18 = Chemokine (C-C motif) Ligand 18
CSF1= Colony Stimulating Factor 1
DNA= Deoxyribonucleic Acid
DAMPs = Damage-Associated Molecular Patterns
DLCO= Diffusing Capacity of the Lungs for Carbon Monoxide
ERAD =ER-Associated Degradation
ECM= Extracellular Matrix Proteins
ELISA = Enzyme Linked Immunosorbent Assay
ER= Endoplasmic Reticulum
FEV1= Forced Expiratory Capacity 1
FBS=Fetal Bovine Serum
FFPE= Formalin Fixed Paraffin Embedded Tissue
FGF= Fibroblast Growth Factor
FVC= Forced Vital Capacity
GRP78= Glucose-Regulated Protein (i.e. immunoglobulin heavy chain binding protein)
H&E=Hematoxylin and Eosin
HLF= Human Lung Fibroblasts
HR-CT = High Resolution Computed Tomography
Hyperpolarized Profibrotic Macrophages = IL-4/IL-13/IL-6 Stimulated Macrophages
IF= Immunofluorescence
IFN=Interferon
IHC= Immunohistochemistry
IPF = Idiopathic Pulmonary Fibrosis
IL = Interleukin
ILD = Intestinal Lung Disease
IRE1=Inositol-Requiring Enzyme 1
LPS = Lipopolysaccharide
M1 Macrophage = Classically Activated Macrophage
M2 Macrophage = Alternatively Activated Profibrotic Macrophage
MCSF = Macrophage Colony Stimulating Factor
NK=Natural Killer Cells
PAMPs = Pathogen-Associated Molecular Patterns
PBMC= Peripheral-Blood Mononuclear Cells
PBS= Phosphate Buffered Saline

PDGF= Platelet-Derived Growth Factor
PERK=PRK-like Endoplasmic Reticulum Kinase
PMA= Phorbol Myristate Acetate
PSR= PicroSirius Red
RNA= Ribonucleic Acid
STAT = Signal Transducer and Activator of Transcription
STF= STF-080310
TEM= Transmission Electron Microscopy
Tc1=T Cytotoxic 1 Cells
TGFβ = Tumor Growth Factor Beta
TH1 = T Helper 1
TH2 = T Helper 2
TLR= Toll Like Receptor
TMA= Tissue Microarray
TNF = Tumor Necrosis Factor
Tuni= Tunicamycin
UPR= Unfolded Protein Response
UIP= Usual Interstitial Pneumonia
VEGF = Vascular Endothelial Growth Factor
XBP-1 =X-box binding protein 1

Declaration of Academic Achievement

This master's thesis was written by Karun Tandon under the supervision of Dr. Kjetil Ask. I personally conducted the majority of the work involved with the design, data collection and analysis. Figures 19 and 23 were done in collaboration with Boehringer Ingelheim (Germany) and Maximilian Ackermann (Johannes Gutenberg University of Mainz).

Chapter 1. Introduction

1.1 General Overview

Interstitial lung disease (ILD) is defined as a diffuse parenchymal lung disorder that leads to the progressive scarring of the lungs (Fischer and du Bois, 2012). This scarring caused by the irreversible accumulation of extracellular matrix proteins in the respiratory system, leads to increased difficulty in a patient's ability to breathe, and is often associated with clinical signs of dyspnea, bibasilar crackles and abnormal chest radiography (Fischer and du Bois, 2012; Schwarz and King, 1998). ILDs are frequently classified according to their specific clinical, radiological and histopathological features and are split into two categories: ILDs of known and unknown etiologies (Fischer and du Bois, 2012). Of the known etiologies, they often include drugs, connective tissue damage, environmental exposure and genetics (Fischer and Du Bois, 2012).

Idiopathic pulmonary fibrosis (IPF) is the most common form of unknown ILD characterized by a progressive decline in lung function (Wuyts et al., 2014). In 2012 approximately 30,000 Canadians were affected with IPF, with predominately Caucasian males older than 60 years of age being at risk (Davidson, 2014; Raghu et al., 2006). The median survival for IPF patients remains poor, ranging between 2.5 to 3.5 years' post-diagnosis, worse than many cancers (Martinez, 2003). Thus, it is important to understand the pathogenesis of this debilitating disease, in order to design novel therapeutics.

While the cellular mechanisms driving IPF remain unclear, it has been noted that IPF patients show an aggregation of activated fibroblasts and myofibroblast cells, responsible for the synthesis and deposition of extracellular matrix (ECM) molecules (Kuhn and McDonald, 1991). It is for this reason researchers have focused on how

mesenchymal or myofibroblast cells are activated and accumulate in pulmonary tissue (Collard et al., 2007). Increasing evidence suggests a role of circulating cells contributing to the accumulation of myofibroblasts, including fibrocytes and profibrotic monocytes (Moeller et al., 2009).

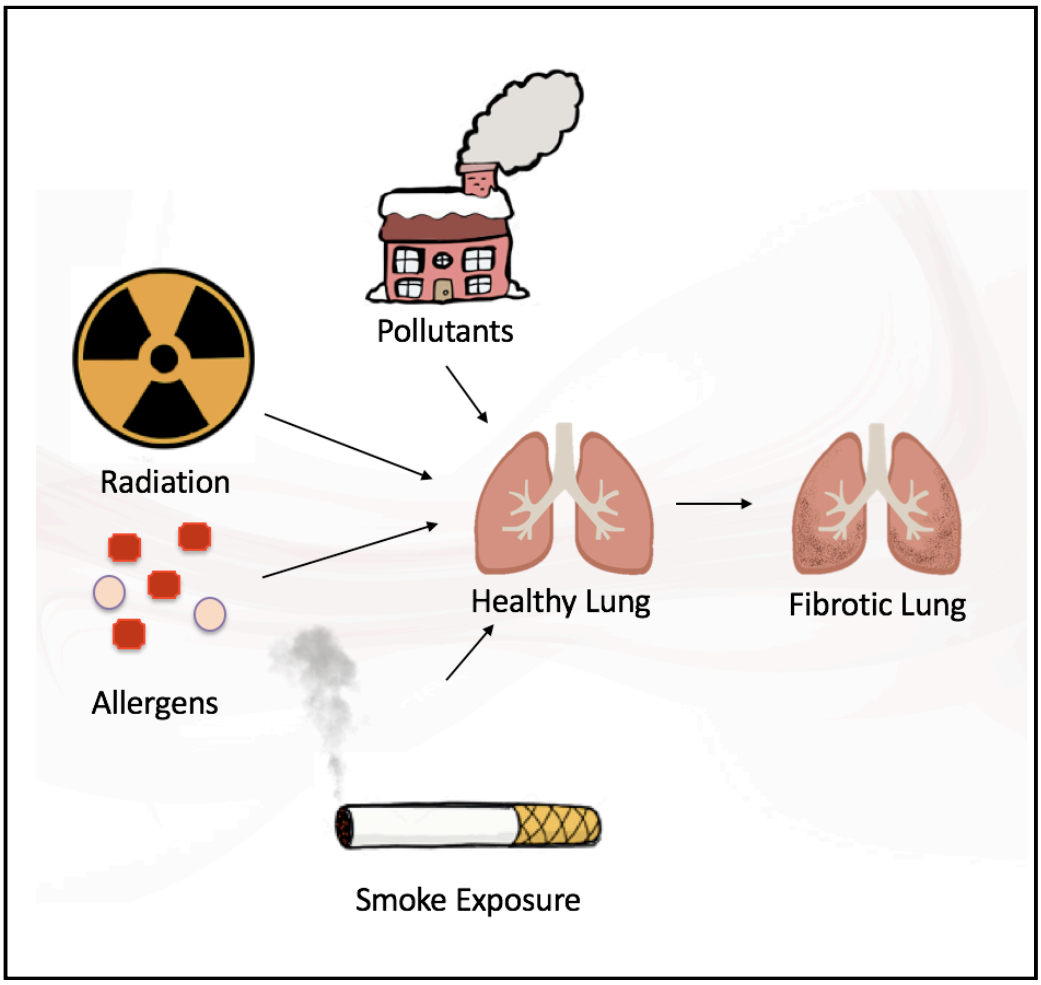

Figure 1: **Initiation of Cellular Damage within the Lung**

Environmental exposure to pollutants, radiation, allergens, and cigarette smoke might lead to the cellular injury seen in certain types of interstitial lung disease.

1.2 Acute Exacerbations of IPF

Patients with IPF may suffer from acute stages of respiratory decline (Papiris et al., 2014). This deterioration may be caused by complications of diagnostic testing, viral or bacterial infection or from unidentified triggers (Hyzy et al., 2007). Additional research has shown that circulating fibrocytes were increased in acute exacerbation of IPF (AE-IPF) and associated with an increased survival (Moeller et al., 2009).

This rapid decline in lung function in IPF patients is characterized by worsening hypoxemia (i.e. fall in PaO_2 of 10 mmHg), dyspnea and radiographic appearance (bilateral ground-class opacities) in the absence of any identifiable cause (Martinez et al., 2003). Patients whom suffer from such conditions in accompaniment with IPF are referred to have an AE-IPF and often have poor outcomes (Collard et al., 2007). Six of the elements from Table 1 must be present to have a confirmed diagnosis of AE-IPF (Hyzy et al., 2007).

Table 1: The table below adapted from Hyzy et al., 2007 lists the diagnostic criteria necessary for a positive diagnosis of AE-IPF.

Diagnostic Criteria For Acute Exacerbation IPF
Previous or current diagnosis of IPF
Unexplained worsening or development of dyspnea within 30 days
High-resolution CT scan with new bilateral ground-glass abnormality and/or consolidation superimposed on a background reticular or honeycomb pattern consistent with a UIP pattern
Worsening hypoxemia from a known baseline arterial blood gas
No evidence of pulmonary infection by endotracheal aspiration or Broncoalveolar Lavage
Exclusion of alternative causes, including Left Heart Failure Pulmonary Embolism Identifiable cause of Acute Lung Injury

1.3 Diagnosis

A diagnosis of IPF usually arises months after a patient first presents with initial manifestations of dyspnea and dry cough as these tend to be overlooked as symptoms of smoking or aging (Cottin and Cordier, 2012). Once these underlying symptoms are properly characterized as an interstitial lung disease, physicians attempt to look for an identifiable etiology. If no detectable cause arises, a high resolution CT (HR-CT) scan or surgical lung biopsy may be conducted to provide a clearer picture of the patient's lungs. After all clinical evidence accumulates, a multi-disciplinary discussion with radiologists, pathologists, and respirologists occur to ultimately diagnose the patient (Wuyts et al, 2014).

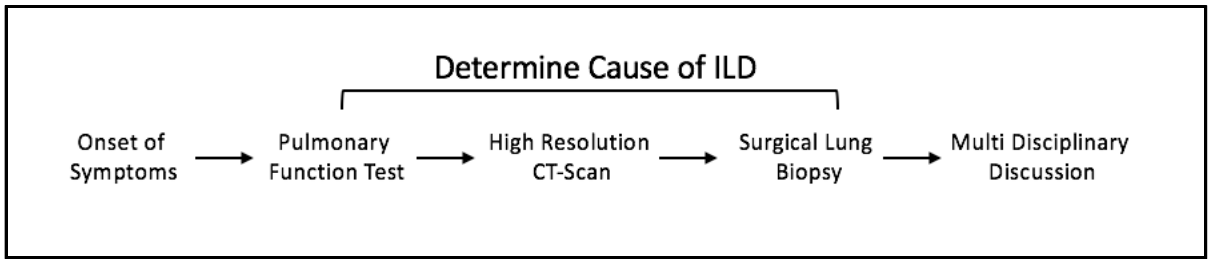

Figure 2: Diagnostic Course of an IPF Patient.

Initial symptoms of an IPF patient are usually not recognized by a primary care physician. A patient will then be seen by a team of radiologists, respirologists and pathologists until they finally are diagnosed.

1.4 Role of Macrophages in Wound Healing and Tissue Repair

Tissue repair and regeneration are fundamental processes in the proper functioning of organisms (Wynn and Vannella, 2016). When cellular injury in the lung epithelium occurs as a result of chemical or physical exposure, the body hosts an inflammatory response through a signal cascade of damage-associated molecular patterns

(DAMPs) and pathogen-associated molecular patterns (PAMPs) (Newton et al., 2012). These triggers stimulate an inflammatory response signaling neutrophils, lymphoid cells, natural killer cells, B cells, fibroblasts and macrophages to repair cellular injury (Wynn and Vannella, 2016). Under normal wound healing processes, fibroblasts differentiate to myofibroblasts, which are key effector cells in the secretion of ECM proteins (Darby et al., 2014). However, when this process becomes unregulated, myofibroblasts develop an increased resistance to apoptosis, resulting in aberrant scarring and impaired tissue function (Robinson et al, 2012). While fibroblasts have been implicated in the repair process, macrophages have also been shown to be critical cells in the process of repair and fibrosis, since different macrophage populations are part of the initiation, maintenance and resolution of fibrosis (Leech et al., 2013; Wynn et al, 2016). Their role in fibrosis is supported with research demonstrating that the amelioration of macrophages (using clodronate) from the bleomycin and AdTGFβ murine model of lung fibrosis has a protective effect on the lungs in this animal system (Gibbons et al., 2011).

1.5 Origins of Macrophages

Tissue macrophages can arise from circulating monocytes derived from the bone marrow, or established prenatally during the embryonic development of the yolk sac (van Furth and Cohn, 1964). When circulating monocytes are recruited to sites of injury and inflammation, they differentiate into macrophages. Different macrophage subtypes include bone-marrow derived precursor cells (BMDCs), peripheral-blood mononuclear cells (PBMCs), and tissue resident macrophages (Italiani et al., 2014). In *in vitro* systems,

these macrophages can display phenotypic characteristics of classically activated M1 or alternatively activated M2 macrophages,[#] which are mononuclear cells measuring 10 to 30 um, and capable of phagocytizing foreign molecules (Gordon, 2003).[*] *In vivo* naïve macrophages can interact with IFN-γ, produced by activated Th1, CD8+ T cytotoxic 1 (Tc1) cells, and natural killer (NK) cells (Chen, 2013). These pre-activated cells can then interact with LPS on bacterial cell walls, for example, to stimulate toll like receptor (TLR) signaling (particularly TLR-4 in this case) causing these preconditioned pro-inflammatory cells to polarize to their classically activated fate through STAT1 signaling (Luu et al., 2014). Alternatively activated macrophages display a Th2 response, serving as anti-inflammatory or pro-fibrotic macrophages and serve to promote ECM development, cell proliferation and angiogenesis (Ginhoux and Jung, 2014). There are three currently known subtypes of alternatively activated macrophages: M2a, M2b, M2c and a potentially new M2d subtype (Ferrante, 2012). M2a is the most studied in diseases of fibrogenesis and is activated by the release of IL-4 and IL-13 to produce the characteristic profibrotic response of regulating wound healing, suppressing T cell responses, host defenses and anti-tumor activity through the activation of STAT6 signaling (Martinez et al., 2012). Recent work has suggested that alternatively activated macrophages may have a primary role in the fibrotic process, through their effect on the transition of fibroblasts to myofibroblasts (Zhu et al., 2017; Binai et al., 2012; Ploeger et al., 2013).

[#] M1 and M2 macrophages are considered to be extremes of a spectrum of multiple macrophage phenotypes. These classifications are made *in vitro* under controlled conditions.

[*] IL-4 stimulated macrophages show decreased phagocytosis (Martinez et al., 2014)

Fibroblasts are central to the wound healing process as they synthesize extracellular matrix proteins and collagen (Darby et al., 2014). The transition from fibroblasts to myofibroblasts occurs through the release of tumor growth factor beta (TGFβ), which induces alpha-smooth muscle actin (αSMA) protein and mRNA expression to help growing myofibroblasts contract around wound edges (Ginhoux and Jung, 2014).

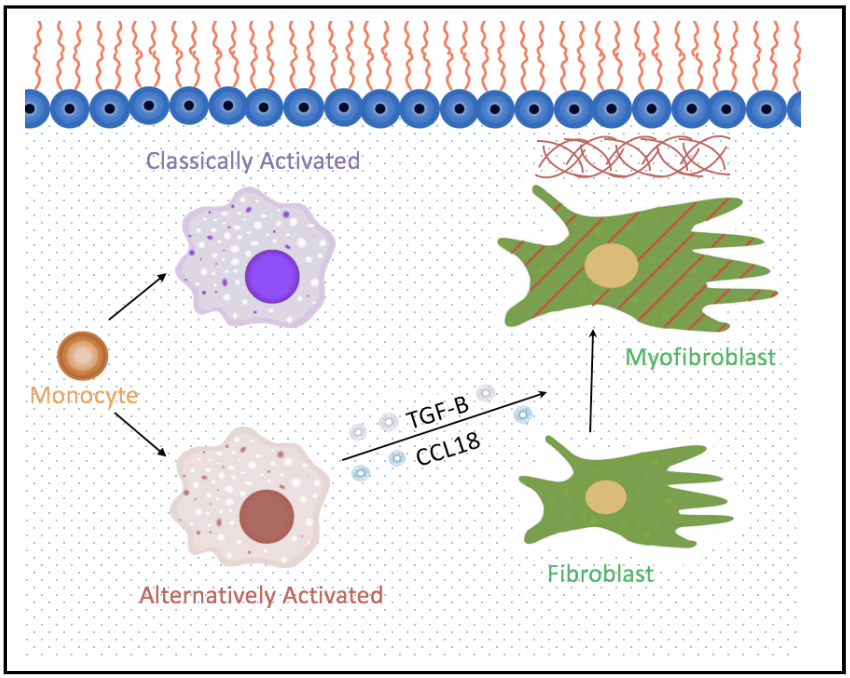

Figure 3: The macrophage paradigm and fibroblast differentiation.

In *in vitro* systems M1 macrophages are termed pro-inflammatory cells while M2 macrophages are termed anti-inflammatory cells that are responsible for wound healing. M2 macrophages release fibrotic cytokines such as TGFβ that may cause fibroblasts to transition to myofibroblasts, accelerating fibrosis.

Evidence for the existence of alternatively activated macrophages in the progression and cause of human disease is well noted. In patients with atherosclerosis, it has been studied that there is an upregulation in CD68 and CD206 positive cells (Rőszer,

2015). CD68 is a glycoprotein that has been characterized to be expressed specifically on monocytes and macrophages. C-type mannose receptor I (CD206), is a human and mouse glycoprotein that is expressed on the surface of alternatively activated macrophages, immature dendritic cells and dermal fibroblasts (Wollenberg et al., 2002). Profibrotic macrophages have also been associated with tumor-associated macrophage cancers, as they are responsible in angiogenesis, matrix remodeling and suppression of adaptive immunity (Sica et al., 2006). Further evidence points to these cells in the progression of IPF as increased amounts of CCL18, a profibrotic macrophage marker, was observed in the bronchoalveolar lavage (BAL) of IPF patients (Schupp et al., 2015).[#]

1.6 CCL18

Chemokine ligand 18 (CCL18) is a small cytokine that is produced and secreted mainly by antigen presenting cells of the innate immune system. It is known to have effects on the adaptive immune system by attracting naïve and Th2 lymphocytes to activated macrophages in lymph nodes (Chang et al., 2010). This ligand has been shown able to inhibit CCR1-, CCR2-, CCR4- and CCR5-mediated chemotaxis and binds to CCR3, PITPNM3, GPR30, and CCR8 (Schutyser et al., 2005). Furthermore, CCL18 production by naïve macrophages is highly upregulated in the presence of fibroblasts, partially because of the collagen produced by the fibroblasts (Schraufstatter et al., 2012). Moreover, fibroblast and macrophages cultured in the presence of CCL18 were observed to have an increased synthesis of collagen and survival capacity (Schraufstatter et al.,

[#] IL-6 was another cytokine that was unregulated in the BAL of IPF patients.[21]

2012; Luzina et al., 2006).

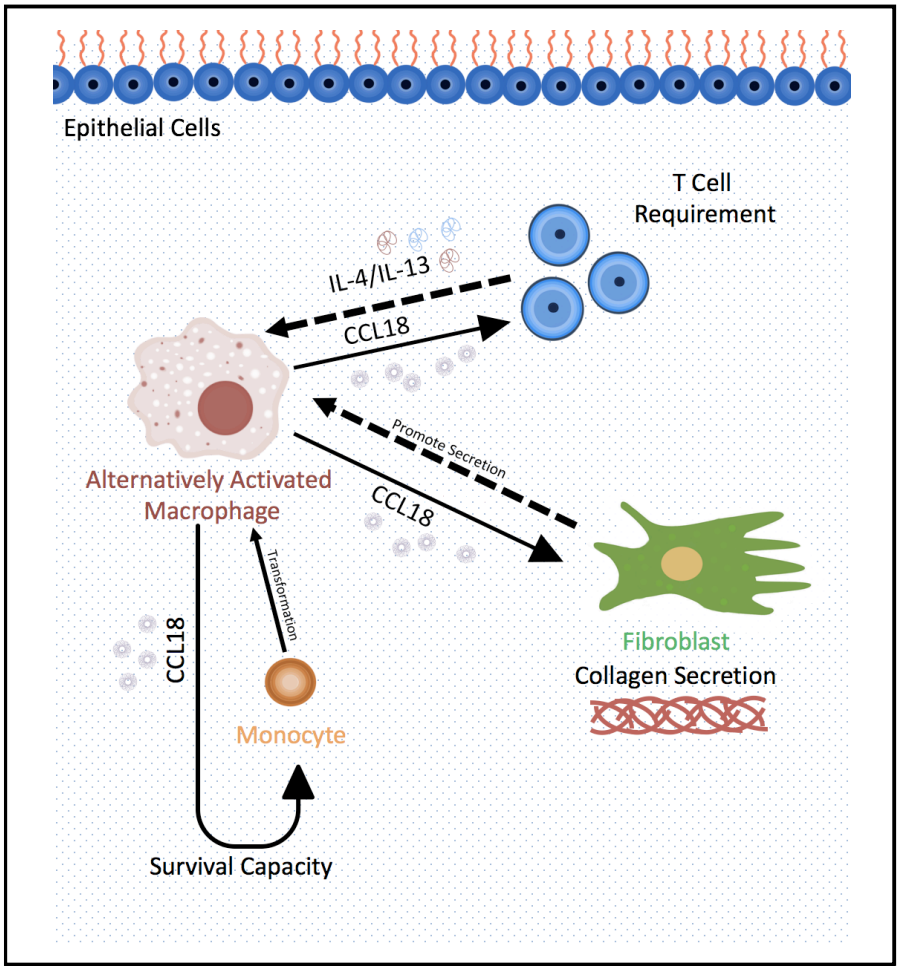

Figure 4: CCL18 functions in immune response.

The chemokine can transform monocytes, promoting collagen secretion from fibroblasts, increase monocyte survival capacity and attract Th2 lymphocytes.

1.7 Endoplasmic Reticulum

The endoplasmic reticulum (ER) is a perinuclear organelle, where the cell stores calcium and synthesizes membrane and secretory proteins. Within the ER, resident molecules called chaperones are responsible for protein folding and preventing protein aggregation. One of the most studied ER chaperones is the glucose-regulated protein

(GRP78), also known as immunoglobulin heavy chain binding protein (BiP) (Kozutusmi et al., 1989). Malfunction in this chaperone results in ER stress through the accumulation of unfolded proteins and triggers the unfolded protein response (UPR) to upregulate ER chaperones, translational machinery and downregulate bulk protein synthesis to achieve homeostasis (Hetz, 2012). However, if this process goes unregulated, the UPR will initiate apoptosis (Woehlbier and Hetz, 2011)

GRP78 has an important function in inhibiting and regulating three membrane bound receptors; activating transcription factor 6 (ATF6), inositol-requiring enzyme 1 (IRE1) and PRK-like endoplasmic reticulum kinase (PERK). PERK serves to detect the aggregation of misfolded proteins through auto-phosphorylation and dimerization, activating the α-subunit of the eukaryotic translational initiation factor 2 to phosphorylate and halt protein synthesis (Zhan, 2002; Welsh, 1992). During the UPR response ATF6 is activated and transported to the Golgi Complex where it is cleaved and moved to the nucleus binding to the cis-acting ER stress response elements (ERSE), which activates the transcription of chaperones (Mimura et al., 2012). Upon activation, IRE-1 homodimerizes and cleaves the X-box binding protein 1 (XBP-1), which moves to the nucleus and binds to ERSE and promotes transcription of ER associated degradation (ERAD) target genes (Hetz, 2012).

In *in vitro* models, the secretory capacity of alternatively activated macrophages can be reduced by blocking the expansion of the endoplasmic reticulum (ER) in bone marrow derived murine macrophages (Unpublished). This expansion, termed the "ER expansion program" is well understood at the molecular level in other cell types and

involves the activation of the IRE1-XBP1 pathway, one of the main activators of the UPR pathway. Although accumulating evidence suggests that UPR response is important in the polarization of immune cells, it is poorly understood if this mechanism is essential for the polarization of profibrotic macrophages and rapid progression of IPF (Welch, 1992).

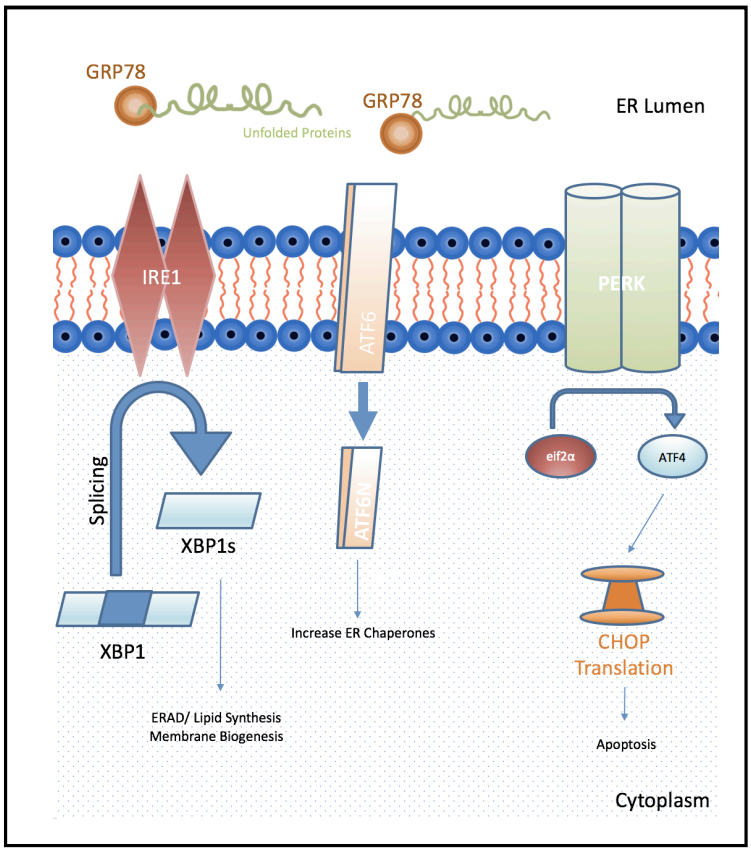

Figure 5: The Unfolded Protein Response.

The ER expansion program is controlled by three arms of the unfolded protein response depicted here; IRE1, ATF6 and PERK (Adapted from Lajoie 2015)

1.8 IRE1/XBP-1

Unfolded protein aggregation causes the ER to activate a transcriptional pathway, called the UPR pathway. One of the main regulators in this response is IRE1, an ER-

resident protein kinase and endoribonuclease. IRE1 was first identified in *S. cerevisiae* as a proximal sensor in which UPR signaling was entirely mediated by the IRE1 pathway (Selman et al., 2001). This receptor is the most conserved ER stress sensor that is activated by oligomerization and autophosphorylation and results in the non-conventional splicing of the mRNA of X-box binding protein 1 (XBP1; inactive), generating a spliced variant of XBP1s (active) to initiate a major UPR program (Jiang et al., 2015). Activation of XBP1s is achieved through the removal of a 26-nucleotide intron from XBP1, resulting in a frame-shift that activates transcriptional activity (Hetz, 2012). XBP1s is a unique transcription factor that regulates genes responsible for ER-associated degradation (ERAD), and those responsible for promoting protein folding through ER formation, such as p58IPK and other ER chaperones (Welch, 1992). Thus, the IRE1-XBP1 pathway has a pro-survival role in the cell. IRE1 also has a pro-apoptotic role when it binds to TRAF2 and activates ASK1, which causes JNK activation, thereby leading to caspase-dependent apoptosis (Mimura et al., 2012).

1.9 Interleukin-6

Although alternatively activated macrophages are associated with various fibrotic diseases, the mechanisms leading to macrophage polarization towards the profibrotic phenotype remains incompletely understood. Recent evidence from our lab indicates that the addition of IL-6 to the conventional polarization cocktail IL-4/IL-13 enhances polarization towards an alternative phenotype (unpublished). IL-6, an important inflammatory cytokine, has been shown to be crucial in inducing Ig production in human

B cells. Additionally, the differentiation of plasma cells is thought to occur through IL6-IRE1 activation (Wu et al, 2015; Reimold et al., 2001; Wen et al, 1999). From studies in murine BMDMs, IL-6 serves to create 'hyperpolarized profibrotic macrophages' with an enlarged endoplasmic reticulum, which could be responsible for an increased secretion of TGFβ. Additional data suggests that the ER stress factor XBP1 is an integral component of the unfolded protein response and crucial in the differentiation and membrane biogenesis of many cell types which possess a high secretory capacity.

1.10 Current Treatments

For over 30 years, IPF was treated with immunosuppressive drugs including corticosteroids, azathioprine, and N-acetylcysteine (Lynch et al., 2001). However, after accumulating evidence suggested that the toxicities and mortality rate for IPF patients on these drugs were substantial, the ATS/ERS recommended that these pharmaceuticals not be used in the treatment of patients as they did not alter the natural history of the disease (Richeldi et al. 2011).

Two drugs have recently been approved for the treatment of IPF: Nintedanib, and Pirfenidone (Lehtonen et al., 2016). Nintedanib is a tyrosine kinase inhibitor that has been shown to reduce FVC decline, which was consistent in slowing disease progression (Richeldi et al., 2014). Pirfenidone is another recently approved anti-fibrotic drug for the treatment of IPF. Its pharmodynamics are thought to affect inflammatory cytokines such as TNFα, downregulating transcription of growth factors including TGFβ and through reductions in lipid peroxidation and oxidative stress. In randomized, placebo-controlled trials, IPF patients given Pirfinidone were shown to have to decelerate disease

progression as measured by decline in FVC over 36-72 weeks (Taniguchi et al., 2010). Despite the advances in the treatment of IPF, lung transplantation remains the only viable treatment option that can improve the respiratory capacity of IPF patients. Transplantation however, has its own unique limitations including a shortage of organ donors and the five-year survival rate being approximately 54 percent (Raghu et al. 2011).

1.11 Nintedanib

IPF patients are believed to have an activation of signaling pathways through phosphorylation of tyrosine kinase domains such as fibroblast growth factor (FGF), vascular endothelial growth factor (VEGF) and platelet-derived growth factor (PDGF) (Richeldi et al., 2014). Nintedanib (BIBF 1120), is potent inhibitor of multiple tyrosine kinases including FGF, VEGF and PDGF receptors (Wollin et al., 2015). Patients with IPF are usually treated with 150 mg of Nintedanib twice daily, as it has been shown to attenuate the decline in lung function and significantly decrease acute exacerbations (Inomata et al., 2015). Furthermore, promising research has shown the inhibitory effect of Nintedanib on the TGFβ-induced transformation of myofibroblasts. However, it is unclear if Nintedanib may have an effect on macrophage polarization.

1.12 Rationale and Objectives

The purpose of this thesis was to examine the role of alternatively activated macrophages in fibrotic lung disease and if the prevention in polarization of these alternatively activated macrophages can be achieved by inhibiting the unfolded protein

response. Because recent work has implicated the ER as a master regulator of many cell functions, it is vital to understand how these processes are entwined in alternatively activated macrophage polarization, since these mechanisms are known to be mediators in the fibrotic process. In order to examine this relationship, a tissue microarray composed of formalin-fixed paraffin-embedded lung tissues was created. Additionally, the establishment of the THP-1 monocyte cell line had not been carried out in the Ask lab prior to this thesis, driving the establishment of this model cell line. To examine how macrophages, affect the differentiation of fibroblasts, a novel co-culture system was developed in order to answer this question. Finally, to determine what role Nintedanib had on macrophage polarization, the *in vivo* bleomycin mouse model of lung fibrosis was examined.

General Hypothesis

I hypothesize that present in IPF patient tissue are alternatively activated macrophages, which contribute to lung fibrogenesis by promoting the secretion of profibrotic cytokines and fibroblast transition.

Hypothesis

I hypothesize that the unfolded protein response pathway in alternatively activated profibrotic macrophages promotes ER expansion and the release of fibrotic cytokines. I further hypothesize that patients have a presence of these macrophages in the lung parenchyma, and that the inhibition of IRE1-XBP1 arm of the UPR is a viable therapeutic strategy to limit the activation of alternatively activated macrophages and the fibroblast to myofibroblast transition.

Chapter 2. Materials and Methods

2.01 Propagation and Culture of THP-1 Monocytes. The THP-1 (ATCC#TIB-202) human monocyte cell line were derived from a 1-year-old male leukemia patient. These suspension cells were grown in RPMI-1640 medium supplemented with 2 mM L-glutamine, 1% Penicillin Streptomycin and 10% FBS (Sigma-Aldrich). The optimal propagation density for these cells were between $1x10^5$ cells/mL to $1x10^6$ cells/mL ($2x10^6$ cells/mL maximum).

THP1 monocytes were differentiated by plating them in a 96-well plate at 80,000 cells per a well, or in a 6 well plate at 1,000,000 cells per a well. Phorbol Myristate Acetate (PMA) (ATCC- 202152) at 10 ng/mL was was added to RPMI-1640 for 48hrs to induce terminal differentiation (Park et al., 2007). At this point cells were adhered, no longer proliferated, metabolized media slowly and took on an appearance that resembled a macrophage.

These naive macrophages were washed with warm PBS to remove residual media and unattached cells. Undifferentiated cells were than polarized with their respective treatment cocktail, for classically activated macrophages LPS (20 ng/mL; *S. enterica*; Sigma Aldrich) and IFNγ (20 ng/mL; PeproTech Canada) for alternatively activated macrophages IL-4 (20 ng/mL; PeproTech Canada and IL-13 were added (20 ng/mL; PeproTech Canada), and for hyper-polarized alternatively activated macrophages an addition of IL-6 (5ng/mL; PeproTech Canada) was added for 72 hrs. Supernatant was then collected and frozen at -20 ^oC for short term storage, or -80 ^oC for long term storage.

2.02 Propagation of Bone Marrow Derived Macrophages. Bone marrow derived macrophages were harvested from C57BL6/J mice (Charles River Laboratories) and exposed to 20 ng/mL M-CSF (PeproTech Canada) in DMEM media for 7 days. Following 7 days, macrophages were washed with PBS then incubated with Accutase (Stem Cell) to disadhere cells. Cells were then treated for 30 hrs. with recombinant IL-4 (20 ng/mL; PeproTech Canada) and IL-13 (50 ng/mL; PeproTech Canada) to induce alternative programming and additional IL-6 (5 ng/mL; PeproTech Canada) for hyperpolarization. Polarization to the profibrotic phenotype was assessed by arginase activity in cell lysates, as described previously by Ayaub et al., 2016.

2.03 Propagation and Culture of Human Primary Lung Fibroblasts. Primary human lung fibroblasts (HLF) were received from Dr. Jack Gauldie's lab at the Michael Degroote Centre for Learning and Discover. They were harvested in 1999 from a patient biopsy and stored in liquid nitrogen using freezing media (DMEM/ F-12, 20% FBS with 10% DMSO). Cells were thawed and propagated in MEM-15 media supplemented with 10% FBS, 2 mM L-glutamine, 1% Penicillin Streptomycin. Fibroblasts, were propagated at a density between 25,000 to 50,000 cells/mL, and appeared elongated with no clumps. Cells were passaged by removing old supernatant and washed with 6 mL of warm PBS to remove residual FBS, this was done because trypsin acts as a serine protease and would act on FBS. Next, 3mL of trypsin was added to T75 flask (1mL= 25cm^2) to detach fibroblasts from plate and incubated at 37^{o}C for 5 min in incubator. Then, 7mL of complete MEM-15 media is added to stop trypsin cleavage of fibroblast surface proteins.

Supernatant was collected and cells were centrifuged in the Beckman Allegra 6R centrifuge at 1250 rpm. Finally, supernatant was removed and 5 mL of MEM media was added to a final concentration of 15,000 cells/mL.

2.04 Fibroblast and Macrophage Cellular Staining. Macrophages and fibroblasts were co-cultured in Biocoat Collagen I coated 96-well black/clear bottom tissue plates (Fisher Scientific) for 72hrs. Macrophages were seeded at 100,000 cells/well and HPF were seeded at 15,000 cells/well in RPMI media. It was determined that 15,000 HPF cells per well was optimal for co-culture and drug intervention experiments. The cells were treated with ± 5 ng/ml TGF-β1 and ± polarized THP1 macrophages ± macrophage secretion or ± macrophages and macrophage secretion in RPMI media. Each treatment had 3 biological replicates.

Upon completion of 72-hour treatment incubation, cells were washed twice with cold PBS and fixed with 4% paraformaldehyde. The cells were washed 3 times with cold PBS for 5 minutes on a shaker. To open up cellular membranes for staining, cells were then permeabilized with 0.1% Triton-X from Bio-Rad in PBS for 5 minutes on ice. The cells were then washed 3 times with room temperature PBS for 5 minutes on a shaker. To obtain specific cellular staining, the plate was blocked with 1% BSA in PBS for 30 minutes at room temperature. Without washing, cells were incubated for 1 hour with the human primary α-SMA antibody from Fitzgerald diluted at 1:100 in PBS with 1% BSA at room temperature. The cells were washed 3 times with PBS for 5 minutes on a shaker. The secondary Alexa Fluor IgG antibody from Invitrogen diluted at 1:200 in PBS with

1% BSA was incubated at room temperature for 30 minutes. The cells were washed 3 times with PBS for 5 minutes on a shaker. Rhodamine Phalloidin (Life Technologies) diluted at 1:200 in PBS with 1% BSA was incubated for 30 minutes at room temperature and again the cells were washed 3 times with PBS for 5 minutes on a shaker. DAPI (Sigma) at 100 ng/ml in PBS with 1% BSA was incubated for 30 minutes at room temperature and the cells were washed 3 times for 5 minutes on a shaker. Cells were imaged using an Olympus IX81 confocal microscope with a DAPI, and FITC filter. Photos were taken with a Rolera-MGi Plus Fast 1394 camera from Qimaging. Fluorescent plate readout was imaged using a Typhoon Trio imager (Amersham Biosciences). Rhodamine Phalloidin, staining cellular filamentous-actin (F-actin), had an excitation, an emission, and cutoff wavelength of 540 nm, 565 nm, and 570 nm, respectively. The secondary α-SMA antibody had an excitation, emission, and cutoff wavelength of 485 nm, 535 nm, and 515 nm, respectively. Cellular staining protocol adapted from Ask Lab Research Associate James Murphy.

2.05 ER-Tracker assay. HPFs were seeded at 20,000 cells per well in 96-clear bottom well plates using MEM/F15 media supplemented with 10% FBS and 1% P/S for 48 hours at 37°C/5% CO_2 to allow cell-plate adhesion. For THP1 macrophages, cells were seeded at 80,000 cells per well in RPMI-1640 media supplemented with 10% FBS and 1% P/S for 72 hours. HPF cells were treated with treated with ± 5 ng/ml TGF-β1 and ± STF-083010 solubilized in MEM/F15 media supplemented for 48 hours at 37°C/5% CO_2. Upon completion of the 48 hours treatment incubation, the cells were washed twice with

room temperature PBS and incubated with ER-Tracker Blue-White DPX (1μM in PBS) from Invitrogen for 30 minutes at room temperature. The cells were washed twice with cold PBS and imaged using an Olympus IX81 confocal microscope and a DAPI filter. Photos were taken with a Rolera-MGi Plus Fast 1394 camera from Qimaging.

2.06 PicroSirius Red Staining of Cell Supernatant. To detect the level of collagen in co-culture system we used an established collagen staining protocol. HPF cells were grown and treated in MEM/F15 serum starved media 0% FBS 1% L-Glut and 1% P/S for 72 hours. Cells supernatant was removed, and cells were then washed with cold PBS. Cells were then washed with cold methanol for 15 minutes and supernatant was replaced back onto cells and incubated overnight to adhere collagen to the plate. The cells were than washed with PBS to remove any residual debris and phenol red. Upon completion cells were stained with PicroSirius Red for two hours. Cells were than washed with acetic acid twice, and then washed with add sodium hydroxide and placed on shaker for 10 mins. Plate was read on Typhoon Trio imager.

2.07 Western blot analysis. This work done in collaboration with Boehringer Ingelheim, and protocol taken from their standard operating procedures. THP-1 monocytes were stimulated with MCSF ± Nintedanib. SDS PAGE and Western blotting were performed following a standard procedure using the Novex NuPAGE system (Life Technologies GmbH, Darmstadt, Germany). Separation of proteins were transferred to a nitrocellulose membrane (Millipore, Billerica, MA) in a wet blotting system (Bio-Rad Laboratories,

Hercules, CA). Afterward, membranes were blocked and then probed with antibodies directed against GAPDH, total CSFR, phosphorylated CSFR (Tyr546, Tyr699, Tyr723, Tyr923), and phosphorylated extracellular signal-regulated kinases 1/2 (pERK1/2, Thr202/Tyr204) (all Cell Signaling Technologies, Danvers, MA). The membranes were then washed in Tris-buffered saline/Tween 20 followed by incubation with horseradish peroxidase-conjugated secondary antibodies (Jackson ImmunoResearch Laboratories, West Grove, PA). Immunoreactive bands were detected by addition of Femto! (Thermo Fisher Scientific, Rockford, IL). The relative signal intensity of each band was determined with the AIDA image analysis software (Raytest Isotopenmessgeraete GmbH, Straubenhardt. Germany) and corrected to the signal intensity of the loading control. Similar method of western staining was completed for XBP1s protein detection as completed by Master's Student Anisha Dubey.

2.08 RNA extraction from THP-1 macrophages. THP-1 monocytes were stimulated with PMA and were seeded at 80,000 cells per well. Cells were washed twice with warm PBS and treated with control media, IL-4/IL-13 ± IL-6 solubilized in RPMI-1640 media supplemented with 10% FBS 1% L-Glutamine and 1% P/S for 72 hours at 37°C/5% CO_2. Each treatment contained three biological replicates. All wells were washed twice with ice cold PBS and lysis buffer RLT (Qiagen) was added while keeping the plate on ice. The lysate was transferred to a 1.5 ml Eppendorf tube and a syringe with a 23-gauge needle was used to mix lysate and lyse cellular membranes. RNA was extracted from the lysate using the RNeasy® Mini Kit (Qiagen). The purity and concentration of the RNA was measured using a Nanovue Plus (GE Life Sciences). Each RNA sample was reverse

transcribed using the SuperScript® II Reverse**.** Expression of *sXBP1* was detected using SYBR Green (Fast SYBR Green Mastermix: Applied Biosystems). The forward and reverse human *sXBP1* primers (Forward: 5'-CTG AGT CCG AAT CAG GTG CAG-3' Reverse: 5'-ATC CAT GGG GAG ATG TTC TGG-3') from MOBIX (McMaster University) were mixed to a concentration of 10 μM. The forward and reverse human *18S mRNA* primers (Forward: 5'-GTA ACC CGT TGA ACC CCA TT-3' Reverse: 5'- CCA TCC AAT CGG TAG TAG CG-3') were mixed to a concentration of 10 μM. Adapted from Research Assistant James Murphy.

2.09 Development of Tissue Microarray. Human lung tissue was obtained from the biobank for lung diseases at St. Joseph's Hospital in Hamilton Ontario. Lung biopsies were obtained from thirty usual interstitial pneumonia patients (confirmed through a clinical history, radiographic appearance and pattern of usual interstitial pneumonia determined by a trained molecular pathologists and radiologists). Upon confirmation of a positive diagnosis patient slides were scanned using the Olympus VS120 Slide Scanner and 0.6mm and 1 mm fibrotic regions and non-fibrotic cores were selected for the TMA and RNA/TEM extraction respectively. Fibrotic regions were determined by looking for features of UIP including; spatial heterogeneity in the parenchyma, architectural distortion and fibroblastic foci. In total 316 cores were selected with at least 4 cores selected for each specified area. Tissue blocks with fibrotic and non-fibrotic regions selected were sent to the Queen's University Department of Molecular Pathology and Medicine to be cored. TMA cores were 0.6 mm in size, while 1mm cores were placed in

RNA-free Eppendorf tubes to be used in RNA extraction and Transmission Electron Microscopy.

2.10 RNA isolation from FFPE cores. FFPE tissues were given to us by pathologists Dr. Cutz and Dr. Naqvi at St. Joesph's Research Hospital. FFPE tissue blocks were cored at the molecular pathology department at Queen's University. Two 1mm FFPE cores were placed into a new Eppendorf tube, and 1 mL of xylene was used to deparaffinize tissue, and vortexed at full speed for 2 min. Supernatant was removed and tissue was washed with 100% ethanol and centrifuged for 2 min. This process was repeated again and residual supernatant was removed. Tube was left open to air dry at room temperature. RNA was extracted from the lysate using the RNAeasy FFPE extraction kit (Qiagen, Toronto, ON), taking note to extract RNA with Proteinase K for 2 hours. The purity and concentration of the RNA was measured using a Nanovue Plus (GE Life Sciences).

2.11 Design and Creation of a Clinical Database. The proper characterization and storage of patient data was crucial in interoperating data in novel ways to represent diverse clinical data in an easily accessible manner. A clinical database of UIP patients was designed by gathering clinical information stored on the Meditech database as well as clinical charts. This information was then incorporated into the REDCap information system by Dr. Anmar Ayoub whom went through past physical examinations, histories and progress notes to record anthropomorphic, physiological, and physical information.

All patient information was de-identified with a unique patient identifier to prevent the linking of patient names and clinical information.

2.12 Immunohistochemistry staining of Tissue Microarray. FFPE tissue was cut and stained by the Molecular Pathology Department located in the Michael Degroote Centre for Learning. Please see Ayaub et al., 2016 for staining protocol. CD206 was purchased from Abcam (AB64693), and diluted at 1:8000 in PBS with 1% BSA. CD68 was purchased from Dako (M0876) and diluted at 1:50 in PBS with 1% BSA. BiP/Grp78 was purchased from Cell Signaling (C3177) and diluted at 1:400 in PBS with 1% BSA. FKBP13 was purchased from R&D Systems (MAB4356) and diluted at 1:300 in PBS with 1% BSA. XBP1s was purchased from Millipore and diluted at 1:100 in PBS with 1% BSA.

2.13 Standard Fixation of FFPE tissue for Resin cores of TEM. With the help of Dr. Jeffery Dickhout FFPE tissue cores were placed in 100% xylene for 3 mins to remove excess paraffin. In serial deparaffinzation steps, cores were placed in 50% xylene for 3 min two times. After, the removal of excess paraffin, tissues were hydrated by washing twice with 100% ethanol. Then in successive washes with 95% and 75% Ethanol for 3 min. Cores were then placed in 0.2M Sodium Cacodylate buffer. Finally, cores were washed and left submerged in 2% Gluteraldehyde for extended storage.

2.14 ELISA. CCL18 (R&D Systems), IL-6 (R&D systems) and MCP1 (R&D Systems) were measured in the supernatant of samples using commercially available ELISA kits. Preparation and analysis were run according to the manufacturer's protocol (R&D Systems, Minneapolis, MN, USA). All samples were measured in quadruplicate.

2.15 Animal Experiments. Wild type C57BL6/J mice were purchased from Charles River Laboratories International (Wilmington, MA, USA). All mice used were between 8 to 12 weeks old and housed at McMaster University. The animals were kept on a 12 h light/12 h dark cycle at a controlled temperature of 20 to 25°C, ambient humidity of ~50% and fed ad libitum. Experimental pulmonary fibrosis was induced using intratracheal intubation of bleomycin at 0.04 U/mouse in a volume of 50 µl sterile saline (Hospira Healthcare Corp., NDC 61703-332-18). Control animals received sterile saline alone. Animal groups were sacrificed after 14 or 21 days. After exsanguination, the lungs were cannulated, excised and washed with phosphate-buffered saline (PBS; 600 µl) for broncheoalveolar lavage fluid (BALF) collection and analysis. The four lobes of the right lung were rinsed with PBS, tied up with a surgical thread, excised and immediately frozen in liquid nitrogen. These were later stored at –80°C for further protein and RNA isolation assays. The left lung was removed and inflated to 30 cmH2O for 3–5 min in 10% formalin solution and fixed for 48-60 h before embedding and subsequent histological analysis. Protocol adapted from Ayaub et al., 2016.

2.16 Statistical analysis: Results were expressed as mean ± SEM. Two groups were compared with a Two-Tailed Unpaired Student's T-Test. When more than two groups were compared, One Way ANOVA followed by Dunnet or Bonferroni multiple comparison test was used. Statistical tests were employed using GraphPad Prism 7.0d (GraphPad Software, Inc). A $p<0.05$ was considered statistically significant.

Chapter 3. RESULTS

3.1 Objective 1: Determining the presence of profibrotic macrophages and UPR proteins in formalin fixed paraffin embedded tissues of pulmonary fibrosis patients

3.1.1 Designing and Optimizing a TMA for target identification

Tissue Microarray (TMA) technology allows for the identification of molecular targets at the RNA, DNA and protein level. This candidate identification tool can then be translated to clinical applications, by elucidating the prevalence, cellular localization and clinical significance of target genes (Kallioniemi et al., 2001). Here, the development of a TMA was used to identify the presence of UPR and macrophage proteins in patients with IPF. To answer the question of whether these molecular targets were present in IPF patients, a retrospective clinical database was created that captured diverse anthropometric and clinical data from usual interstitial pneumonia (UIP) patients. Additionally, formalin fixed lung biopsies, Hematoxylin and Eosin (H&E) stained slides, and longitudinal patient information were made available by St. Joesph's Research Hospital. Initially, 121 UIP patients were provided, but 30 UIP patients were selected who had lung biopsies with features including; usual intestinal pneumonia, parenchyma spatial and temporal heterogeneity and architectural distortion. Supplementary Figure A1.A depicts spatial heterogeneity as abrupt transitions from normal to diseased lung. Supplementary Figure A1.B shows architectural distortion, as parenchymal areas where fibrotic scars obliterate normal alveolar tissue, and dense tissue could be seen to replace normal air pockets. In Figure Supplementary Figure A1.C temporal heterogeneity was evident due to fibroblastic foci, which were areas of current injury consisting of dome-shaped regions of fibroblast activity (Flaherty, 2003). These areas were also noted by

their honeycombing, which were indicative of preexisting lung injury.

Patient slides were scanned using the Olympus VS120 Slide Scanner and fibrotic regions and non-fibrotic regions were selected based on the criteria mentioned in Supplementary Figure A1. For most UIP patients 16 cores were selected, 4 fibrotic areas and 4 non-fibrotic areas (0.6 mm in size), with adjacent areas chosen from each core for RNAseq or Transmission Electron Microscopy (1mm in size).[#] Figure 6 illustrates the steps of creating a tissue microarray.

Staining was validated with the help of a trained molecular pathologist, with stains being done using different retrieval methods and dilutions. Supplementary Figure A2 and A3 show staining for CD206 a macrophage receptor stain and CD68. Staining for alternatively activated macrophages, was seen in serial sections, and areas positive for CD206 were also positive for CD68. To determine if CD68 and CD206 staining was co-localized a TMA section was cut and stained for dual immunofluorescence (IF). CD68 and CD206 were found to stain similar membrane bound regions Supplementary Figure A3.

[#] Some UIP patients did not have enough non-fibrotic tissue present and only 8 cores were taken

Table 2: Cohort information of 30 UIP patients selected for TMA

Disease	Sample Size	Gender		Average Age	Average Pack Years	FVC (%predicted)
IPF Fibrotic	24	Male	15	58.9	23.2	63
		Female	9	58.4	17.5	62.5
IPF Non-Fibrotic	21	Male	13	58.1	26.1	65.92
		Female	8	59.5	17.5	62.5
Non Classifiable UIP	3	Male	2	64	0.57	71
		Female	1	50	20	71
Cryptogenic Organizing Pneumonia	1	Male	0	0	0	0
		Female	1	59	20	59
Connective Tissue Lung Disease	2	Male	2	69	17.5	62.5
		Female	0	0	0	0
Control	17					

* Patient information missing from four IPF patients

3.1.2 Target Identification of Alternatively Activated Macrophages Proteins in FFPE tissues of IPF lung biopsies

TMA technology was aimed to elucidate if alternatively activated macrophages were present in IPF patients by examining for CD68 and CD206 macrophage proteins within FFPE lung tissue. Relative staining for each core was then analyzed using ImageJ to assess the presence and amount of area stained or the amount of cells positively stained in each TMA core (Supplementary Figure A5).

Figure 7 shows that there was a presence of CD68 and CD206 staining found in IPF patients. CD68 and CD206 staining appeared to be localized near blood vessels and within the parenchyma of lung tissue. Furthermore, when staining was quantified no relative increase in the amount of CD68 area stained was seen in IPF patients versus control patients. However, there was a 1.5-fold increase in the amount of CD206 staining

in both fibrotic and non-fibrotic areas in IPF patients versus control patients.

3.1.3 Target identification of *UPR Proteins in FFPE tissues of IPF lung biopsies*

Next to determine if there was a presence of UPR proteins in IPF patients, TMA slides were stained using the automated BondRX stainer and percent area stained was quantified using ImageJ. The presence of three resident ER proteins XBP1s, GRP78 and FKBP13 a chaperone thought to be associated in the ER stress response were investigated. Intracellular ER straining was observed and calculated through the ImageJ software program. All three protein stains were observed to be cytoplasmic, with abundant FKBP13 staining seen in IPF tissues, although XBP1s showed minimal staining.

There were not significant differences found in XBP1s staining between IPF and control patients Figure 8. However, there was an increase in the relative abundance of GRP78 and FKBP13 in fibrotic areas of IPF patients versus control patients.

3.1.4 Endoplasmic reticulum enlargement in macrophage like cells of IPF patients

To investigate if UPR proteins found in IPF patients were enhancing ER expansion in macrophage, IPF patient lung biopsies positive for CD206 were examined and compared to control samples. Figure 9 shows images at 1000x - 50000x magnification which appear to be macrophage-like cells taken from formalin fixed lungs. There was a noticeable increase and dilation in the endoplasmic reticulum of macrophage-like cells in IPF patients. This same dilation was not seen in control patients.

This may suggest that the UPR may play a role in the fibrotic process in IPF patients. Similar findings were seen in fibroblasts of IPF patients (Supplementary Figure A6)

3.2 Objective 2: Characterizing the role of IRE-1/XBP-1 pathway in polarized THP-1 human macrophage cell line.

In this second aim, a human monocyte cell line (THP-1) was used to investigate the role of the UPR pathway in the alternative activation process of macrophages. It was hypothesized that the activation of the IRE1-XBP1 pathway was required for the polarization of IL-4/IL-13 and IL-4/IL-13/IL-6 stimulated macrophages. To test this hypothesis, the IRE1 UPR-arm was inhibited with STF-083010 and 4μ8C, to understand if this led to a reduction in the polarization of naive macrophages to alternatively activated macrophages as assessed through CCL18 secretion.

3.2.1. Validation and control experiments for THP-1 stimulated macrophages

The THP-1 human monocyte cell line was derived from a one-year-old leukemia patient and is well defined in understanding macrophage function, signaling, and nutrient transport (Chanput et al., 2013). To validate the responsiveness of these cells, naïve THP1 macrophages were stimulated with four different conditions, either supplemented RPMI-1640 media, LPS/IFNγ, IL-4/IL-13, or IL-4/IL-13/IL-6. Cells were stimulated for 72 hours and 50μL of supernatant was collected and examined by EVE technologies (Calgary, AB) to determine relative cytokine secretions. Figure 11 shows cells were responsive to recombinant human cytokine and displayed differing phenotypes. Alternatively activated (IL-4/IL-13) and hyperpolarized (IL-4/IL-13/IL-6) macrophages induced the induction of profibrotic cytokines such as VGEF and TGFα. Classically

activated macrophages (LPS/IFNγ) promoted the stimulation of inflammatory cytokines such as TNFα, G-CSF, and IL-6.

3.2.2 Increased concentration of CCL18 from IL-4/IL-13/IL-6 stimulated THP-1 macrophages and human IPF serum

In the context of idiopathic pulmonary fibrosis, chemokine ligand 18 concentrations have shown to be predictive in the pathogenesis of IPF and may become a useful tool in the clinical management of patients (Prasse et al., 2006). To replicate these findings, IPF serum was collected from patient samples and quantified for concentration of CCL18. Fig 11 demonstrates that there was a two-fold increase of CCL18 in IPF patients. Furthermore, CCL18 serum concentrations were shown to be predictive in determining FVC decline in patients.

To characterize if alternatively activated THP-1 macrophages secreted CCL18, naïve macrophages were treated with IL-4/IL-13 and IL-4/IL-13/IL-6. Figure 12 depicts an increased secretion of CCL18 from alternatively activated macrophages over 72 hours, this secretion was significantly upregulated in the presence of IL-6. Furthermore, CCL18 expression was limited to alternatively activated macrophages, and IL-6 nor LPS/IFNγ treated macrophages had a noticeable concentration of the chemokine.

3.2.3 ER Expansion upregulated in hyperpolarized- alternatively activated macrophages

Previous data from our group has shown that IL-4/IL-13/IL-6 stimulated macrophages had an enlarged ER in bone marrow derived murine macrophages

(Unpublished). To further phenotype these findings in a human system, THP-1 macrophages were stimulated with control media, IL-4/IL-13 or IL-4/IL-13/IL-6 supplemented media, and examined at 50000x magnification (Fig. 13). THP1 macrophages treated with IL-4/IL-13 had an enlarged ER versus control macrophages but this affect was enhanced with the addition of IL-6 where the ER became extensively dilated and expanded, appearing as a plasma cell. Additionally, IL-4/IL-13/IL-6 macrophages had an increased presence of mitochondria versus control macrophages.

3.2.4. Elucidating the involvement of IRE1-XBP1 in the polarization of THP-1 macrophages

To identify if XBP1 splicing was increased as alternatively activated macrophages were polarized, THP-1 macrophages were treated for 8, 15 and 24 hours and RNA fold change was assessed through rt-PCR. Fig. 14 depicts at 8 hours there was a significant fold change in IL-4/IL-13 and IL-4/IL-13/IL-6 macrophages versus control macrophages but after that time point level of expression decreased.

Next to determine if these results were similarly seen at the protein level, THP-1 macrophages were treated for 2, 8 and 24 hours, and protein expression was assessed through Western Blot analysis. Tunicamycin (tuni) was used as a positive control, as it has been shown to promote ER stress. No noticeable levels of protein upregulation were seen in treated IL-4/IL-13 or IL-4/IL-13/IL-6 macrophages, but tunicamycin treated cells appear to produce a significant band of XBP1s protein at the 8-hour and 24-hour time point.

Finally, to determine if ER expansion could be seen visually, THP-1 macrophages were treated and stained with an ER-tracker dye (Fig. 14c). ER- Tracker permeated cell membranes and stained the endoplasmic reticulum of polarized macrophages. Hyperpolarized macrophages had an enlarged ER versus, control and IL-4/IL-13 macrophages. STF-083010 appeared to lower the ER expansion process as suggestive through reduced ER stain. This IRE1 inhibitor also appeared to inhibit the expansion of ER in human primary fibroblasts (Supplementary Figure A7).

3.2.5 Inhibition of IRE1-XBP1 axis prevents profibrotic secretion of IL-4/IL-13 and IL-4/IL-13/IL-6 macrophages

To determine if inhibition of the unfolded protein response could prevent the pronounced ER seen in polarized alternatively activated macrophages of macrophages, XBP1 splicing was inhibited. This was achieved by administering two drugs STF-083010 and 4μ8C which block the IRE1 RNase domain of the UPR pathway. Macrophage polarization was assessed through CCL18 or MCP1 secretions.

Macrophages were treated with STF-083010 and metabolic activity of the THP-1 cells was assessed through MTS assay. Fig. 15A shows that STF-083010 at concentrations lower than 6uM were not affected. When the production of CCL18 and MCP1 secretions was assessed in this system, results demonstrate that STF-083010 prevented the secretion of IL-4/IL-13 treated cells at 0.06, 0.6, 6 μM & 0.6, 6 μM respectively. Similar results were seen when alternatively activated macrophages where exposed to another inhibitor of the IRE1 axis 4μ8C at concentrations of 30 μM. At these

concentrations there was a reduction in polarization of alternatively activated macrophages as assessed by CCL18 secretion.

To investigate whether these findings were similarly found in hyperpolarized IL-4/IL-13/IL-6 macrophages. THP1 cells exposed to hyperpolarization cocktail for 72 hrs. ± STF-083010/4μ8C and CCL18 secretion was assessed. Fig. 15 E and F demonstrate that STF-083010 prevented the polarization of alternatively activated macrophages at (0.06, 0.6, 6 μM) and by 4μ8C (0.3, 3 & 30 μM). Although the THP-1 response may elucidate potentially novel responses that might occur *ex vivo* or *in vitro*, these findings should be further validated by *in vivo* studies to draw concrete conclusions.

3.3 Objective 3: Examining whether IL-4/IL-13 polarized THP-1 macrophages effect the transition of fibroblasts to myofibroblasts

3.3.1 TGFβ Secretion is Upregulated in Alternatively Activated THP-1 macrophages

Alternatively activated macrophages have been known to be profibrotic cells, but their direct action on the differentiation of fibroblasts to myofibroblasts has not been elucidated (Gibbons et al., 2011). Here tumor growth factor beta (TGFβ) secretion was assessed in THP-1 macrophages, as this growth factor has been shown to be crucial in fibroblast to myofibroblast transition. THP-1 macrophages were polarized for 72 hours and total TGFβ was assessed through ELISA. These results demonstrate that IL-4/IL-13 and IL-4/IL-13/IL-6 macrophages had a 1.5 fold increased secretion of TGFβ over naive/control macrophages (Fig 16).

3.3.2 Optimization and control experiments for co-culture of human pulmonary fibroblasts and THP-1 macrophages

To further assess these findings, a human *in vitro* macrophage fibroblast co-culture system was developed to determine if and how macrophages may be affecting the fibroblast to myofibroblast differentiation. Polarized macrophages were co-cultured with fibroblasts on a 96-black coated flat bottom well plate. In the experimental setup 15,000 primary fibroblasts taken from a healthy or fibrotic lungs were plated on a 96-well plate with 100, 000 polarized macrophages. After co-culture supernatant was removed and αSMA expression was determined via cellular staining in each well.

These preliminary experiments investigated the length of time to co-culture macrophages with fibroblasts Sup Fig. A7 shows that after 72 hours of co-culture, fibroblast transition plateaued as assessed through αSMA staining. Additionally, a noticeable difference in the presence of αSMA staining at this time-point was seen when control fibroblasts were stimulated with TGFβ. These results led us to select the 72-hour time point for the co-culture system.

Next to determine the difference in expression of healthy and fibrotic fibroblasts, both types of fibroblasts were treated with TGFβ and αSMA expression was assessed. Supplementary Figure A7. D shows fibrotic fibroblasts converted more readily to myofibroblasts than healthy fibroblasts when exposed to TGFβ.

3.3.3 Determining the effects of macrophages on healthy and fibrotic primary fibroblasts

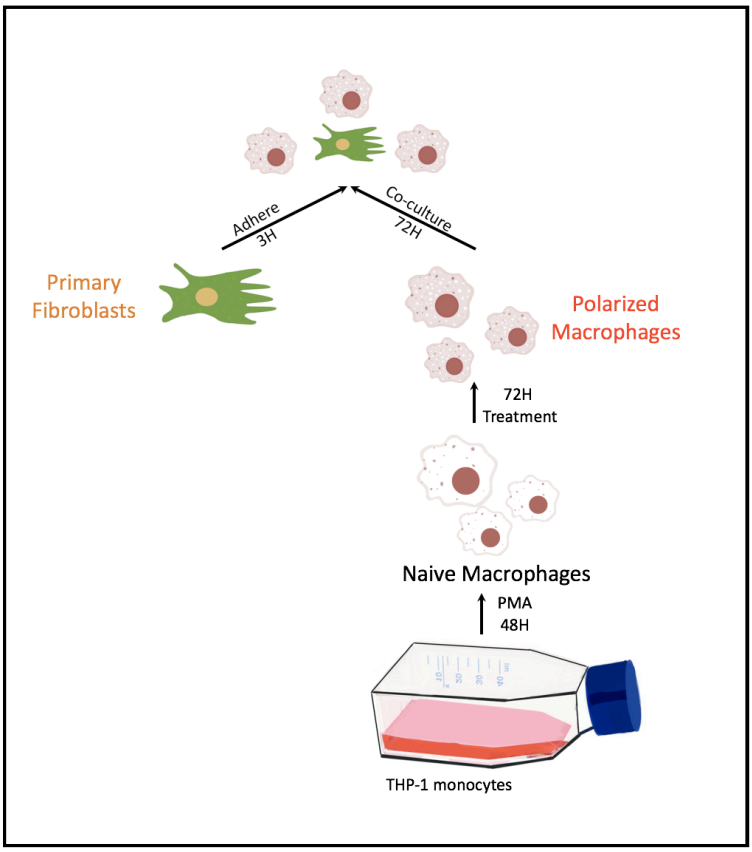

Figure 17: Design of Co-Culture System

In order to identify if macrophages promote myofibroblast formation, a co-culture system was designed. In this *in vitro* experimental system 15,000 primary lung fibroblasts were plated with 100,000 THP-1 macrophages. Fluorescent cellular staining was used to assess for αSMA staining.

As depicted in Fig. 18, a novel co-culture system was designed to analyze the effect of macrophages on fibroblast to myofibroblast transition as assessed through level of αSMA/f-actin. Filamentous actin (F-actin) was used to modulate differences in proliferation. In primary healthy fibroblasts, variously polarized macrophage populations

were assessed on fibroblast differentiation, and whether it was soluble autocrine, paracrine, or juxtacrine signals that affected this process. These results indicate that IL-4/IL-13/IL-6 stimulated macrophages resulted in an increase in αSMA/f-actin staining in healthy fibroblasts. Furthermore, in this system STF acted to block fibroblast transition. Similar effects were not seen in fibrotic fibroblasts suggesting differing phenotypical characteristics.

3.4. Objective 4: Investigating the effect of the antifibrotic drug Nintedanib on alternatively activated macrophages.

3.4.1 Nintedanib inhibits the phosphorylation of tyrosine residues (Tyr546, Tyr699, Tyr723, Tyr923) on CSF1R on THP-1 monocytes.

Circulating monocytes in the lung vasculature have been thought to be involved in the pathogenesis in the early fibrotic response resulting in the destruction in the lung architecture. These immune cells were thought to infiltrate the lung parenchyma transitioning to macrophages and contributing to the fibrotic progression. Our group in collaboration with Boehringer Ingelheim examined whether Nintedanib prevented the phosphorylation of tyrosine residues on the CSF1 receptor critical for monocyte to macrophage differentiation.

Accordingly, THP-1 monocytes were exposed to macrophage colony stimulating factor (MCSF) for 48 hours with or without Nintedanib at biologically significant concentrations of (10, 30, 100, 300nM). Western blot analysis on cell lysates was analyzed to determine the relative phosphorylation states of tyrosine residues (Tyr546,

Tyr699, Tyr723, Tyr923) on CSF1 receptor. This data indicated that at 300nM Nintedanib significantly inhibited the phosphorylation of these tyrosine residues (Fig. 19).

3.4.2 Nintedanib attenuates the polarization of naive macrophages to alternatively activated or hyperpolarized profibrotic macrophages

CCL18 is a small cytokine thought to be involved in the chemotaxis of T-cells, B-cells and immature dendritic cells. One of the main producers of this cytokine in the immune system are alternatively activated profibrotic macrophages. Since the addition of IL-6 to the standard profibrotic cocktail of IL-4/IL-13 dramatically increased the CCL18 production of these cells, the role of Nintedanib was examined in this system.

To determine if Nintedanib could affect the polarization of naive macrophages to alternatively activated and hyperpolarized profibrotic macrophages, bone marrow derived murine macrophages from C57BL/6 mice and THP-1 macrophages were treated with IL-4/IL-13 or IL-4/IL-13/IL-6 with or without Nintedanib at concentrations of 0.1, 0.3 and 1μM. This results demonstrate that Nintedanib prevented the polarization of alternatively activated macrophages mediated by IL-4/IL-13 (0.3 and 1μM) and by IL-4/IL-13/IL-6 (0.1, 0.3 and 1μM) in both murine and human model systems examined (Fig. 20).

3.4.3 *Nintedanib prevents the secretion of collagen in IPF-derived fibroblasts.*

In connective tissues, fibroblasts are the most common immune cell and one of the primary sources of the extensive extracellular matrix (ECM). These cells also serve as central mediators of pathological fibrotic accumulation of ECM and their cellular

proliferation and differentiation are known to be key contributors in pulmonary fibrosis. To determine the effect of Nintedanib on the secretion of collagen from fibroblasts primary lung fibroblasts from patients with IPF or healthy donors were treated with TGFβ (1ng/mL) with or without Nintedanib and the level of collagen secretion was determined through PicroSirius Red staining. Fibrotic fibroblasts treated with low dose TGFβ demonstrated significant collagen secretion versus healthy fibroblasts (Fig 21). Nintedanib prevented the secretion of collagen from fibrotic fibroblasts at doses of 300nm and 100nm, but did not affect healthy fibroblasts treated with TGFβ.

3.4.4 The effects of Nintedanib on the bleomycin mouse model of fibrosis.

The bleomycin mouse model of fibrosis is a well characterized system to highlight the pathological features of pulmonary fibrosis. To determine if Nintedanib affected the expression of alternatively activated cells in this system, C57BL6/J mice were exposed to a single intratracheal administration of bleomycin, followed by BID Nintedanib treatment from day 5 to day 20. Level of alternatively activated cells present in mice was examined using immunohistochemical staining via two well characterized profibrotic macrophage proteins YM1 and arginase-1.

In the bleomycin mouse model of fibrosis, Nintedanib although not significant led to lowered fibrotic outcomes as assessed to pressure volume loops and lung elastance measurements (Fig. 22). FFPE lungs resected from mice showed although not statistically significant reduced YM1- positive immunohistochemical staining in the Nintedanib group (Fig. 23).

Chapter 4. Discussion

Macrophages are plastic cells that are considered to be important effector leukocytes of the innate immune system (Janeway et al., 2016). In the context of fibrosis and tissue regeneration, macrophages are thought to play a role in the recruitment of immune cells and are an imperative source of chemokines such as CCL18 and MCP1 and growth factors such as TGFβ and VEGF-1 (Kharraz et al., 2014; Luzina et al., 2006). Accumulating research points to the importance of these cells in fibrotic disorders, as the depletion of macrophages from models of fibrosis ameliorates disease (Kim et al., 2015). Additionally, several researchers have proposed macrophage-derived CCL18 as crucial in the pathogenesis of fibrotic lung disease, due to its role in driving collagen production from fibroblasts in the lung (Prasse, 2006). Consequently, CCL18 was found to be elevated in the serum of IPF patients, where its concentration was increased in patients with a respiratory decline (Fig. 11). This was similar to other findings that revealed patients with fibrotic lung disease had an increased percentage of CCL18-positive alveolar macrophages (Prasse et al., 2006). CCL18 may therefore be a potential therapeutic target for the treatment of IPF or serve as a prognostic indicator. While numerous research from other groups has focused on the role of alternatively activated macrophages in *in vivo* animal models, the presence of these cells in IPF patients and whether we could affect their polarization by inhibiting IRE1 activation in a human cell-line was examined.

Human tissue biopsies have been preserved in formalin and embedded in paraffin for over a century, for the purpose of microscopic examination (Kallioniemi et al., 2001).

While this method has become the standard method in histopathological analysis, it comes with consequences as the process is slow and tedious. The advent of the tissue microarray in 1988, allowed for the high throughput screening of multiple specimens by taking small cores from a pre-existing block and embedding them into a master block (Kallioniemi et al., 2001). The goal in creating a tissue microarray was to assemble numerous IPF patient lung samples onto a single histological wedge, which were characterized from a clinical standpoint. This technology would easily allow for the investigation in changes of tissue microarchitecture through TEM or for target identification. Targeted genes of interest could then could be correlated with respiratory measurements such as FVC or DLCO. The correlation between gene signatures and respiratory measurements was only possible through the development of a clinical database on the REDCap servers used for the collection of patient information. This clinical database is a highly modifiable, stream-lined network, which allows for the future development of epidemiological projects, by interoperating and extrapolating data in novel ways. One of the goals of this thesis and information system was to create and design a database that would allow for the correlation of clinical outcomes with genomic and architectural changes.

Through examining TMA slides, the identification of $CD206^{+}$ and $CD68^{+}$ macrophage markers and UPR staining in IPF tissue were assessed. Analysis of staining was quantified in various ways such as area stained or number of positive cells present, in order to develop an optimal calculation of staining (Supplementary Figure A5). While not presented here, the percent of $CD206^{+}$ and $CD68^{+}$ staining was found to have no

correlation with respiratory measurements (i.e. FVC and DLCO). This negative outcome could be attributed to factors such as not selecting representative tissue, obtaining overlying fibrotic lung biopsies, or the non-existing pathological mechanism between CD206 cells and respiratory decline. Furthermore, fibrotic areas of IPF patients showed increased expression of the chemical chaperones FKBP13 and GRP78 (Fig.8), as compared to the control cohort. This increased expression of molecular chaperones may suggest that patients have a robust aggregation of unfolded proteins found in the endoplasmic reticulum. This aberrant accumulation of misfolded proteins has been seen in other pathological diseases such as cardiac fibrosis where aggregated proteins are a major driver in the persistent remodeling of tissue (Groenendyk et al., 2016). Furthermore, it has been found that the attenuation of the transiently activated UPR prevented cardiac fibrosis, and improved prognosis (Groenendyk et al., 2016).

These TMA results however, should not be over-interpreted due to the small sample size and clinical heterogeneity. Additional experiments in a larger, stratified population are necessary to confirm the data presented here. This data may instead suggest that the presence of these UPR and macrophage proteins to be important targets for future clinical and preclinical investigation.

While this preliminary TMA is a powerful tool that can be used to identify unique gene signatures for target development and drug discovery, the precious tissue used to create TMAs becomes difficult to access and create, as clinical guidelines change and HR-CT becomes the predominate method to diagnosis IPF patients (Hunninghake et al., 2001). This patient cohort also becomes valuable as these patients were not on the current

standard of care drugs Nintedanib and Pirfenidone. Thus, it becomes important to characterize the unique gene signatures expressed in these IPF patients. While RNAseq was not completed in this patient population, RNA extraction from TMA cores were completed and a relative RNA yield was measured to be 150 ug/mL with an RNA integrity of 2.5. Our group has already completed Nanostring analysis on IPF patient tissue cores of this quality showing the upregulation of various UPR markers in human IPF FFPE lung biopsies including GRP78 and FKBP65. Furthermore, from these cores transmission electron microscopy images were done to look at the microarchitecture of the tissues, which has revealed the dilated and enlarged ER found in immune cells of IPF patients (Fig. 9).

After noting the presence of alternatively activated macrophages and UPR proteins in pathological regions of the fibrotic lung, the link between the UPR response and the polarization of profibrotic macrophages was investigated. Detailed experiments done *in vitro* on plasma cell differentiation have shown that XBP1 splicing is required for cellular differentiation (Todd et al., 2009). Furthermore, XBP1 activation was shown to be potentially mediated through pro-inflammatory cytokine IL-6. Thus, the XBP1-IL6 axis of the UPR pathway was examined to determine its potential effects on the polarization of alternatively activated macrophage through the secretion of profibrotic cytokine, CCL18. It is important to note that previous groups have found an upregulation of proinflamatory cytokine IL-6 in IPF patients, however here we were not able to determine such an effect in IPF serum (Fig. 11) (Ioannis et al., 2016). This result may be attributed to a small sample size, assessing patients too early or late in their disease, or

before onset of an acute exacerbation. To examine this polarization process in the THP-1 system, macrophages were treated with IL-4/IL-13 alone or with/without the addition of IL-6. Fig 11 and 13 show the addition of IL-6 to the conventional IL-4/IL-13 polarization cocktail resulted in a hyperpolarization of alternatively activated macrophages as assessed through the enhanced production of profibrotic factors CCL18, TGFβ & VGEF. Notably, CCL18 has been shown to skew circulating monocytes to profibrotic macrophages with increased cell survival and robust capacity for phagocytosis (Schraufstatter et al., 2012). Moreover, CCL18 cytokine may act through a positive feedback mechanism by attracting Th2 helper cells to secrete cytokines such as IL-4/IL-13, in turn stimulating alternatively activated macrophages (Chang et al., 2010). Another interesting finding was that IL-4/IL-13/IL-6 treated THP-1 macrophages had an expanded and dilated ER as assessed through TEM (Fig. 13). The function of the UPR in promoting ER biogenesis is clear, as splicing of XBP1 stimulates lipid biosynthesis and ER expansion in fibroblasts and B lymphocytes (Sriburi et al., 2004). Conversely, XBP1 deficiency ablates ER expansion during the maturation of specialized secretory cells (Reimold et al., 2001). It is important to note that IL-6 alone did not appear to upregulate expression of CCL18 production in THP-1 macrophages. This finding suggests a synergistic effect between cytokines IL-6 and IL-4/IL-13 (Fig. 12).

To investigate if this induction in profibrotic cytokines and ER expansion in IL-4/IL-13 and IL-4/IL-13/IL-6 macrophages was linked to the activation and XBP-1 splicing, the RNA signature from these macrophage populations was examined. At the 8-hour time point, XBP1 splicing was increased in hyperpolarized versus IL-4/IL-13 and

control macrophages. This increase in IL-6 signaling is thought to occur through the induction of IL-4 receptor, promoting the induction of IL-4- and STAT-6-mediated polarization (Mauer et al., 2014). However, the precise mechanism of which XBP1 splicing affects IL-4/STAT-6 signaling still remains unclear. No visible difference was seen in XBP1 protein expression at the 2-, 8- or 24-hour time point.

To determine if manipulation of the UPR prevented the polarization of naive macrophages to alternatively activated macrophages, THP-1 macrophages were treated with IRE1 inhibitors 4μ8C and STF-038010. Macrophages were polarized with IL-4/IL-13 or IL-4/IL-13/IL-6, with or without addition of IRE1 inhibitors. At non-cytotoxic levels, STF-038010 demonstrated a reduction in fibrotic cytokines CCL18 and MCP1 at 0.06, 0.6 and 6 μM and at 30μM with 4μ8C. Similar findings were seen with IL-4/IL-13/IL-6 treated macrophages (Fig. 15). These findings were validated visually through the use of ER tracker dye, where there is a reduction in the ER expansion process through the administration of 4μ8C and STF-038010 (Fig. 14). These results indicate that alternative activation and hyperpolarization of macrophages may occur through the IRE-XBP1 splicing and that inhibiting the UPR, may serve as a potential therapeutic avenue to prevent alternatively activated macrophages in pulmonary fibrosis.

Fibroblasts and macrophages are multi-functional immune regulatory cells that modulate important mechanisms in the functional behavior of inflammation and tissue regeneration (Wynn and Vannella, 2016). It is thought that the two cells play an important role in regulating the actions of one another through the communication of soluble autocrine, paracrine, and juxtacrine signaling (Ploeger et al., 2013). Hence, fibroblast

activation through the chemical and physical interactions between both recruited and tissue-resident macrophages are thought to play an important role in the modulation of cellular proliferation, enzymatic activity and protein synthesis. Furthermore, as noted previously, alternatively activated macrophages are a primary source of CCL18, an important cytokine that has been shown to stimulate collagen production in primary pulmonary fibroblasts (Schraufstatter et al., 2012; Luzina et al., 2006).

However, the detailed mutual effects of these two cell types in fibrogenesis remain unknown. Here the design of a preliminary co-culture system begins to remediate some of these questions. In this *in vitro* system, fibrotic fibroblasts were more prone to TGFβ-associated myofibroblast transition, as assessed through *in vitro* αSMA staining and collagen production (Supp. Fig. A8). This data is congruent with published literature showing scleroderma fibroblasts to show greater expression of αSMA, in addition to increased maturation toward myofibroblasts as compared to their healthy counterparts when stimulated with TGFβ (Binai et al., 2012).

Subsequently, when healthy fibroblasts were co-cultured with macrophages they appeared to be more susceptible to juxtacrine signaling by IL-4/IL-13/IL-6-stimulated macrophages (Fig. 18). Macrophages are known to secrete mediators that activate local and recruited tissue fibroblasts to differentiate into myofibroblasts (Murray and Wynn, 2011). These soluble mediators secreted by hyperpolarized macrophages include CCL18, TGFβ and VEGFα (Fig. 17). TGFβ and VEGFα are two growth factors known to promote cellular proliferation and angiogenesis. However, these findings may provide a potentially novel mechanism as to how fibroblasts may be transitioning to myofibroblasts. In this co-

culture system, physical interaction between macrophages and fibroblasts may be required for fibroblasts to transition into myofibroblasts. This may explain macrophages were noted to be in close proximity to areas of active fibroblast fibrogensis in the fibroblastic foci of IPF patient lungs. This adhesion may be occurring through the binding of fibroblast activation protein-α (FAP) and class A scavenger receptor (SR-A) on macrophage membranes. Co-localization studies done *in vivo* show SR-A expressing macrophages to localize in the stromal environments of breast tumors with activated fibroblasts (Mazur et al., 2016). FAP-cleaved collagen serves a substrate for SR-A-dependent macrophage adhesion, as macrophages do not adhere well to native collagen proteins. This may elucidate a mechanism as to how macrophages physically interact in the tissue environment with fibroblasts.

The next question that arose was whether the inhibition of the UPR pathway through STF-038010 treatment could attenuate the ability of alternatively activated macrophages to activate fibroblast-myofibroblast transition. While STF-038010 attenuated the transition of healthy fibroblasts, the same effect was not observed in fibrotic pulmonary fibroblasts. This data reveals how fibrotic pulmonary fibroblasts substantially differ from their control counterparts, exhibiting pro-fibrotic features matched by their increased ability to differentiation through the interaction with TGFβ. This data may suggest that it is important to identify fibrogenesis at an early stage in patients to prevent the irreversible transition of fibroblasts to key effector cells. While the cell-culture system provides a simplified, cost-effective and focused analysis of cellular

interaction, there are limitations, as it does not replicate the positive and negative feedback loops seen in *in vivo* signaling.

Nintedanib is a tyrosine kinase inhibitor recently approved for the treatment of IPF with unclear pharmokinetics. Research has already shown the effects of Nintedanib on fibroblast migration and proliferation of fibroblasts, as well as myofibroblast differentiation (Wollin et al., 2015). However, the effects of Nintedanib on macrophage polarization have not been fully elucidated. The role of this pharmaceutical on the polarization of THP1 monocytes and macrophages, its effects on the phosphorylation of CSF1 receptor, its role on collagen secretion from fibroblasts and whether it ablated alternatively activated macrophage polarization in the bleomycin model of lung fibrosis were investigated. What was demonstrated was that Nintedanib effectively inhibited phosphorylation of tyrosine domains of the CSFR1 receptor (300nM), which has been associated with the monocyte to macrophage differentiation process (Fig. 21). Accumulating evidence suggests that the loss of the CSF1 receptor depletes tissue- and tumor-associated macrophages in cancer models, which were major pathological drivers for tissue inflammation and fibrosis. It also was an important regulator in the migration, proliferation and survival of myeloid progenitors. MacDonald and colleagues found that depletion of CSF-1 signaling attenuates the maturation and replacement of resident monocytes and tissue macrophages while not altering the numbers of pro-inflammatory monocytes (MacDonald et al., 2010). This may suggest that the inhibition of CSF1R by Nintedanib may directly affect the population of profibrotic macrophages without altering the inflammatory macrophage response. Nintedanib also attenuated IL-4/IL-13 and IL-

4/IL-13/IL-6 macrophage secretion of CCL18 at pharmacologically relevant doses (Fig. 20). IL-4-stimulated macrophages have been indicated in accelerating repair in tissues, and sustained activation of IL-4 macrophages has been thought to contribute to developing fibrosis. Interestingly, IL-6 acts to increase IL-4 receptor on macrophages and contributes to the fibrotic response (Mauer et al., 2014). Nintedanib's effect on lowering CCL18 production by IL-4-stimulated macrophages may translate *in vivo* into effects of mitigating survival and activation of myofibroblasts, the key effector cell in the production of ECM. This novel mechanism may suggest a novel response of how Nintedanib might be acting to reduce CCL18-dependent collagen production in pulmonary fibroblasts. Furthermore, Nintedanib has been previously shown to reduce fibroblast to myofibroblast differentiation, however in this study, Nintedanib acted directly on fibrotic fibroblast to attenuate TGFβ stimulated collagen production (Fig. 21). Moreover, while not statistically significant, Nintedanib reduced lung elastance in the bleomycin murine model of lung fibrosis. This antifibrotic effect was additionally associated with a non-significant decrease in alternatively activated macrophage markers (YM1-positive cells in the lungs of mice; Fig. 23). Taken into whole, this data may reveal Nintedanib's role in the attenuation of AAM in diseases of fibrosis.

In summary, these findings suggest that there is a presence of UPR and macrophage proteins in the lungs of IPF patients and the UPR response may be necessary in the polarization of alternatively activated macrophages. Furthermore, the addition of IL-6 to the conventional alternatively activated cocktail of IL-4/IL-13 resulted in the upregulation of profibrotic cytokines and enhanced ER. This hyperpolarization process

may occur through the action XBP1 splicing and can be prevented through the treatment of IRE1 inhibitors 4μ8C and STF-038010. Finally, Nintedanib a current therapy for the treatment of IPF patients may work to prevent CSFR1 phosphorylation on monocytes and the CCL18 secretion from AAM. However, no link between Nintedanib and the unfolded protein response was established. Future work should look at the role of Nintedanib in tunicamycin treated THP-1 macrophages.

Chapter 5. Limitations:

Future work utilizing the techniques of this thesis should help in demonstrating the involvement of the UPR pathway in alternatively activated macrophages. Furthermore, the development of a novel co-culture system, TMA, and clinical database could be used in the identification of novel therapeutic targets. However, limitations to this research arise as recent studies have demonstrated the functional plasticity of macrophages. While macrophages can be polarized *in vitro* to the "M1" state, which promotes host inflammation, or to the "M2" state, which is vital in promoting wound healing, the *in vitro* methods employed in defining M1 and M2 macrophages as distinct subtypes rather than a continuum of various functional characteristics remains problematic. In this thesis, M2 macrophages were stimulated by Th2 cytokines IL-4/IL-13 and expression of cellular markers CD68 & CD206 in humans and YM1/Arg1 in murine systems. Future studies should instead focus on better characterizing these macrophages and their ability to promote fibrogenesis or host inflammation and phagocytosis. To characterize these cells, RNAseq could be used to define the

upregulation of various gene signatures in macrophage subtypes. Additionally, the development of functional assays to characterize phagocytic and fibrotic activity would be more precise. This data would help to differentiate the various subtypes, in addition to showing which ER stress genes are upregulated through the macrophage polarization process. Another important consideration is that the cell systems used in this thesis are perhaps overly simplified and may inaccurately mimic the disease pathology found in patients. Hence, using the THP1 cancer cell line may fails to consider much of the essential feedback signals necessary to truly simulate the *in vivo* aspects of fibrogenesis. Future work could instead focus directly on human peripheral blood mononuclear cells, in order to increase translational relevance.

Another limitation involved the transmission electron microscopy completed in the FFPE cores of IPF patients. Here, $CD206^{+}$ regions from FFPE blocks were cored and submitted them for TEM. This was done to assess level of ER expansion in macrophages and fibroblasts of IPF patients. However, it cannot definitively be proven whether these cells were macrophages. Future work could label macrophages through immunogold staining or quantify relative expansion of ER from immunohistochemical staining.

Finally, the construction of a tissue microarray allowed for the examination in the upregulation of various proteins through immunohistochemical staining. This high throughput method of identification, also had its limitations. The first limitation was the use of adenocarcinoma patient lungs as control specimens. TMA staining depicted large increases in ER chaperones in both control in addition to IPF patients. This relative presence of staining in control tissue may have been skewed because of the disease

pathology present in the lungs of these adenocarcinoma patients. Accessing truly normal pathology lung specimens is difficult to collect as routine lung biopsies are not taken from healthy individuals and specimens taken post-autopsy have deterioration in protein folding. Another limitation in staining arises from the quantification of immunohistochemical staining, as there is no standard method for quantification of IHC staining in histopathologic analysis. The amount of staining was validated in various ways to correct for the density of tissue (i.e. CD206/CD68), as well as quantifying the area stained by IHC and quantifying the number of cells stained by IHC. Staining was presented in various ways as there was no one definitive way to quantify stain. The actual method of quantifying levels of staining in IPF lungs is much more complex and can be done through flow cytometry on frozen lung specimens. Instead data was presented in a much more simplistic way of quantifying an increase in alternatively activated macrophages through an increase in CD68, and CD206 staining in this study. Future work should instead focus on the presence proteins in disease tissue for target identification. Additionally, in-situ hybridization staining of tissue samples could be done to determine if there was the presence of RNA or DNA in tissues and whether it is co-localized in the cellular staining of tissue. A future goal of this research is to optimize an algorithm for cellular staining to take into account the intensity of stain as well as the proportion of staining present.

Significance:

The data presented in this thesis may contribute to better understanding the importance of the IRE1-XBP1 activation pathway and ER expansion process related to the accumulation of alternatively activated macrophages in patients with fibrotic ILD. Furthermore, this work sets a foundation that will help to create a clinical and translational framework that may help guide cellular and pre-clinical experiments, where we aim to demonstrate the requirement of the IRE1-XBP1 pathway in the macrophage polarization process, in addition to target identification at the protein and gene level by combining immunohistochemistry and in-situ hybridization. We predict that the examination of these clinical samples and human cells systems will allow for the investigation of cellular and molecular pathways that once identified could be further examined in experimental models. This may allow us to propose novel anti-fibrotic therapies targeting ER expansion and macrophage polarization that are clinically relevant.

References

Alberts, S. M., Sonntag, C., Schäfer, A., & Wolf, D. H. (2009). Ubx4 modulates cdc48 activity and influences degradation of misfolded proteins of the endoplasmic reticulum. *Journal of biological chemistry, 284*(24), 16082-16089.

Ayaub, E. A., Kolb, P. S., Mohammed-Ali, Z., Tat, V., Murphy, J., Bellaye, P. S., ... & Lhoták, Š. (2016). GRP78 and CHOP modulate macrophage apoptosis and the development of bleomycin-induced pulmonary fibrosis. *The journal of pathology*, *239*(4), 411-425.

Binai N., O'Reilly S., Griffiths B., van Laar J. M., Hugle T. (2012). Differentiation potential of CD14+ monocytes into myofibroblasts in patients with systemic sclerosis. *PLoS ONE* 7:e33508 10.1371/journal.pone.0033508.

Briken, V., & Mosser, D. M. (2011). Editorial: switching on arginase in M2 macrophages. *Journal of leukocyte biology, 90*(5), 839-841.

Burnham, E. L., Janssen, W. J., Riches, D. W., Moss, M., & Downey, G. P. (2014). The fibroproliferative response in acute respiratory distress syndrome: mechanisms and clinical significance. *European respiratory journal, 43*(1), 276-285.

Byrne, A. J., Maher, T. M., & Lloyd, C. M. (2016). Pulmonary macrophages: a new therapeutic pathway in fibrosing lung disease?. *Trends in molecular medicine*, *22*(4), 303-316.

Camp, R. L., Charette, L. A., & Rimm, D. L. (2000). Validation of tissue microarray technology in breast carcinoma. *Laboratory investigation*, *80*(12), 1943-1949.

Chanput, W., Mes, J. J., Savelkoul, H. F., & Wichers, H. J. (2013). Characterization of polarized THP-1 macrophages and polarizing ability of LPS and food compounds. *Food & function, 4*(2), 266-276.

Chanput, W., Mes, J. J., Savelkoul, H. F., & Wichers, H. J. (2013). Characterization of polarized THP-1 macrophages and polarizing ability of LPS and food compounds. *Food & function, 4*(2), 266-276.

Chang, Y., De Nadai, P., Azzaoui, I., Morales, O., Delhem, N., Vorng, H., ... & Chenivesse, C. (2010). The chemokine CCL18 generates adaptive regulatory T cells from memory CD4+ T cells of healthy but not allergic subjects. *The FASEB journal, 24*(12), 5063-5072.

Chen, K., & Kolls, J. K. (2013). T cell–mediated host immune defenses in the lung. *Annual review of immunology*, *31*, 605-633.

Collard, H. R., Moore, B. B., Flaherty, K. R., Brown, K. K., Kaner, R. J., King Jr, T. E., ... & Raghu, G. (2007). Acute exacerbations of idiopathic pulmonary fibrosis. *American journal of respiratory and critical care medicine*, *176*(7), 636-643.

Cottin, V. & Cordier, J.F. (2012). ACR practice guideline for HRCT in adults 2009. Available at www.acr.org. *European Respiratory Journal;40*(3):519-521.

Cross, B. C., Bond, P. J., Sadowski, P. G., Jha, B. K., Zak, J., Goodman, J. M., ... & Harding, H. P. (2012). The molecular basis for selective inhibition of unconventional mRNA splicing by an IRE1-binding small molecule. *Proceedings of the National Academy of Sciences, 109*(15), E869-E878.

Darby, I. A., Laverdet, B., Bonté, F., & Desmoulière, A. (2014). Fibroblasts and myofibroblasts in wound healing. *Clinical, cosmetic and investigational dermatology*, (*7)*, 301.

Davidson, R. (2013). Idiopathic pulmonary Fibrosis: A patient's guide. Retrieved from http://www.canadianpulmonaryfibrosis.ca/wordpress/wp-content/uploads/2013/02/IPF_Guide_2012_Final.pdf.

Fazio, E. N., & Lajoie, P. (2015). Endoplasmic Reticulum Homeostasis in Huntington's Disease. *Austin Journal of Anatomy*, *1*(5), 1025th ser. Retrieved June 2, 2017, from http://austinpublishinggroup.com/anatomy/fulltext/Anatomy-v1-id1025.php

Ferrante, C. J., & Leibovich, S. J. (2012). Regulation of macrophage polarization and wound healing. *Advances in wound care*, *1*(1), 10-16.

Fischer, A., & du Bois, R. (2012). Interstitial lung disease in connective tissue disorders. *The Lancet*, *380*(9842), 689-698.

Flaherty, K. R., Colby, T. V., Travis, W. D., Toews, G. B., Mumford, J., Murray, S., ... & Martinez, F. J. (2003). Fibroblastic foci in usual interstitial pneumonia: idiopathic versus collagen vascular disease. *American journal of respiratory and critical care medicine, 167*(10), 1410-1415.

Genin, M., Clement, F., Fattaccioli, A., Raes, M., & Michiels, C. (2015). M1 and M2 macrophages derived from THP-1 cells differentially modulate the response of cancer cells to etoposide. *BMC cancer, 15*(1), 577.

Ginhoux, F., & Jung, S. (2014). Monocytes and macrophages: developmental pathways and tissue homeostasis. *Nature Reviews Immunology*, *14*(6), 392-404.

Gibbons, M. A., MacKinnon, A. C., Ramachandran, P., Dhaliwal, K., Duffin, R., Phythian-Adams, A. T., ... & Hirani, N. (2011). Ly6Chi monocytes direct alternatively activated profibrotic macrophage regulation of lung fibrosis. *American journal of respiratory and critical care medicine, 184*(5), 569-581.

Gordon, S. (2003). Alternative activation of macrophages. *Nature reviews immunology*, *3*(1), 23-35.

Groenendyk, J., Lee, D., Jung, J., Dyck, J. R., Lopaschuk, G. D., Agellon, L. B., & Michalak, M. (2016). Inhibition of the unfolded protein response mechanism prevents cardiac fibrosis. *PloS one, 11*(7), e0159682.

Hetz, C. (2012). The unfolded protein response: controlling cell fate decisions under ER stress and beyond. *Nature reviews molecular cell biology,13*(2), 89-102.

Hunninghake, G. W., Zimmerman, M. B., Schwartz, D. A., KING JR, T. E., Lynch, J., Hegele, R., ... & Galvin, J. (2001). Utility of a lung biopsy for the diagnosis of idiopathic pulmonary fibrosis. *American journal of respiratory and critical care medicine, 164*(2), 193-196.

Hyzy, R., Huang, S., Myers, J., Flaherty, K., & Martinez, F. (2007). Acute exacerbation of idiopathic pulmonary fibrosis. *CHEST Journal*, *132*(5), 1652-1658.

Idiopathic Pulmonary Fibrosis Clinical Research Network. (2012). Prednisone, azathioprine, and N-acetylcysteine for pulmonary fibrosis. *New England Journal Medicine*, *2012*(366), 1968-1977.

Italiani, P., & Boraschi, D. (2014). From monocytes to M1/M2 macrophages: phenotypical vs. functional differentiation. *Frontiers in immunology*, *5*.

Inomata, M., Nishioka, Y., & Azuma, A. (2015). Nintedanib: evidence for its therapeutic potential in idiopathic pulmonary fibrosis. *Core evidence, 10*, 89.

Jackson, D. A., & Elsawa, S. F. (2015). Factors regulating immunoglobulin production by normal and disease-associated plasma cells. *Biomolecules*, *5*(1), 20-40.

Janeway CA Jr, Travers P, Walport M, et al. Immunobiology: The Immune System in Health and Disease. 5th edition. New York: Garland Science; 2001. Available from: https://www.ncbi.nlm.nih.gov/books/NBK10757/.

Jiang, D., Niwa, M., & Koong, A. C. (2015). Targeting the IRE1α-XBP1 Branch of the Unfolded Protein Response in Human Diseases. *Seminars in Cancer Biology*, *33*, 48–56. http://doi.org/10.1016/j.semcancer.2015.04.010.

Kallioniemi, O. P., Wagner, U., Kononen, J., & Sauter, G. (2001). Tissue microarray technology for high-throughput molecular profiling of cancer. *Human molecular genetics, 10*(7), 657-662.

Kharraz, Y., Guerra, J., Pessina, P., Serrano, A. L., & Muñoz-Cánoves, P. (2014). Understanding the process of fibrosis in Duchenne muscular dystrophy. *BioMed research international*, *2014*.

Kim, M. G., Kim, S. C., Ko, Y. S., Lee, H. Y., Jo, S. K., & Cho, W. (2015). The role of M2 macrophages in the progression of chronic kidney disease following acute kidney injury. *PLoS One, 10*(12), e0143961.

Kozutsumi, Y., Normington, K., Press, E., Slaughter, C., Sambrook, J., & Gething, M. J. (1989). Identification of immunoglobulin heavy chain binding protein as glucose-regulated protein 78 on the basis of amino acid sequence, immunological cross-reactivity, and functional activity. *Journal of Cell Science. Supplement, 11*, *115–137.*

Kuhn, C., & McDonald, J. A. (1991). The roles of the myofibroblast in idiopathic pulmonary fibrosis. Ultrastructural and immunohistochemical features of sites of active extracellular matrix synthesis. *The American journal of pathology*, *138*(5), 1257.

Kulkarni, M. M. (2011). Digital multiplexed gene expression analysis using the NanoString nCounter system. *Current protocols in molecular biology, 25*B-10.

Lech, M., & Anders, H. J. (2013). Macrophages and fibrosis: How resident and infiltrating mononuclear phagocytes orchestrate all phases of tissue injury and repair. *Biochimica et biophysica acta (BBA)-molecular basis of disease*, 1832(7), 989-997.

Lehtonen, S. T., Veijola, A., Karvonen, H., Lappi-Blanco, E., Sormunen, R., Korpela, S., ... & Kaarteenaho, R. (2016). Pirfenidone and nintedanib modulate properties of fibroblasts and myofibroblasts in idiopathic pulmonary fibrosis. *Respiratory research*, *17*(1), 14.

Ley, B., Collard, H. R., & King Jr, T. E. (2011). Clinical course and prediction of survival in idiopathic pulmonary fibrosis. *American journal of respiratory and critical care medicine*, *183*(4), 431-440.

Luu, K., Greenhill, C. J., Majoros, A., Decker, T., Jenkins, B. J., & Mansell, A. (2014). STAT1 plays a role in TLR signal transduction and inflammatory responses. *Immunology and cell biology*, *92*(9), 761-769.

Luzina, I. G., Tsymbalyuk, N., Choi, J., Hasday, J. D., & Atamas, S. P. (2006). CCL18-stimulated upregulation of collagen production in lung fibroblasts requires Sp1 signaling and basal Smad3 activity. *Journal of cellular physiology*, *206*(1), 221-228.

Lynch III, J. P., White, E., & Flaherty, K. (2001). Corticosteroids in idiopathic pulmonary fibrosis. *Current opinion in pulmonary medicine, 7(*5), 298-308.

Mauer, J., Chaurasia, B., Goldau, J., Vogt, M. C., Ruud, J., Nguyen, K. D., ... & Estevez, E. (2014). Signaling by IL-6 promotes alternative activation of macrophages to limit endotoxemia and obesity-associated resistance to insulin. *Nature immunology, 15*(5), 423-430.

Martinez, J. A. B. (2003). Mortality by idiopathic pulmonary fibrosis. *Jornal de Pneumologia*, *29*(3), 119-120.

Martinez, F. O., Helming, L., & Gordon, S. (2009). Alternative activation of macrophages: an immunologic functional perspective. *Annual review of immunology, 27*, 451-483.

Mazur, A., Holthoff, E., Vadali, S., Kelly, T., & Post, S. R. (2016). Cleavage of type I collagen by fibroblast activation protein-α enhances class A scavenger receptor mediated macrophage adhesion. *PloS ONE, 11*(3), e0150287.

Mimura, N., Fulciniti, M., Gorgun, G., Tai, Y. T., Cirstea, D., Santo, L., ... & Kiziltepe, T. (2012). Blockade of XBP1 splicing by inhibition of IRE1α is a promising therapeutic option in multiple myeloma. *Blood*, *119*(24), 5772-5781.

Moeller, A., Ask, K., Warburton, D., Gauldie, J., & Kolb, M. (2008). The bleomycin animal model: a useful tool to investigate treatment options for idiopathic pulmonary fibrosis? *The international journal of biochemistry & cell biology, 40(*3), 362–382. http://doi.org/10.1016/j.biocel.2007.08.011.

Moeller, A., Gilpin, S. E., Ask, K., Cox, G., Cook, D., Gauldie, J., ... & O'byrne, P. M. (2009). Circulating fibrocytes are an indicator of poor prognosis in idiopathic pulmonary fibrosis. *American journal of respiratory and critical care medicine, 179*(7), 588-594.

Murray, P.J., and Wynn, T.A. (2011). Protective and pathogenic functions of macrophage subsets. *Nature Review Immunology 11*, 723–737.

Newton, K., & Dixit, V. M. (2012). Signaling in innate immunity and inflammation. *Cold Spring Harbor perspectives in biology*, *4*(3), a006049.

Papiris, S. A., Kagouridis, K., Kolilekas, L., Bouros, D., & Manali, E. D. (2014). Idiopathic pulmonary fibrosis acute exacerbations: where are we now?.

Park, E. K., Jung, H. S., Yang, H. I., Yoo, M. C., Kim, C., & Kim, K. S. (2007). Optimized THP-1 differentiation is required for the detection of responses to weak stimuli. *Inflammation research, 56*(1), 45-50.

Pechkovsky DV, Prasse A, Kollert F, Engel KM, Dentler J, Luttmann W, Friedrich K, Muller-Quernheim J, Zissel G: Alternatively activated alveolar macrophages in

pulmonary fibrosis-mediator production and intracellular signal transduction. *Clinical Immunology* 2010, 137:89-101.

Ploeger, D. T., Hosper, N. A., Schipper, M., Koerts, J. A., de Rond, S., & Bank, R. A. (2013). Cell plasticity in wound healing: paracrine factors of M1/M2 polarized macrophages influence the phenotypical state of dermal fibroblasts. *Cell Communication and signaling, 11*(1), 1.

Prasse, A., Pechkovsky, D. V., Toews, G. B., Jungraithmayr, W., Kollert, F., Goldmann, T., ... & Zissel, G. (2006). A vicious circle of alveolar macrophages and fibroblasts perpetuates pulmonary fibrosis via CCL18. *American journal of respiratory and critical care medicine*, *173*(7), 781-792.

Raghu, G., Weycker, D., Edelsberg, J., Bradford, W. Z., & Oster, G. (2006). Incidence and prevalence of idiopathic pulmonary fibrosis. *American journal of respiratory and critical care medicine*, *174*(7), 810-816.

Reimold, A.M., N.N. Iwakoshi, J. Manis, P. Vallabhajosyula, E. Szomolanyi- Tsuda, E.M. Gravallese, D. Friend, M.J. Grusby, F. Alt, and L.H. Glimcher. 2001. Plasma cell differentiation requires the transcription fac- tor XBP-1. *Nature. 412*:300–307. doi:10.1038/35085509.

Richeldi, L., Davies, H. R. H., Spagnolo, P., & Luppi, F. (2003). Corticosteroids for idiopathic pulmonary fibrosis. *The Cochrane Library.*

Richeldi, L., du Bois, R. M., Raghu, G., Azuma, A., Brown, K. K., Costabel, U., ... & Kim, D. S. (2014). Efficacy and safety of nintedanib in idiopathic pulmonary fibrosis. *New england journal of medicine*, 370(22), 2071-2082.

Robinson, C. M., Watson, C. J., & Baugh, J. A. (2012). Epigenetics within the matrix: A neo-regulator of fibrotic disease. *Epigenetics*, *7*(9), 987–993. http://doi.org/10.4161/epi.21567.

Rőszer, T. (2015). Understanding the mysterious M2 macrophage through activation markers and effector mechanisms. *Mediators of inflammation*. Article ID 816460, 16 pages, 2015. doi:10.1155/2015/816460.

Selman, M., King, T. E., & Pardo, A. (2001). Idiopathic pulmonary fibrosis: prevailing and evolving hypotheses about its pathogenesis and implications for therapy. *Annals of internal medicine*, *134*(2), 136-151.

Selman, M., Pardo, A., Barrera, L., Estrada, A., Watson, S. R., Wilson, K., ... & Zlotnik, A. (2006). Gene expression profiles distinguish idiopathic pulmonary fibrosis from hypersensitivity pneumonitis. *American journal of respiratory and critical care medicine*, *173*(2), 188-198.

Schraufstatter, I. U., Zhao, M., Khaldoyanidi, S. K., & DiScipio, R. G. (2012). The chemokine CCL18 causes maturation of cultured monocytes to macrophages in the M2 spectrum. *Immunology, 135*(4), 287-298.

Schutyser, E., Richmond, A., & Van Damme, J. (2005). Involvement of CC chemokine ligand 18 (CCL18) in normal and pathological processes. *Journal of leukocyte biology, 78*(1), 14-26.

Schupp, J. C., Binder, H., Jäger, B., Cillis, G., Zissel, G., Müller-Quernheim, J., & Prasse, A. (2015). Macrophage activation in acute exacerbation of idiopathic pulmonary fibrosis. *PloS ONE, 10*(1), e0116775.

Schwarz MI & King TE. (1988). Interstitial lung disease. Philadelphia, PA: BC Decker Inc.; 350 p.

Sica, A., Schioppa, T., Mantovani, A., & Allavena, P. (2006). Tumour-associated macrophages are a distinct M2 polarised population promoting tumour progression: potential targets of anti-cancer therapy. *European journal of cancer*, *42*(6), 717-727.

Sriburi, R., S. Jackowski, K. Mori, and J.W. Brewer. 2004. XBP1: a link be- tween the unfolded protein response, lipid biosynthesis, and biogenesis of the endoplasmic reticulum. *Journal Cell Biololgy 167*:35–41. doi:10.1083/ jcb.200406136.

Taniguchi, H., Ebina, M., Kondoh, Y., Ogura, T., Azuma, A., Suga, M., ... & Takeuchi, M. (2010). Pirfenidone in idiopathic pulmonary fibrosis. *European Respiratory Journal, 35*(4), 821-829.

Todd, D. J., McHeyzer-Williams, L. J., Kowal, C., Lee, A. H., Volpe, B. T., Diamond, B., ... & Glimcher, L. H. (2009). XBP1 governs late events in plasma cell differentiation and is not required for antigen-specific memory B cell development. *Journal of Experimental Medicine, 206*(10), 2151-2159.

Tomos, I., Manali, E., Karakatsani, A., Spathis, A., Korbila, I., Analitis, A., ... & Papiris, S. (2016). IL-6 and IL-8 in stable and exacerbated IPF patients and their association to outcome. *European respiratory journal. 48* (60) DOI: 10.1183/13993003.congress-2016.PA3890.

van Furth, R. & Cohn, Z.A. (1968). The origin and kinetics of mononuclear phagocytes. *Journal Experimental Medicine*.128, 415–435.

Wang, N., Liang, H., & Zen, K. (2014). Molecular Mechanisms That Influence the Macrophage M1–M2 Polarization Balance. *Frontiers in immunology, 5,* 614. http://doi.org/10.3389/fimmu.2014.00614.

Wei J, Rahman S, Ayaub EA, Dickhout JG, Ask K: Protein misfolding and endoplasmic reticulum stress in chronic lung disease. *Chest 2013, 143*:1098-105.

Welch, W. J. (1992). Mammalian stress response: cell physiology, structure/function of stress proteins, and implications for medicine and disease. *Physiological reviews, 72*(4), 1063-1081.

Woehlbier, U., & Hetz, C. (2011). Modulating stress responses by the UPRosome: a matter of life and death. *Trends in biochemical sciences, 36*(6), 329-337.

Wollenberg, A., Oppel, T., Schottdorf, E. M., Günther, S., Moderer, M., & Mommaas, M. (2002). Expression and function of the mannose receptor CD206 on epidermal dendritic cells in inflammatory skin diseases. *Journal of Investigative Dermatology*, *118*(2), 327-334.

Wollin, L., Wex, E., Pautsch, A., Schnapp, G., Hostettler, K. E., Stowasser, S., & Kolb, M. (2015). Mode of action of nintedanib in the treatment of idiopathic pulmonary fibrosis. *European Respiratory Journal*, ERJ-01749-2014; doi:10.1183/09031936.00174914.

Wu, R., Zhang, Q.-H., Lu, Y.-J., Ren, K., & Yi, G.-H. (2015). Involvement of the IRE1α-XBP1 Pathway and XBP1s-Dependent Transcriptional Reprogramming in Metabolic Diseases. *DNA and Cell Biology*, *34*(1), 6–18. http://doi.org/10.1089/dna.2014.2552.

Wuyts, W. A., Cavazza, A., Rossi, G., Bonella, F., Sverzellati, N., & Spagnolo, P. (2014). Differential diagnosis of usual interstitial pneumonia: when is it truly idiopathic?. *European Respiratory Review*,*23*(133), 308-319.

Wynn, T. A., & Vannella, K. M. (2016). Macrophages in tissue repair, regeneration, and fibrosis. *Immunity*, *44*(3), 450-462.

Zhan, K., Vattem, K. M., Bauer, B. N., Dever, T. E., Chen, J.-J., & Wek, R. C. (2002). Phosphorylation of Eukaryotic Initiation Factor 2 by Heme-Regulated Inhibitor Kinase-Related Protein Kinases in *Schizosaccharomyces pombe* Is Important for Resistance to Environmental Stresses. *Molecular and Cellular Biology*, *22*(20), 7134–7146. http://doi.org/10.1128/MCB.22.20.7134-7146.2002.

Zhu, Z., Ding, J., Ma, Z., Iwashina, T., & Tredget, E. E. (2017). Alternatively activated macrophages derived from THP- 1 cells promote the fibrogenic activities of human dermal fibroblasts. *Wound Repair and Regeneration.* doi:10.1111/wrr. 12532.

CHAPTER 6. FIGURES

Figure 6: Tissue microarray construction to allow for high throughput screening.

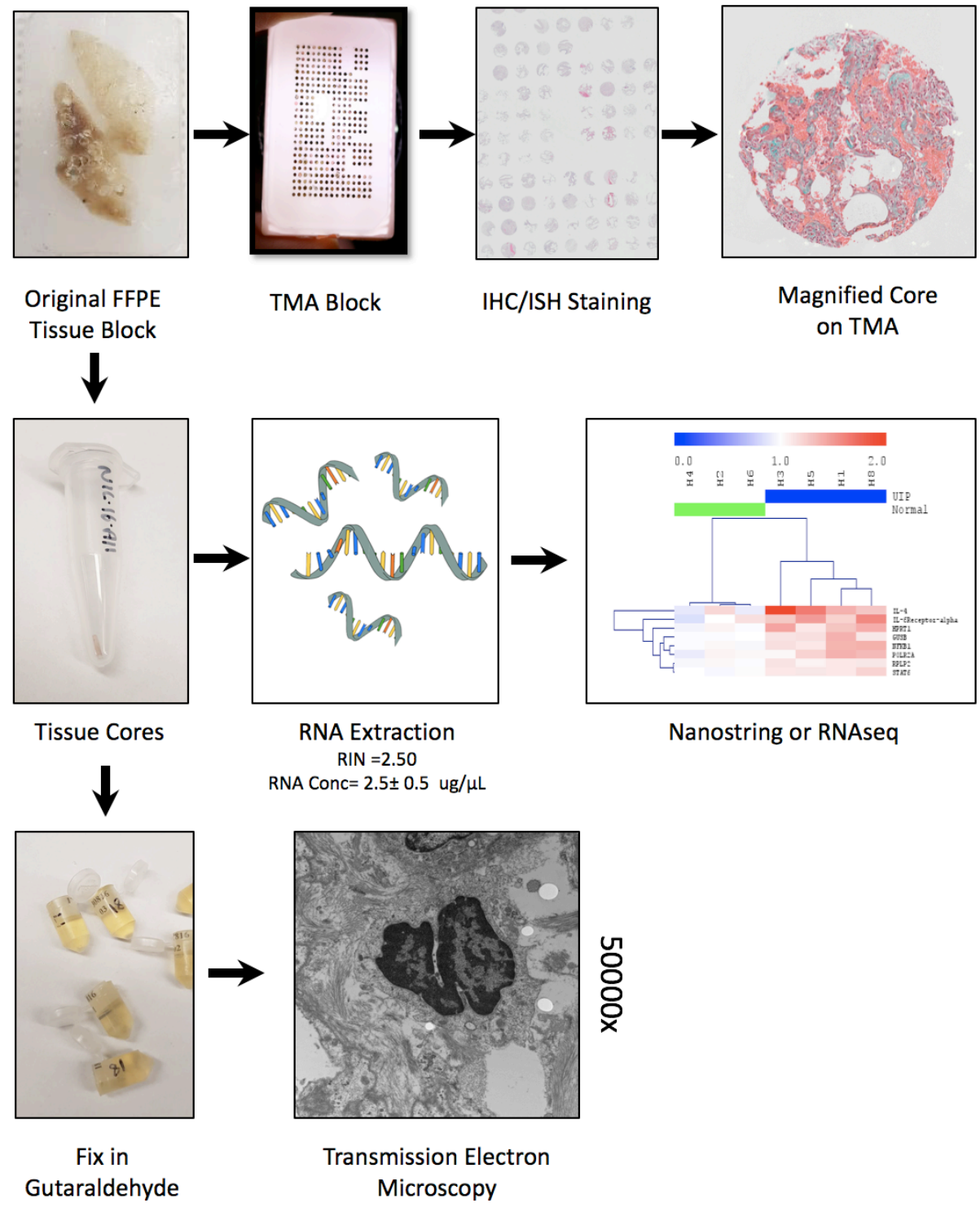

Figure 6: Construction of a TMA block begins by selecting formalin fixed paraffin embedded blocks. An original FFPE tissue block was cored out, and these cores were put into a donor block. In total 360 cores, 0.6 mm in size, were taken from a total of twenty-four IPF patients and seventeen control subjects. Four cores were taken from each specified area. Fibrotic areas in IPF patients were determined with the help of a trained molecular pathologist by selecting areas of increased fibroblastic foci, parenchymal thickening, and angiogenesis. A slide was cut from the TMA block and stained, with each individual core being magnified allowing for the quantification of staining through image analysis program ImageJ.

Additional 1mm cores were taken from the original FFPE tissue blocks for RNA extraction or Transmission Electron Microscopy. RNAseq and TEM, was designed for target validation, that could help in identification of genes or cells that were important in the progression of IPF patients.

Figure 7: Target Identification of CD206 expression in IPF patients as assessed through TMA staining

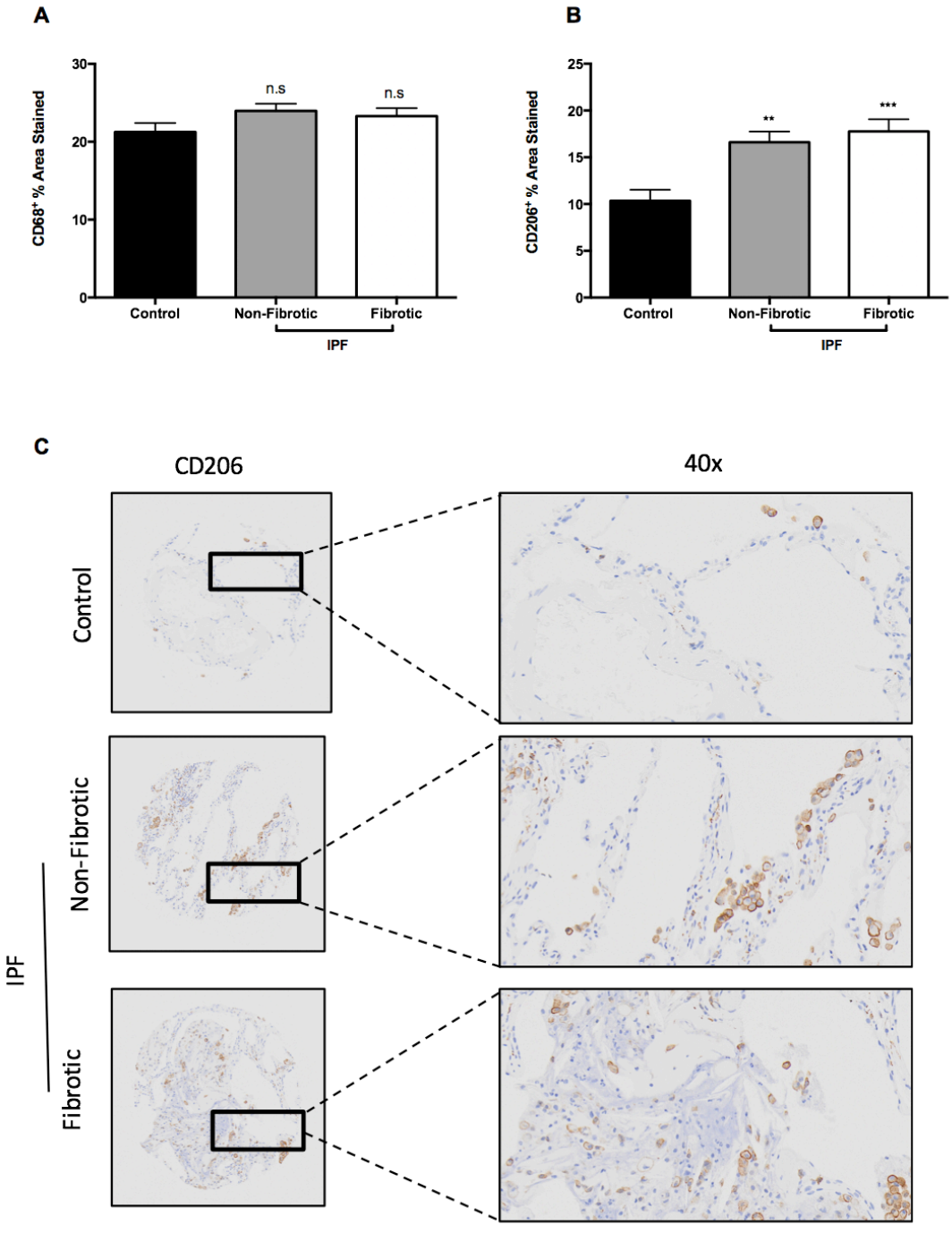

Figure 7. TMA slides were used to compare the relative expression of CD68 and CD206 in IPF and control cohorts. There was no relative increase in the amount of CD68 in IPF patients versus control patients (*A*). However, there was an increase in the amount of CD206 in fibrotic and non-fibrotic areas of IPF patients versus control patients (*B and C*).

Figure 8: Target Identification of UPR proteins GRP78 and FKBP13 in IPF patients as assessed through TMA staining

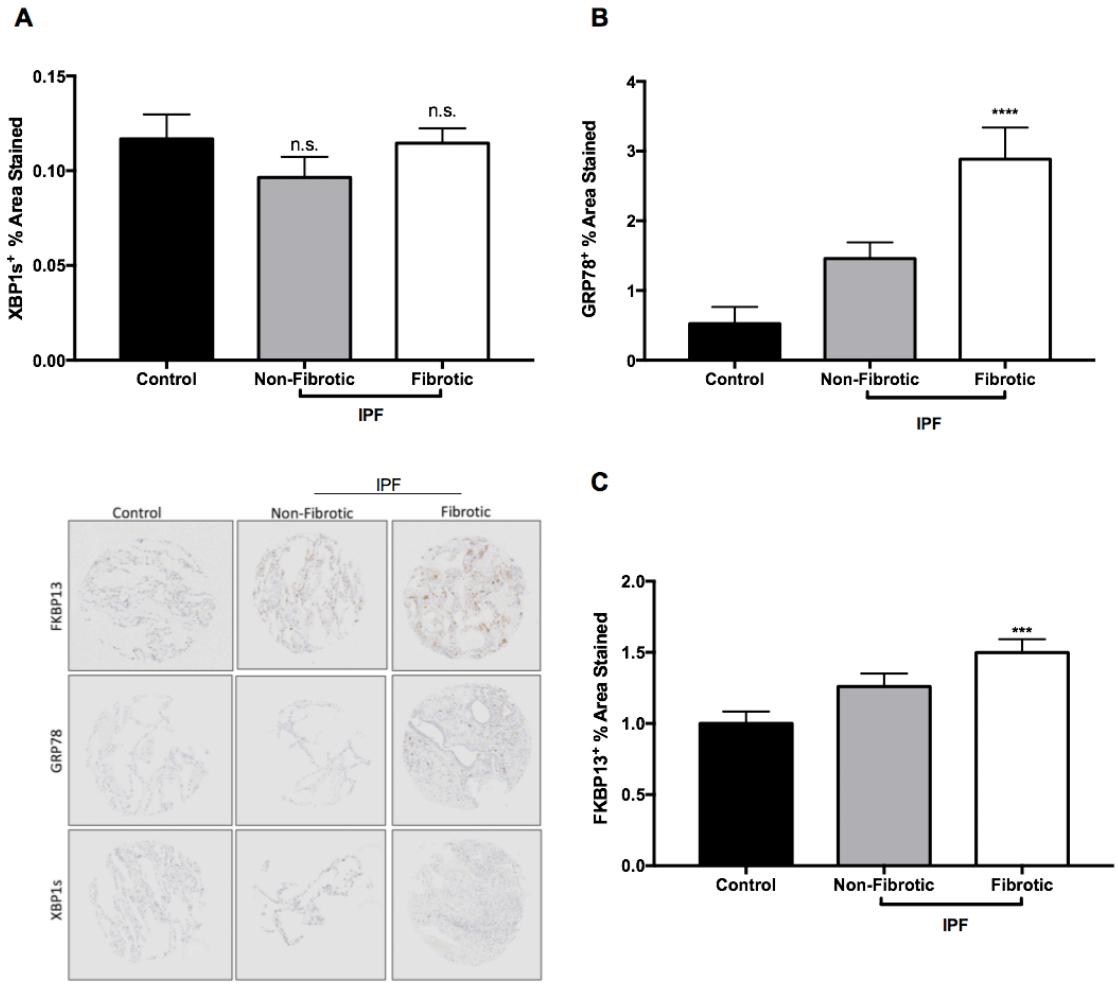

Figure 8: TMA slides were used to examine the expression of Endoplasmic Reticulum associated proteins XBP1s, GRP78, and FKBP13 in the lungs of patients with IPF. There was little staining of XBP1s in IPF lungs which was not significantly different than control patients *(A*). Calculation of FKBP13 and GRP78 staining was optimized to detect for intracellular staining. Patient-derived fibrotic lung sections from IPF patients had higher detected levels of expression of FKBP13 and GRP78 than in control patients (*B and C*).

Figure 9: Enlarged Endoplasmic Reticulum of Immune Cells in IPF patients versus Control Subjects.

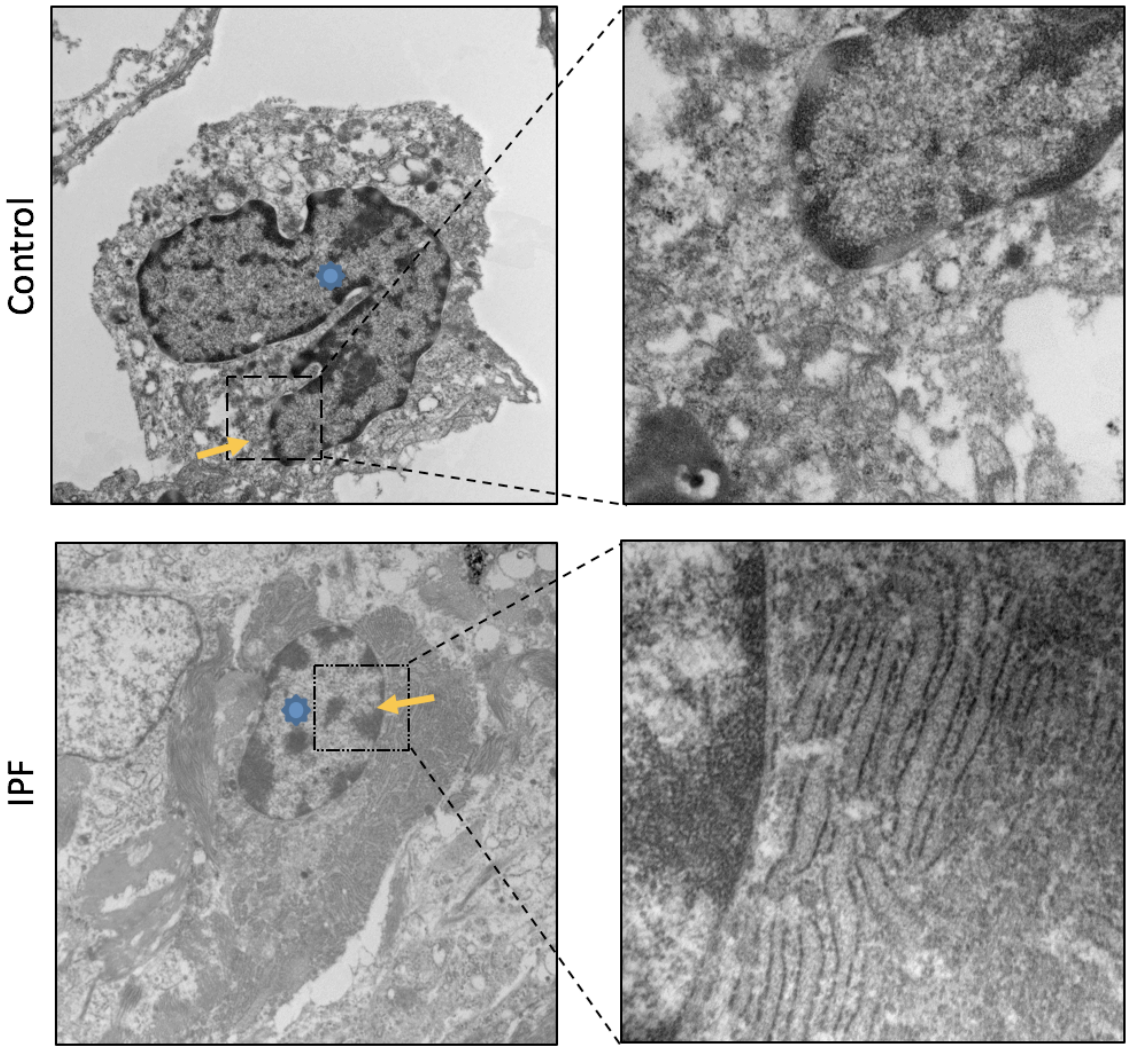

Figure 9: FFPE tissue lung biopsies were fixed in gluteraldehyde for TEM. The blue star denotes the nucleus, while the gold arrow shows the endoplasmic reticulum. Image represent a macrophage-like cells in both IPF and control subjects (n=5 cells). Work was done with the help of Dr. Jeffery Dickhout at McMaster University.

Figure 10: Identifying cytokine secretions of polarized THP-1 macrophages

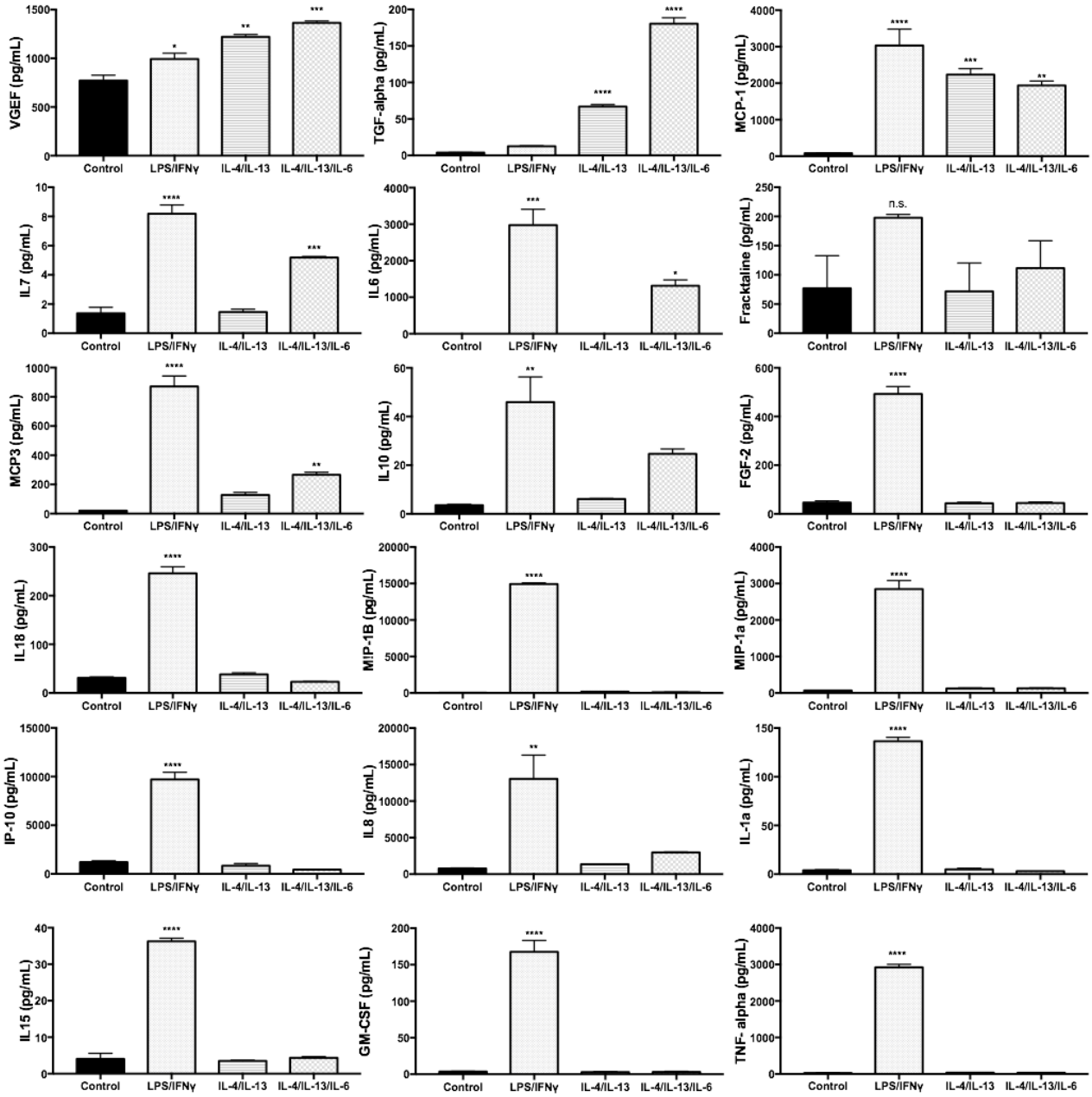

Figure 10: THP-1 macrophages were polarized for 72 hrs. to their respective phenotypes and cytokine secretions were analyzed by EVE Technologies. IL-6 addition to IL-4/IL-13 treatment enhances VGEF and TGF-α secretion. LPS/IFNγ stimulated macrophages augment cells to produce inflammatory cytokines such as TNFα and IL-10. Cell experiments were executed in 96-well plates with 3 biological replicates per condition. Data is presented as mean ± SEM. Statistical analysis used a ANOVA test with a post hoc Dunnet's comparison.

Figure 11: Baseline Serum Concentrations in IPF and Control Groups as compared to FVC

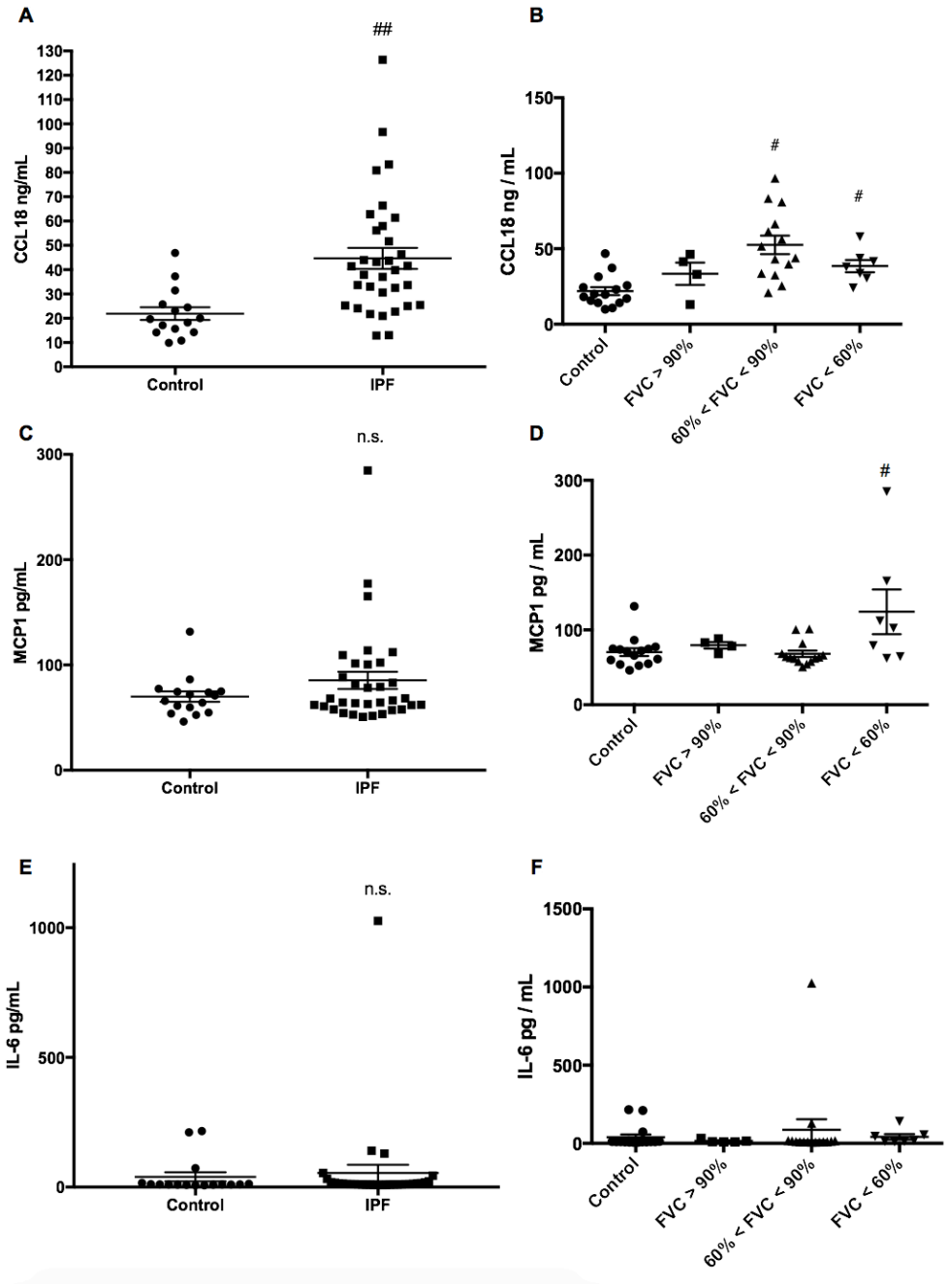

Figure 11: Serum was collected from thirty-two IPF patients and fifteen control patients. Serum concentrations from IPF patients were then compared to FVC. IPF patients had an increased presence of CCL18 in their serum (*A*). There was a negligible change in the amount of MCP1 and IL-6 (*C and E*). Patients with a FVC below 90% predicted had an increased concentration of CCL18 in their serum (*B*). MCP1 levels in IPF patients were significantly up regulated in patients with a FVC less than 60 (*C*). Data is presented as mean ± SEM. Statistical analysis used a Student's T-test or ANOVA test with a post hoc Dunnet's comparison. *Note*: Some IPF patients were missing FVC measurements.

Figure 12: IL-4/IL-13/IL-6 stimulated THP-1 macrophages show a significant induction of CCL18

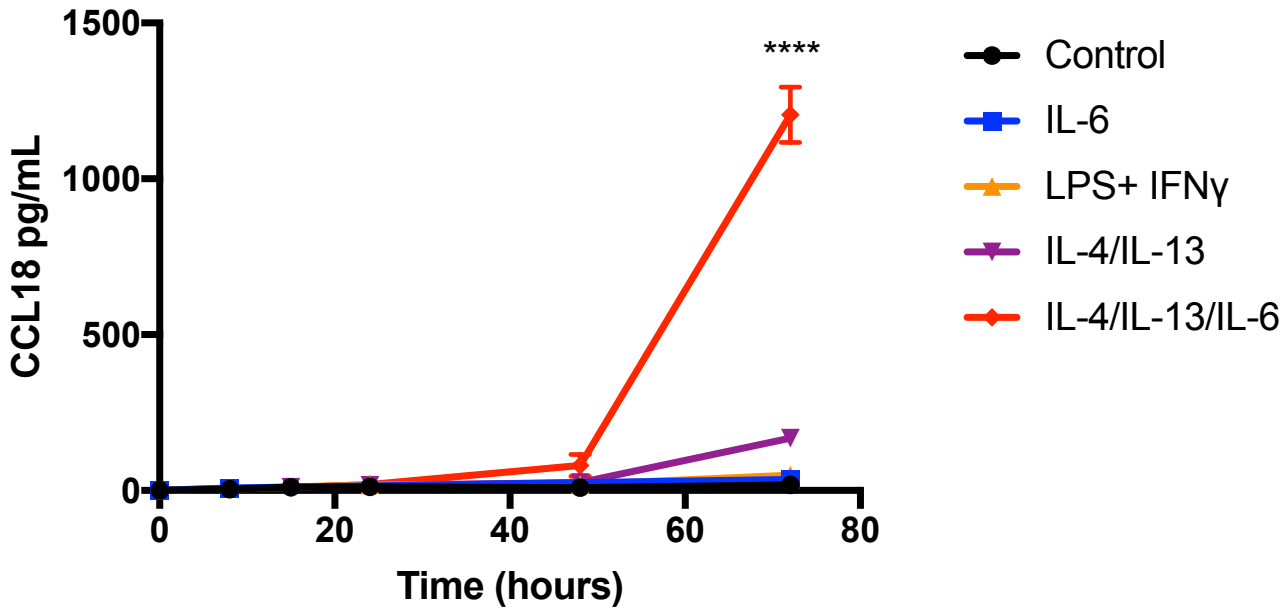

Figure 12: THP-1 monocytes were treated with PMA for 48 hours and then were stimulated to their respective phenotypes. Stimulated macrophages supernatant was collected and CCL18 secretion was measured at various time-points through ELISA measurements. IL-4/IL-13/IL-6 treated macrophages had an induction of CCL18 secretion at the 72-hour time point. Additionally, control polarized LPS/IFNγ and IL-6 stimulated THP-1 macrophages had a negligible secretion of CCL18. Data is presented as mean ± SEM. Cell experiments were executed in 96-well plates with 4 biological replicates per condition (n=3).

Figure 13: Transmission Electron Microscopy of polarized THP-1 macrophages show enhanced ER in IL-4/IL-13/IL-6 stimulated macrophages

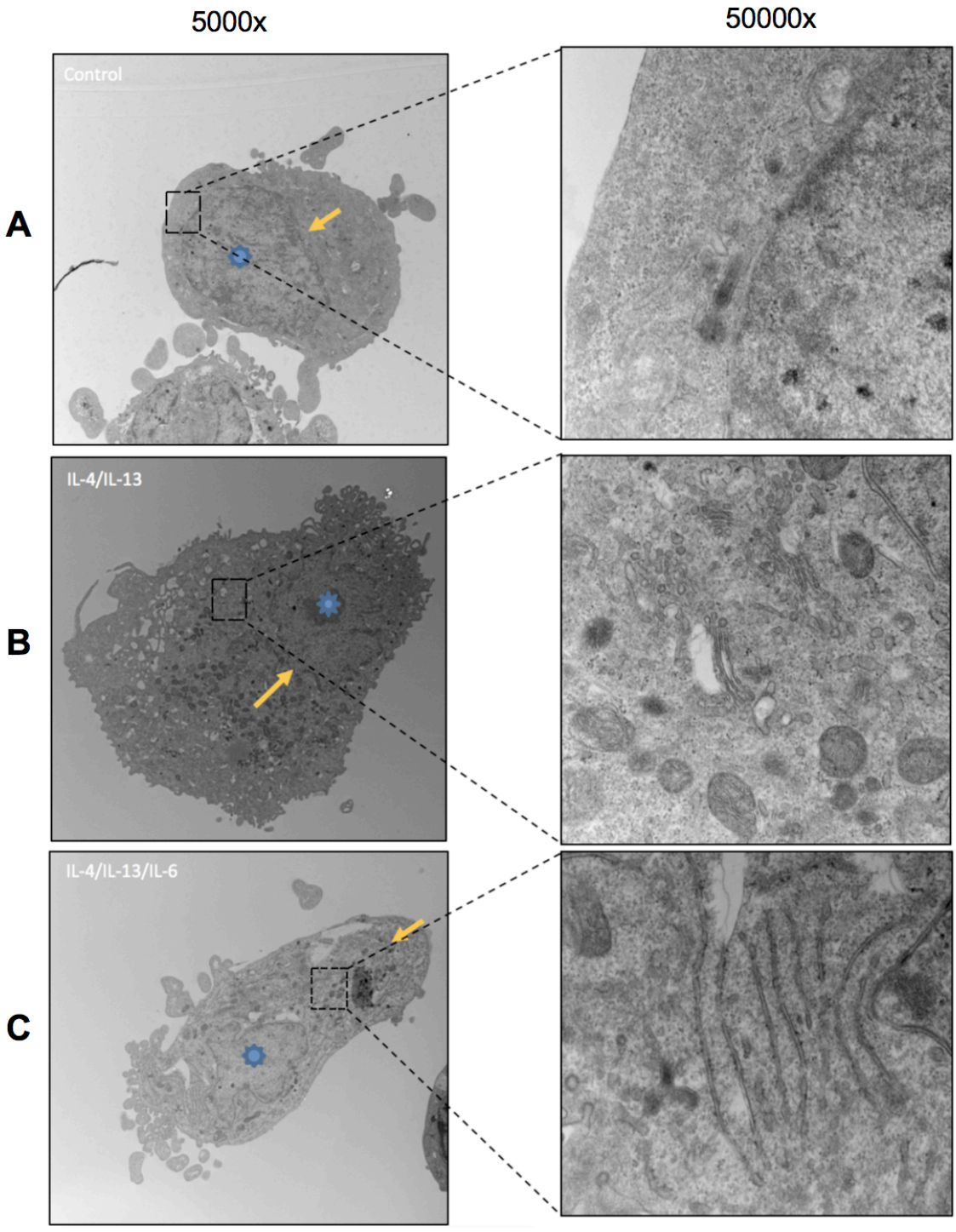

Figure 13: THP-1 macrophages were polarized with either control or IL-4/IL-13 or IL-4/IL-13/IL-6 media (*A, B, C respectively*). The blue star denotes the nucleus, while the gold arrow denotes the endoplasmic reticulum. IL-4/IL-13 macrophages show an increased ER versus control macrophages, however this induction is enhanced in IL-4/IL-13/IL-6 macrophages. Additionally, IL-4/IL-13/IL-6 macrophages show increased number of mitochondria (n=5 cells). Work was done with help of Dr. Jeffery Dickhout at McMaster University.

Figure 14: Investigating level of spliced XBP1 and ER expansion through IRE1 inhibitor treatment.

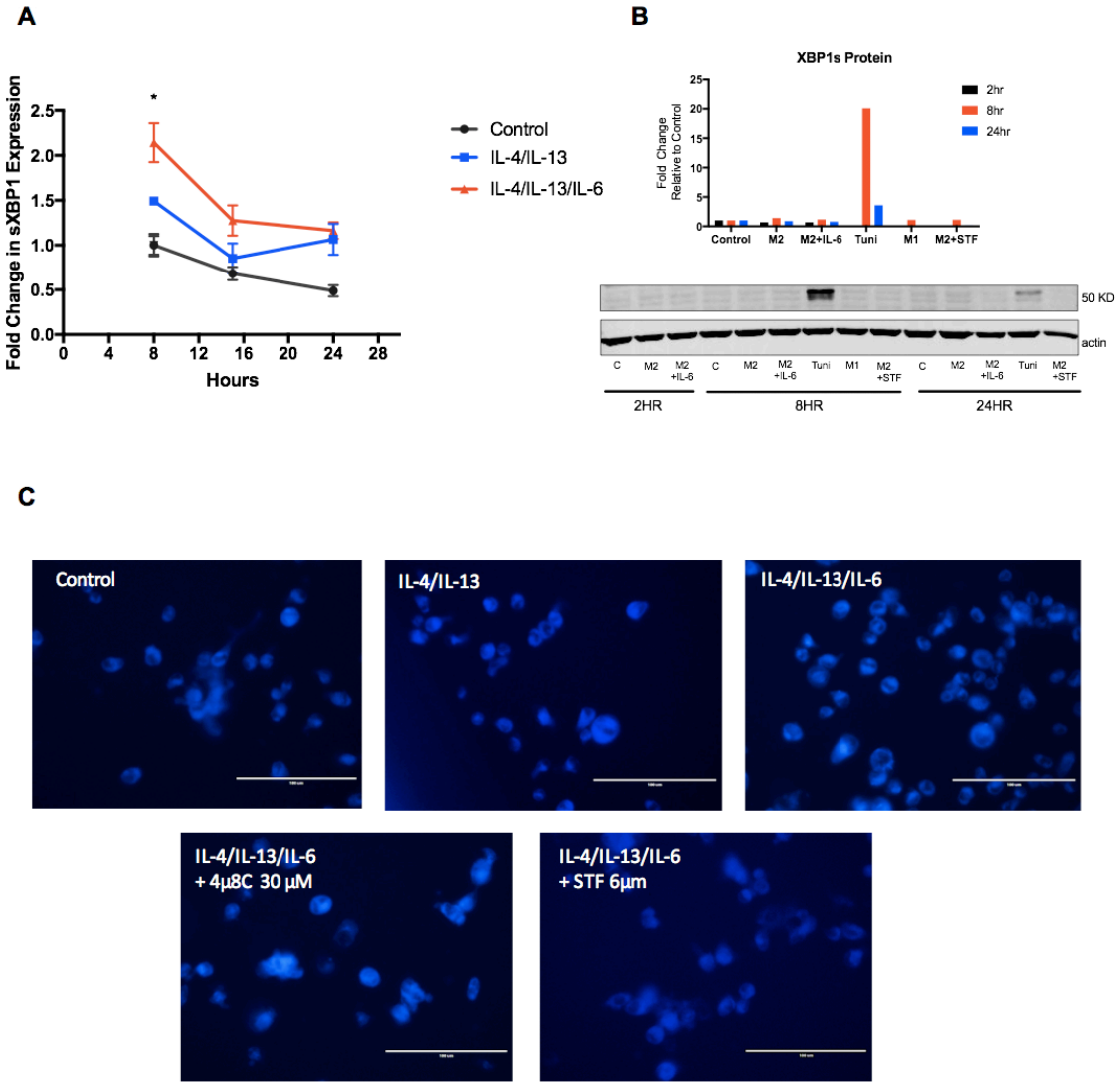

Figure 14: RNA expression of XBP1s in THP1 polarized macrophages at different time points was examined through rt-PCR. At the 8-hour time point there was an increased expression of XBP1s RNA (*A*). Western blot analysis was completed to show the relative expression of XBP1s at various time points. Tunicamycin (Tuni) treated macrophages were used as a positive control. Actin was used as a house keeping protein. STF-083010 was delivered at 6uM. No detectable band at 50KD was seen in XBP1s protein expression in IL-4/IL-13 or IL-4/IL-13/IL-6 stimulated macrophages (*B*). ER tracker dye was used to visually stain the endoplasmic reticulum of cells blue. IL-4/IL-13/IL-6 stimulated macrophages appear to have an enlarged ER as determined visually through fluorescence staining versus control or IL-4/IL-13 macrophages. This ER expansion in IL-4/IL-13/IL-6 stimulated macrophages was limited through the administration of 4μ8C and STF-083010 *(C)*. Data is presented as mean ± SEM.

Figure 15: Limiting the polarization of THP-1 macrophages with IRE1-XBP1 inhibitor STF-080310/4μ8C

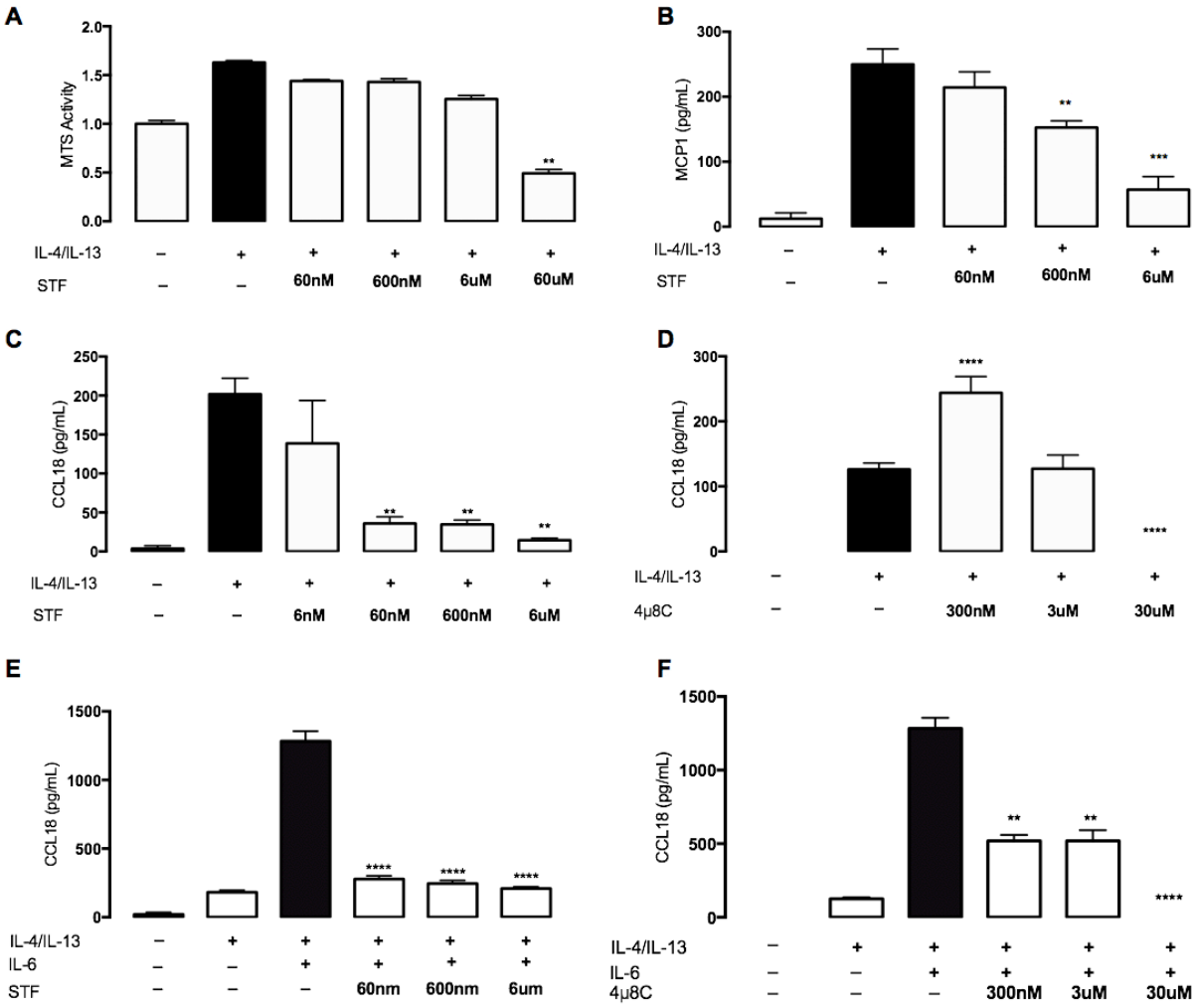

Figure 15: STF-083010 and 4μ8C were solubilized in DMSO, all cells received 0.12% DMSO vehicle per well. MTS metabolic assay was run to determine colorimetric quantification of viable cells by proliferation and cytotoxicity. THP-1 cells treated with STF-083010 show no difference in MTS activity below 6 μM (*A*). MCP1 and CCL18 were used to measure polarization of THP1 macrophages. STF-083010 reduced MCP1 secretion at 6um and 600nm and CCL18 secretion at 6uM, 600nM and 60nM (*B and C*). Another IRE1 inhibitor, 4μ8C, reduced CCL18 expression in IL-4/IL-13 stimulated macrophages (*D*). THP-1 macrophages were also polarized with IL-4/IL-13/IL-6. Here the inhibition with STF-083010 and 4μ8C significantly reduces CCL18 secretion (*E* and *F*). Cell experiments were executed in 96-well plates with 4 biological replicates per condition, and performed thrice. Data is presented as mean ± SEM. Statistical analysis used a ANOVA test with a post hoc Dunnet's comparison.

Figure 16: Increase in TGFβ secretion from alternatively activated THP-1 macrophages

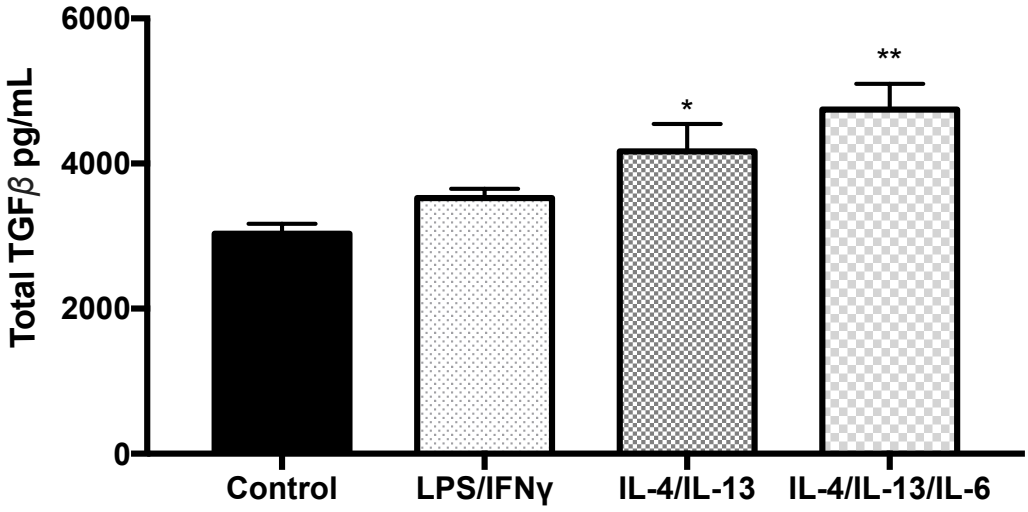

Figure 16: Assessing the level of TGFβ secretion by THP-1 macrophages, as assessed through ELISA. In the THP-1 macrophage system there was an increased secretion of TGFβ in IL-4/IL-13 and IL-4/IL-13/IL-6 macrophages. Cell experiments were done with 4 biological replicates per condition. Data is presented as mean ± SEM. Statistical analysis used a ANOVA test with a post hoc Dunnet's comparison.

Figure 18: αSMA expression after macrophage co-culture between primary fibrotic and healthy fibroblast

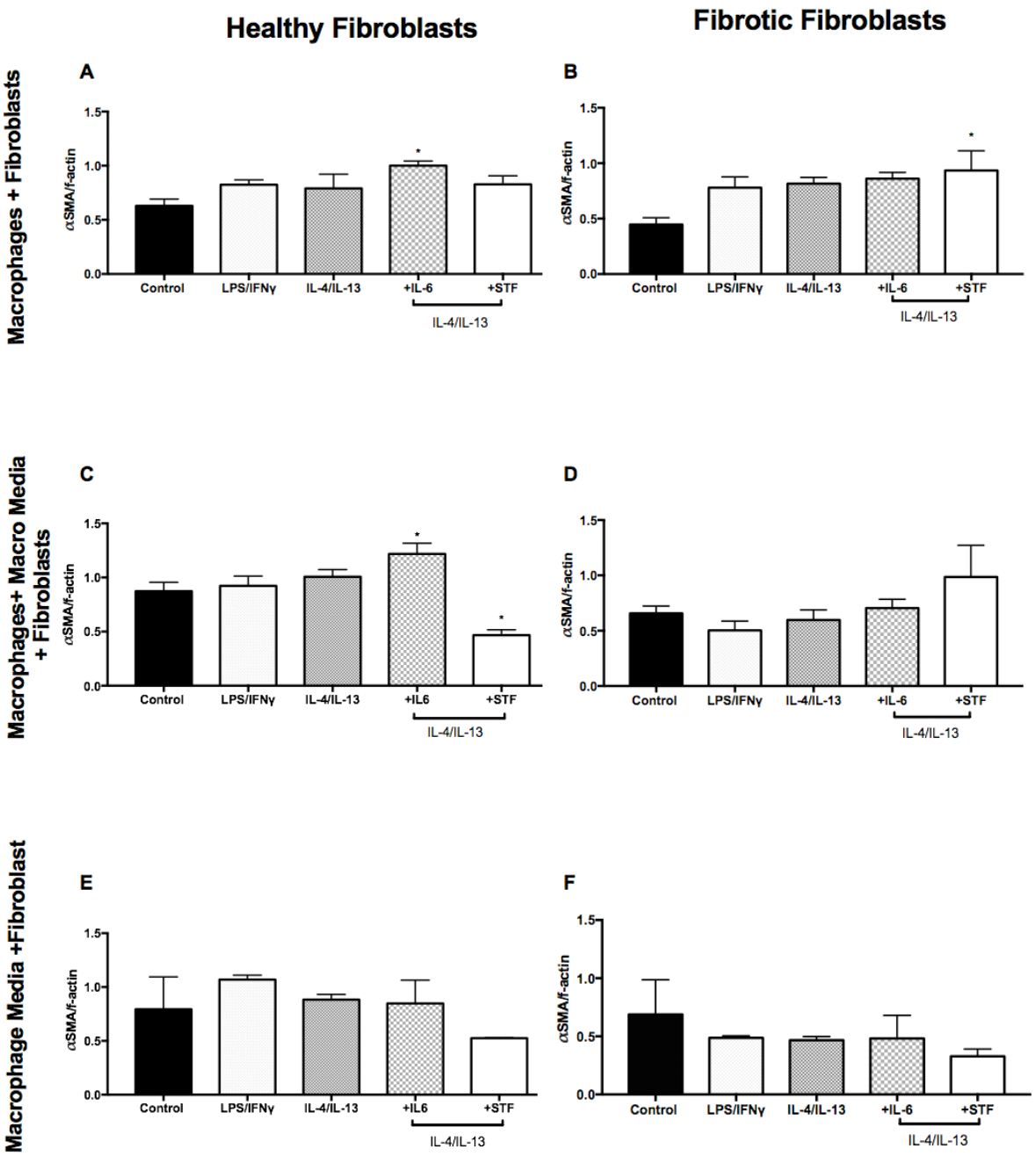

Figure 18: To determine if and how macrophages may be affecting the differentiation of primary healthy and fibrotic fibroblasts to myofibroblasts. Naïve macrophages were stimulated with LPS/IFNy**,** IL-4/IL-13, IL-4/IL-13/IL-6, IL-4/IL-13+STF-083010 (6uM), or supplemented with RPMI-1640 media (control). Results were expressed as a ratio between αSMA and f-actin. Healthy fibroblasts were plated and co-cultured with macrophages alone (*A*), or with macrophages and their milleu (*C*) or macrophage milleu alone for 72 hours (*D*). Results show that IL-4/IL-13/IL-6 stimulated macrophages and their milleu may act together to increase the differentiation of fibroblasts. STF-083010 reduces the expression αSMA/f-actin. In fibrotic fibroblasts STF-083010 stimulated macrophages appear to increase αSMA/f-actin ratio *B*). Cell experiments were executed in 96-well plates with 3 biological replicates per condition and repeated twice. Data is presented as mean ± SEM. Statistical analysis used a ANOVA test with a post hoc Dunnet's comparison.

Figure 19: Nintedanib attenuates the polarization of profibrotic macrophages through the inhibition of tyrosine phosphorylation on CSF1 receptor

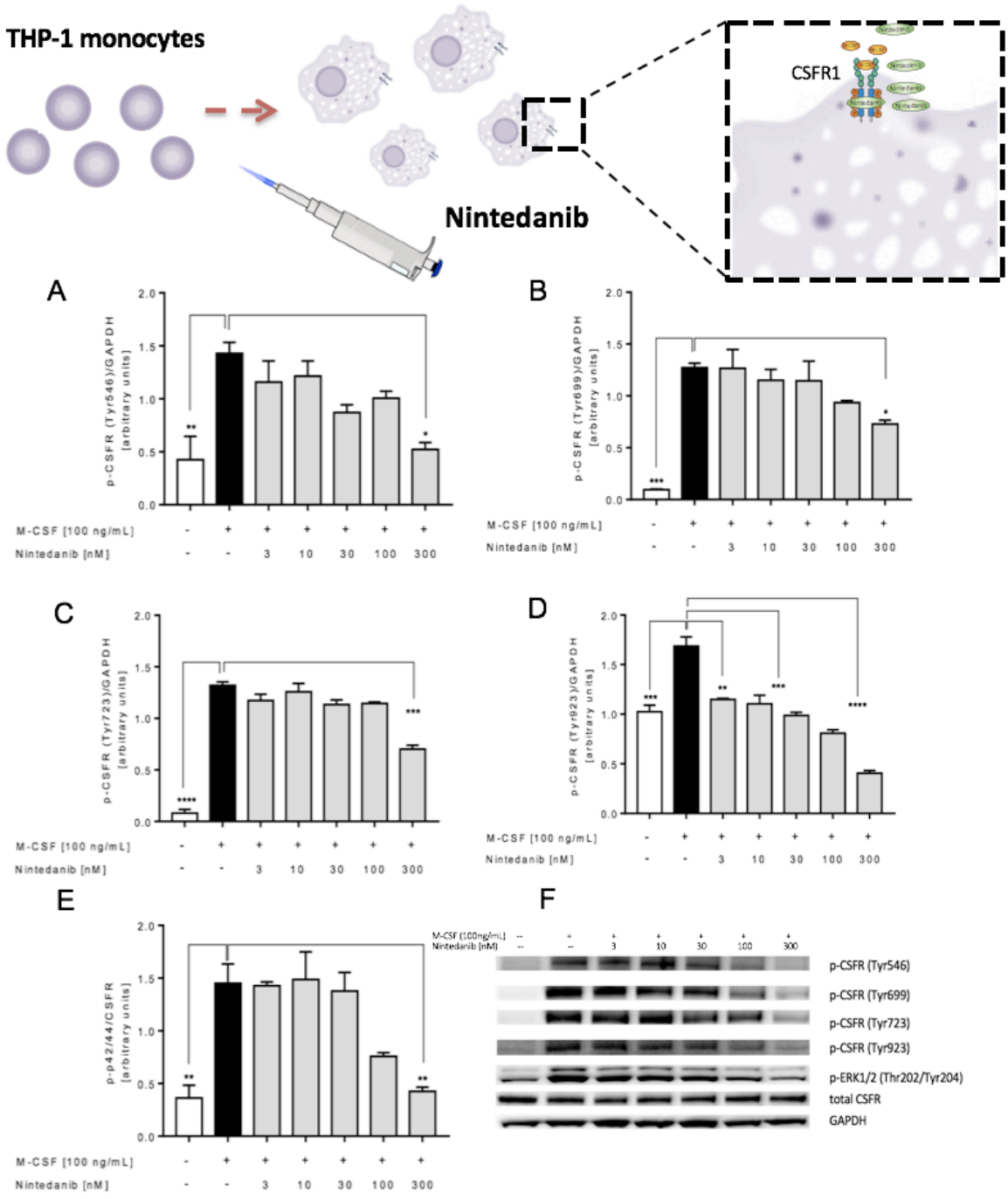

Figure 19: Nintedanib reduces CSFR1 phosphorylation by M-CSF. THP-1 monocytes obtained from ATCC were pre-incubated with different concentrations of BIBF1120 (3-300 nM) for 30 minutes. After pre-incubation, the cells were stimulated with 100 ng/mL M-CSF for 5 minutes and lysed in RIPA buffer. The effect of Nintedanib on M-CSF stimulated THP-1 was demonstrated by looking at the phosphorylation of tyrosine sites of the colony stimulating factor-1 receptor through western blotting. THP-1 monocytes were incubated with Nintedanib for 30 min. The colony stimulating factor 1 receptor (CSF1R) was stimulated with macrophage-stimulating factor (M-CSF) and the receptor activation was assessed by Western blot analysis of the phosphorylation of the tyrosine residues (Tyr546, Tyr699, Tyr723, Tyr923). Nintedanib significantly affected the phosphorylation of tyrosine receptors at 300nm (*A-F*). All data are presented as means ± SEM of n=2 experiments. Unless otherwise noted statistically significant differences were determined by one-way ANOVA followed by Dunnett's multiple comparison test. *Graph done in partnership with Boehringer Ingelheim.*

Figure 20: Nintedanib prevents alternatively activated profibrotic macrophage polarization

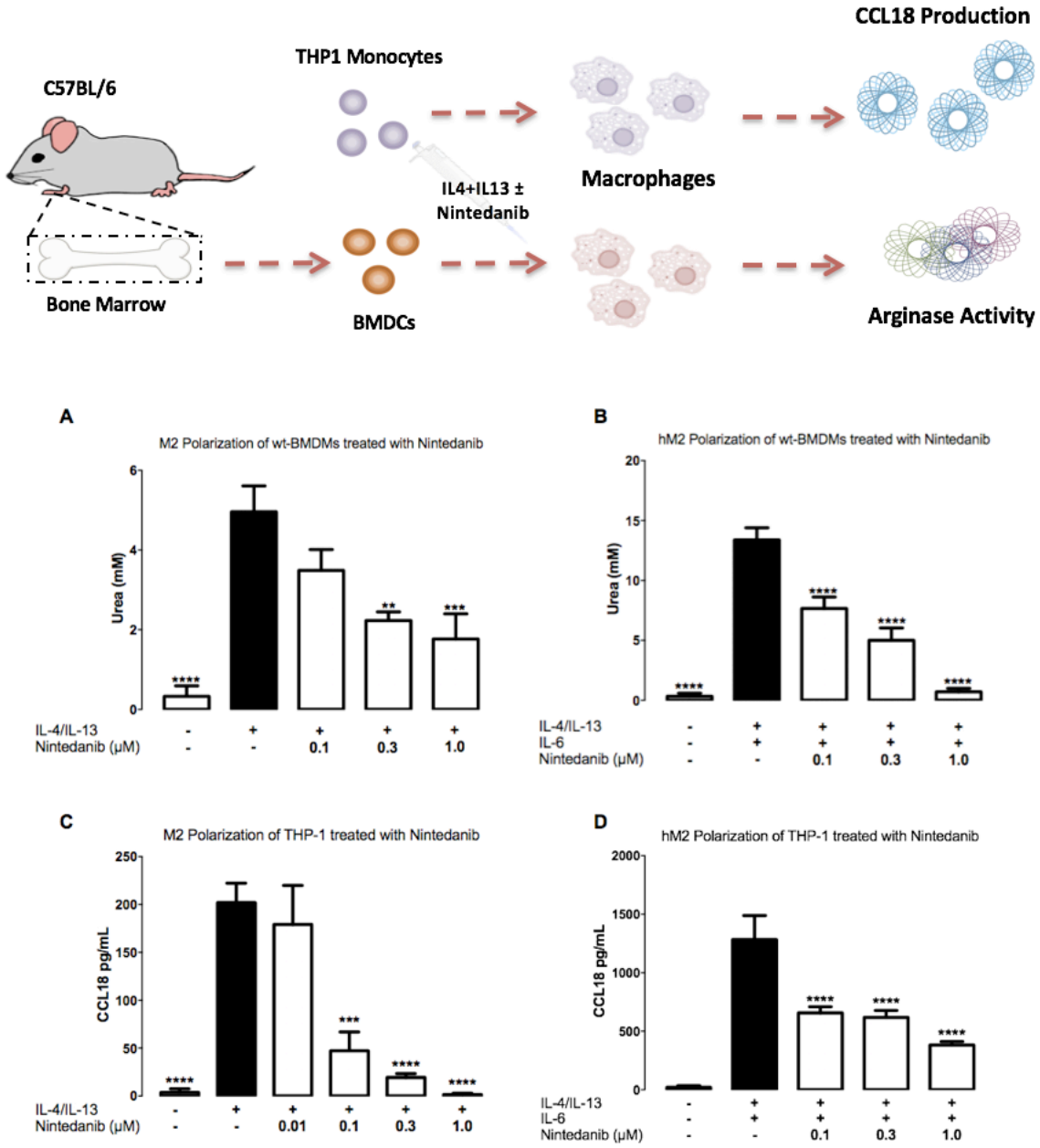

Figure 20: Bone marrow derived and THP-1 macrophages were exposed to IL-4/IL-13 or IL-4/IL-13/IL-6 ± Nintedanib, followed by the assessment of Urea (a marker for arginase activity) or CCL18. Nintedanib was solubilized in DMSO, all cells received 0.12% DMSO. Nintedanib prevented the polarization of IL-4/IL-13 macrophages (0.3 and 1μM) and by IL-4/IL-13/IL-6 (0.1, 0.3 and 1μM) in both murine and human model systems examined. Cell experiments were executed in 96-well plates with 4 biological replicates per condition. All data was presented as means ± SEM of n=3 experiments. Statistical significant differences were determined by one-way ANOVA followed by Dunnett's multiple comparison test.

Figure 21: Effect of Nintedanib on Collagen Production of Healthy and Fibrotic Fibroblasts

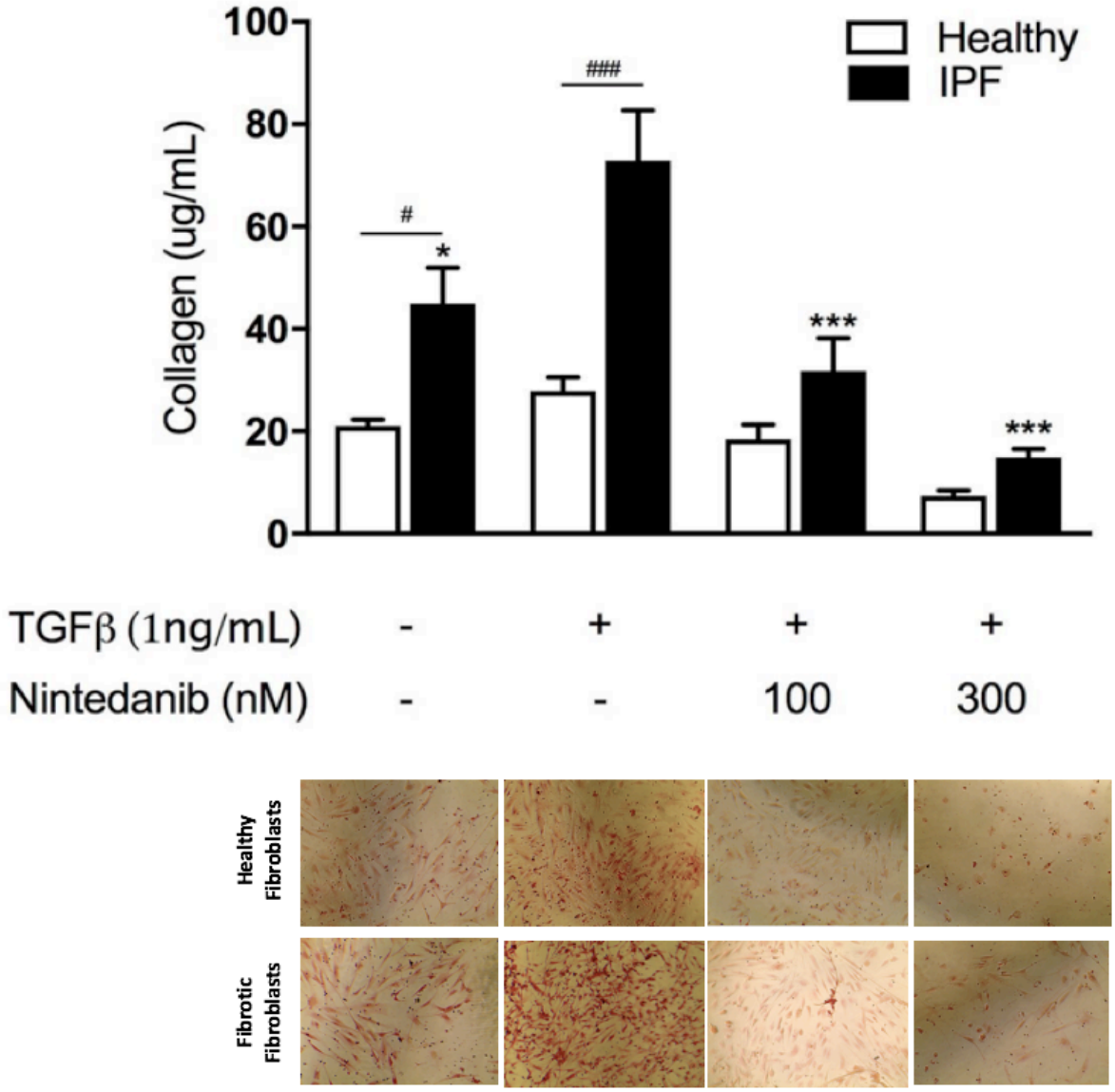

Figure 21: The affect of Nintedanib on primary healthy and fibrotic fibroblasts. At a low dose of TGFβ (1ng/mL), fibrotic fibroblasts had a significant induction of collagen. Lung fibroblasts from patients with IPF or control donors were treated with TGFβ with/without Nintedanib and determined the level of collagen through PicroSirius Red staining. Representative images are shown below. Cell experiment was executed in 96-well plates with 4 biological replicates per condition. All data was presented as means ± SEM. Statistical analysis used a ANOVA test with a post hoc Dunnet's comparison.

Figure 22: The effect of Nintedanib on lung elastance in the murine model of bleomycin lung fibrosis

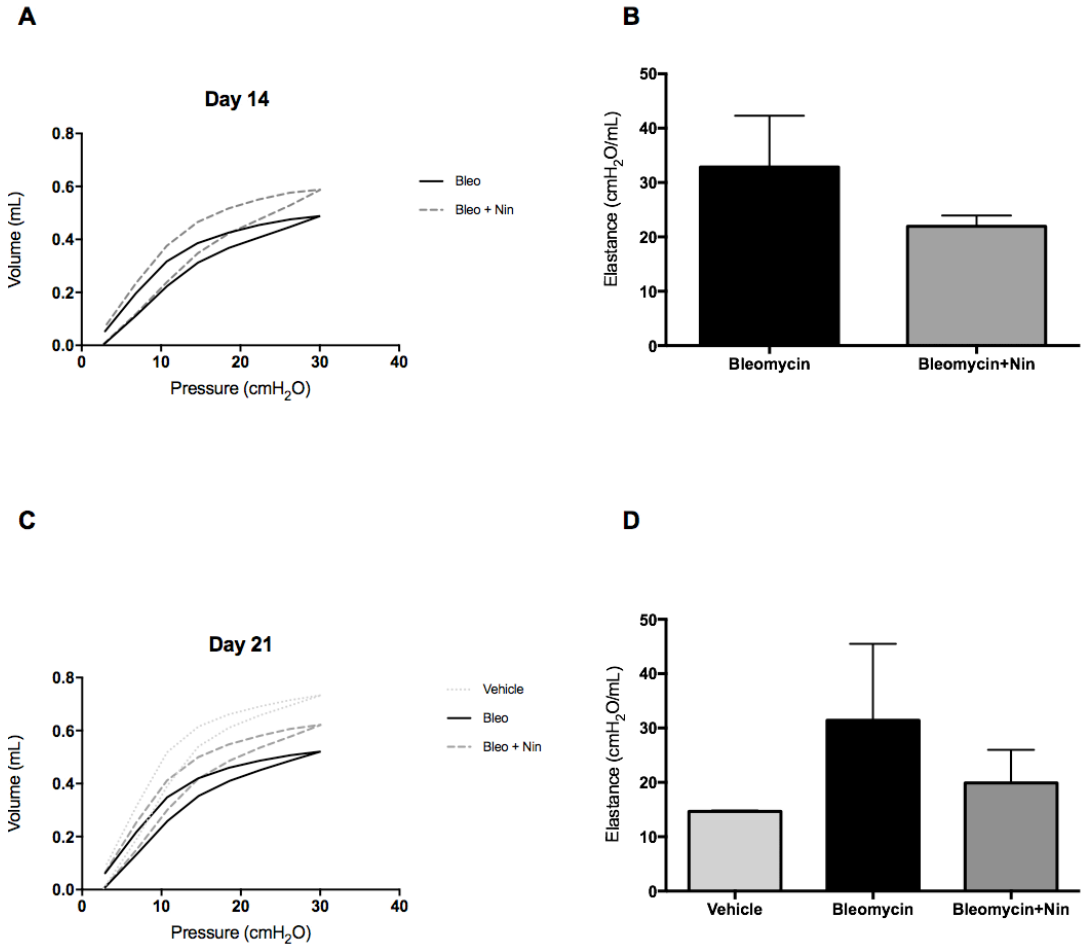

Figure 22: Average pressure volume curves from naïve mice as exposed to bleomycin and/or Nintedanib were measured with flexivent. The curves from fibrotic animals demonstrate, although not significant shift downward and to the right. Nintedanib treatment shifted PV loops upwards at day 14 and day 21 (*A and C*), suggesting an improvement in lung function. Additionally, elastance of lung function was measured with no significance seen in groups *(B and D)*. All data was presented as means ± SEM of n= 1 experiments (3-5 mice per group). Statistical analysis used a ANOVA test with a post hoc Dunnet's comparison.

Figure 23: Nintedanib's effect on YM1^{+} and Arg1^{+} cells *in vivo* bleomycin murine model

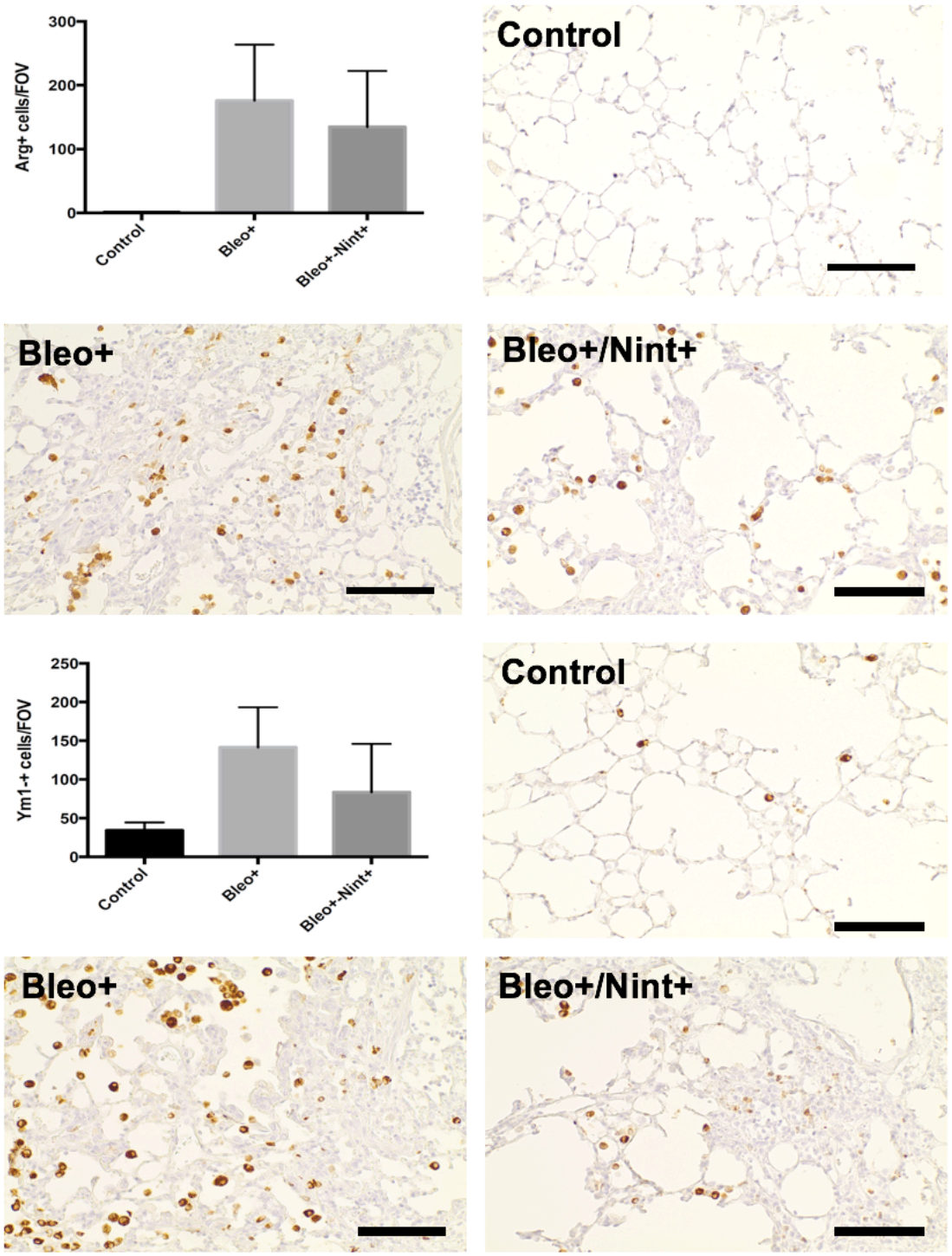

Figure 23: The bleomycin mouse model of fibrosis is a well characterized system to highlight the pathological features of pulmonary fibrosis. To determine if Nintedanib affected the expression of alternatively activated cells, C57BL6/J mice were exposed to a single intratracheal administration of bleomycin, followed by BID Nintedanib treatment from day 5 to day 20. To determine the level of alternatively activated cells present in mice, immunohistochemical staining via two well characterized profibrotic macrophage proteins YM1 and arginase-1. In the bleomycin mouse model of fibrosis, Nintedanib although not significant lowered lung elastance. Lungs were resected and preserved in formalin and fixed in paraffin. Immunohistochemical staining showed that Nintedanib non-significantly reduced YM1- and arginase-1- positive cells as determined by IHC assessment. *Graph produced in collaboration with Maximilian Ackermann, Johannes Gutenberg University of Mainz.*

Supplementary Figures

Supplementary Figure A1: Determining the pathological differences in the parchemymal architecture of usual interstitial pneumonia patients

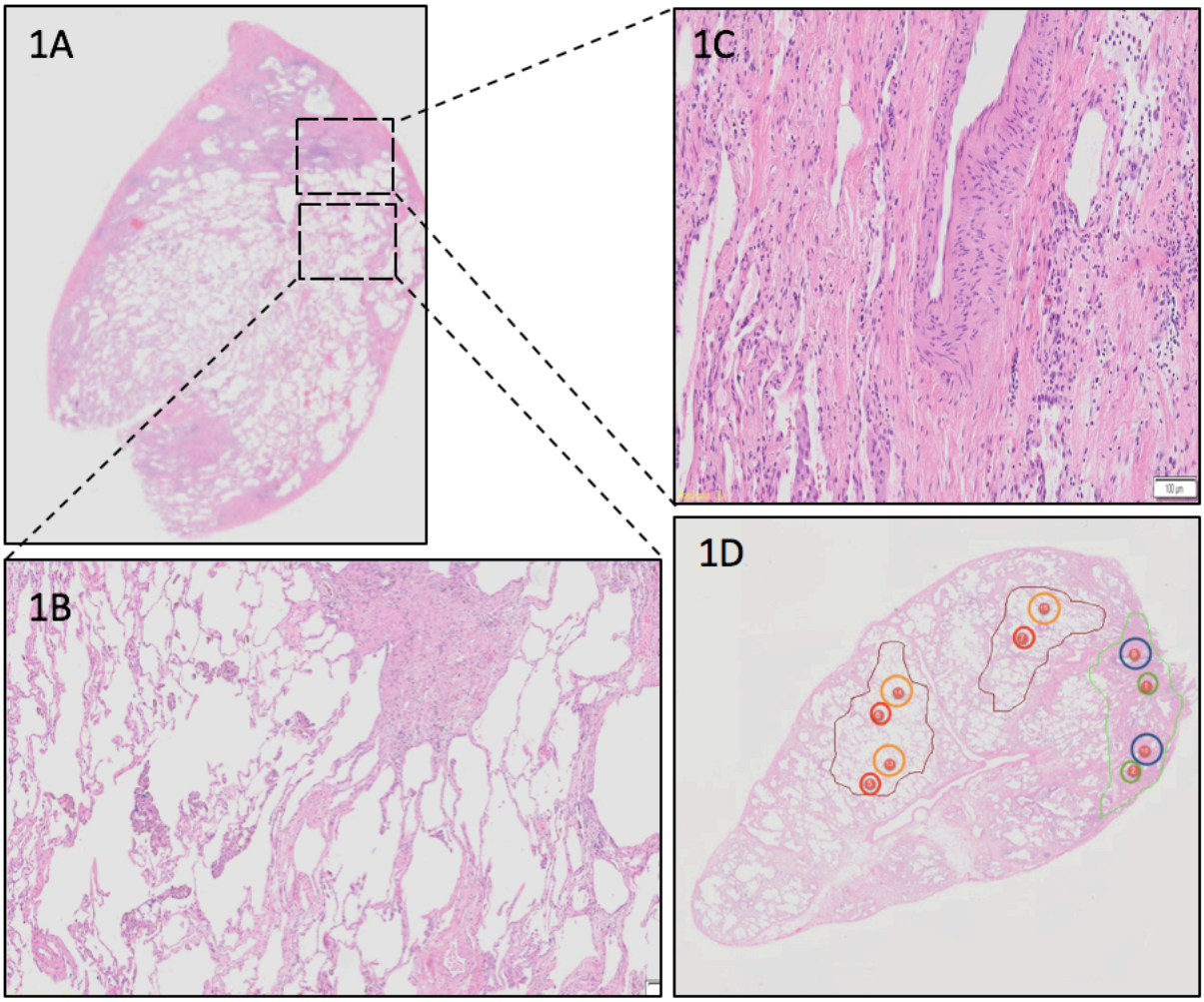

Supplementary Figure A1: Figure 1A shows spatial heterogeneity this is evident through the abrupt transitions from densely packed fibrotic tissue to normal healthy looking lung. Figure 1B shows architectural distortion, in the upper right of the image you can see how scars obliterate the normal alveolar tissue, and dense tissue can be seen to replace normal air pockets. In Figure 1C temporal heterogeneity is evident due to fibroblastic foci. These foci are areas of ongoing remodeling, embedded in a background of scar tissue and honeycombing, which are suggestive of preexisting lung injury. Figure 1D shows how areas of the lungs are marked to get 0.6mm cores for tissue microarray and 1mm cores for RNA extraction and TEM. Fibrotic regions were selected to be cored out for TMA in green, with an adjacent area in blue to analyze RNAseq/TEM. Red regions represent non-involved/fibrotic regions selected for TMA and an adjacent area in orange selected for RNAseq/TEM.

Supplementary Figure A2: Optimization of immunohistochemical staining for Mannose receptor CD206

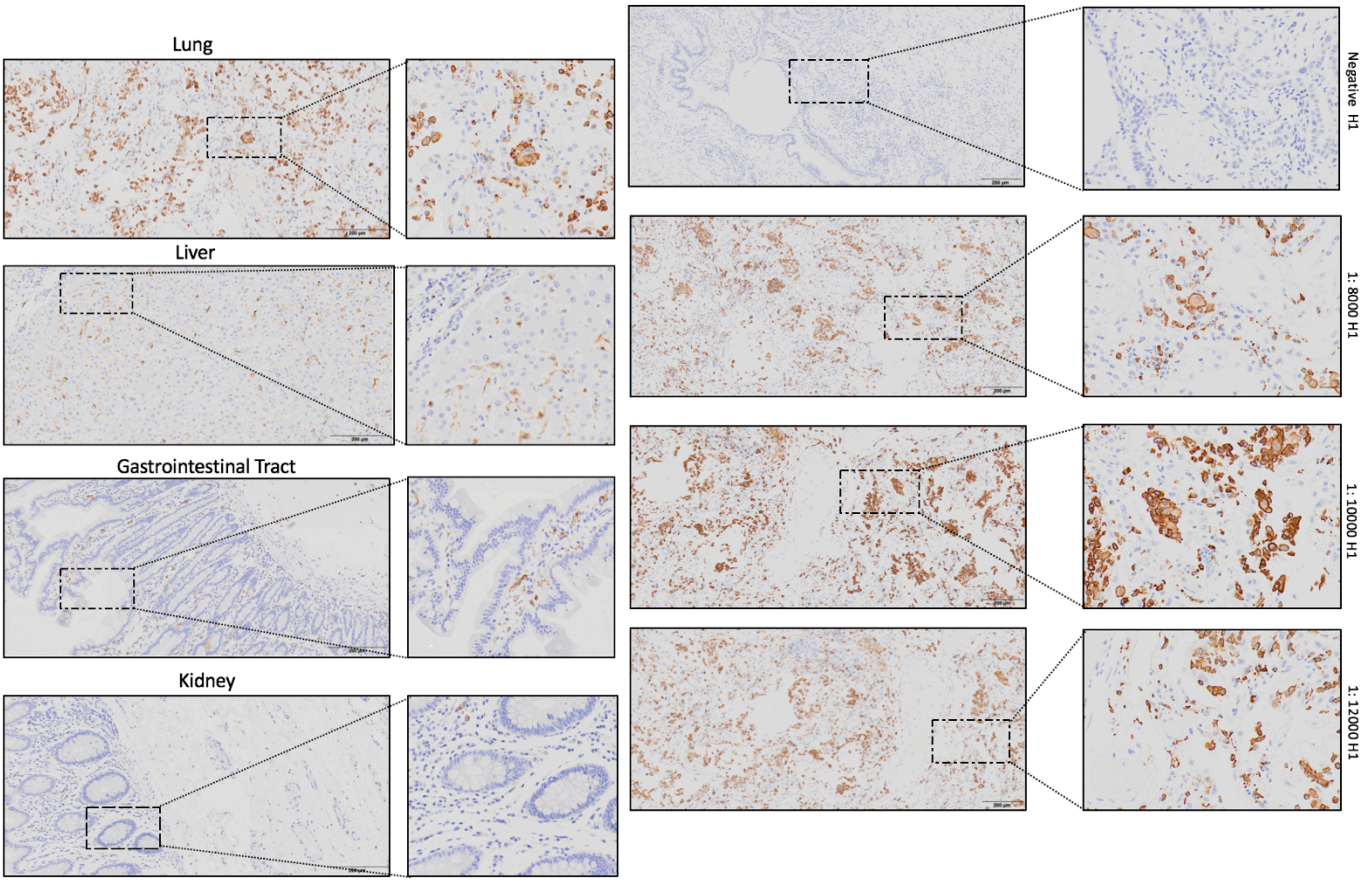

Supplementary Figure A2: Validation of immunohistochemical staining was done with the help of a trained molecular pathologist. Representative images of CD206 staining at various dilutions and tissues was completed. CD206 expression can be seen in human lung cells showing intense and uniform cellular membrane staining of medium intensity. Human kidney used as negative control. All samples were counterstained with Mayer's hematoxylin.

Supplementary Figure A3 : Optimization of CD206 and CD68 immunohistochemical Staining in IPF tissue

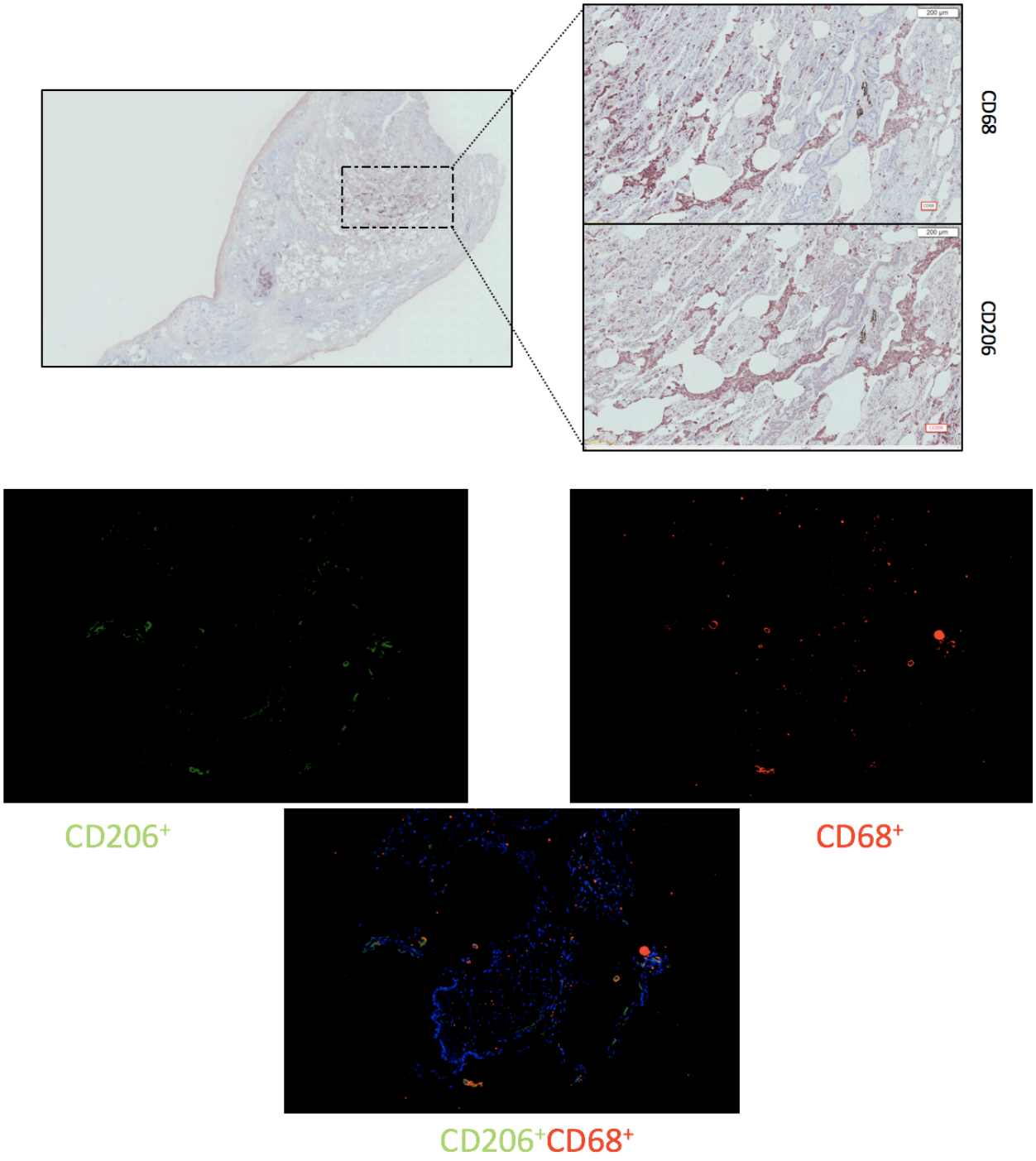

Supplementary Figure A3: *A)* Patient lung FFPE lung biopsy was cut and stained in serial sections. Staining was validated with the help of a pathologist being done with different retrevial methods and human kidney used as a positive control. What was evident was that CD68 and CD206 could be seen in similar areas of serial sections, validating the stain. *B)* To determine colocalization of CD206 and CD68, tissue was cut and immunofluroescene staining was done co-localization of CD68 in red and CD206 in green can be seen.

Supplementary Figure A4: Algorithm illustrating calculation of cellular immune-staining

1) Open ImageJ/Fiji
→ Import Tiff image

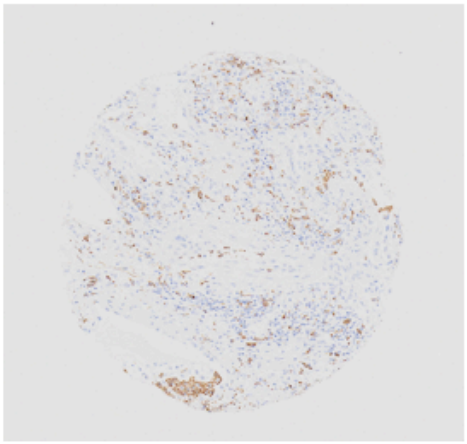

2) Convert to 16-bit

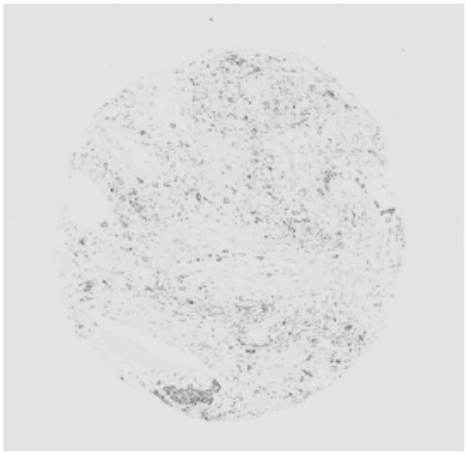

3) setAutoThreshold("Default")
//run("Threshold...");
→ setThreshold(0, 180);
→ setOption("BlackBackground", false);

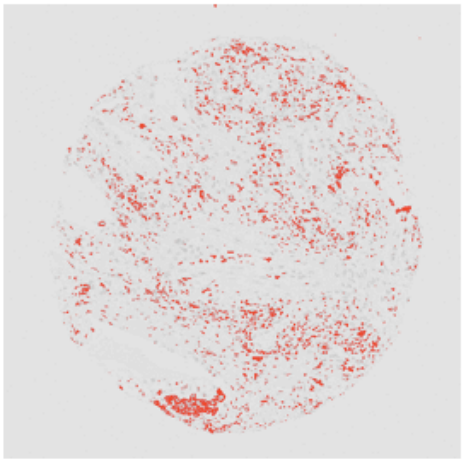

4) run("Analyze Particles...",
"size=20-Infinity circularity
=0.65-1.00 clear summarize");

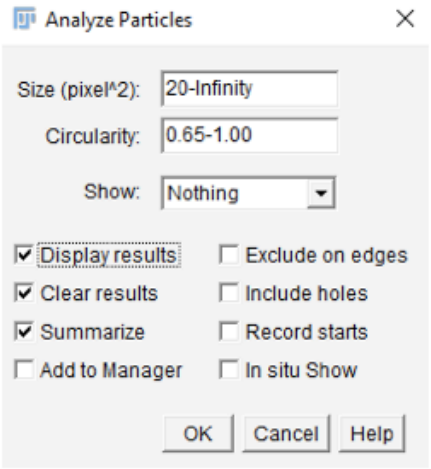

Supplementary Figure A4: Quantification of cellular staining was done in Fiji6. Background of TMA cores were cleaned to remove background particles. Tiff images were converted to 16-bit to quantify cellular intensity. Only staining present at a circularity of 65 percent was measured.

Supplementary Figure A5: Measuring expression of CD206 and CD68 through various methods

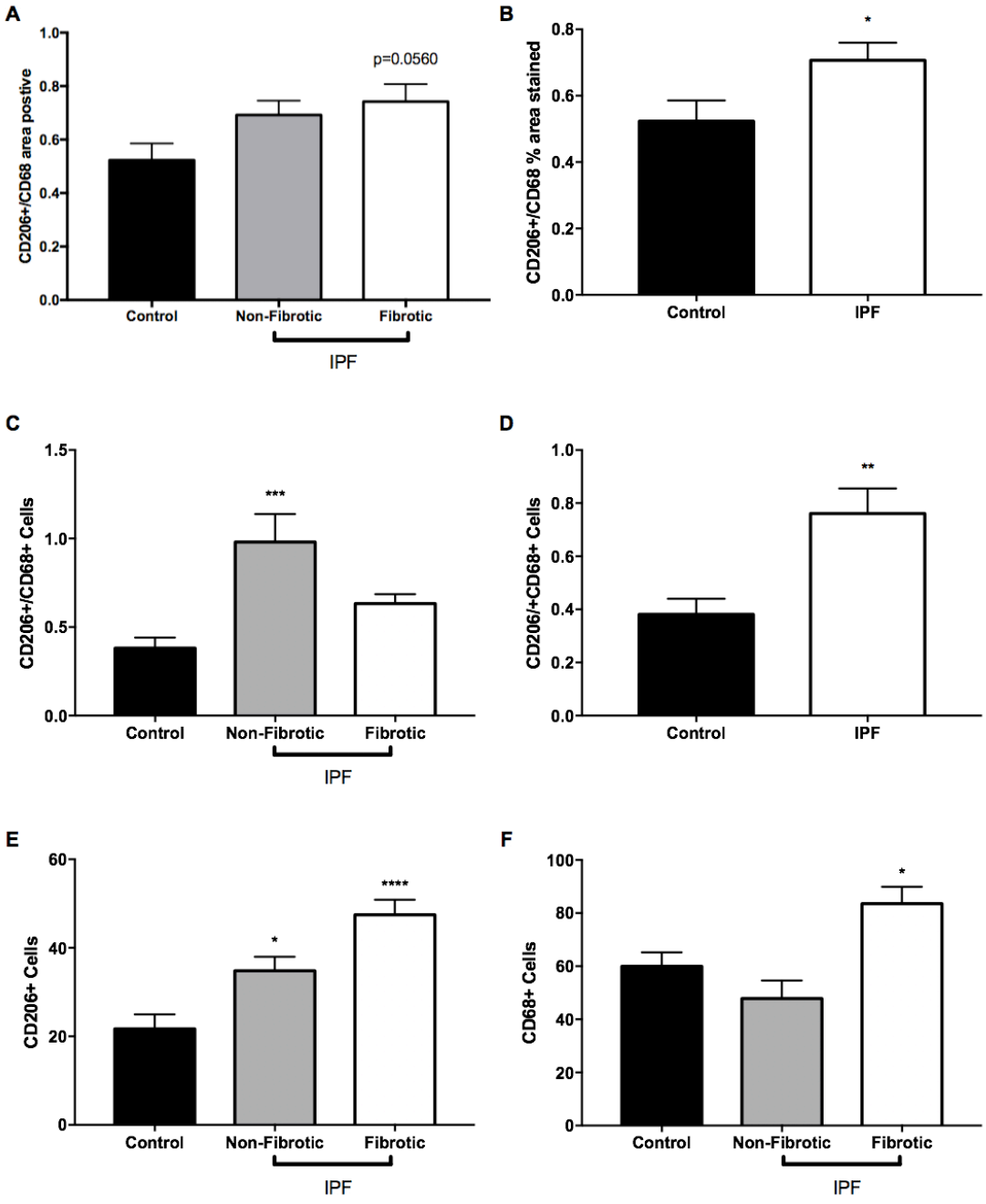

Supplementary Figure A5: Expression of CD68 and CD206 was measured through different algorithms and methods to validate method of quantification. Staining was assessed through percent area stained (A and B), as well as counting the number of cells present which were stained in each TMA core (C to F). All data was presented as means ± SEM. Statistical analysis used a student's T-Test or ANOVA test with a post hoc Dunnet's comparison.

Supplementary Figure A6: Inhibition of Fibroblast ER Expansion achieved through treatment with STF-083010 and 4μ8C

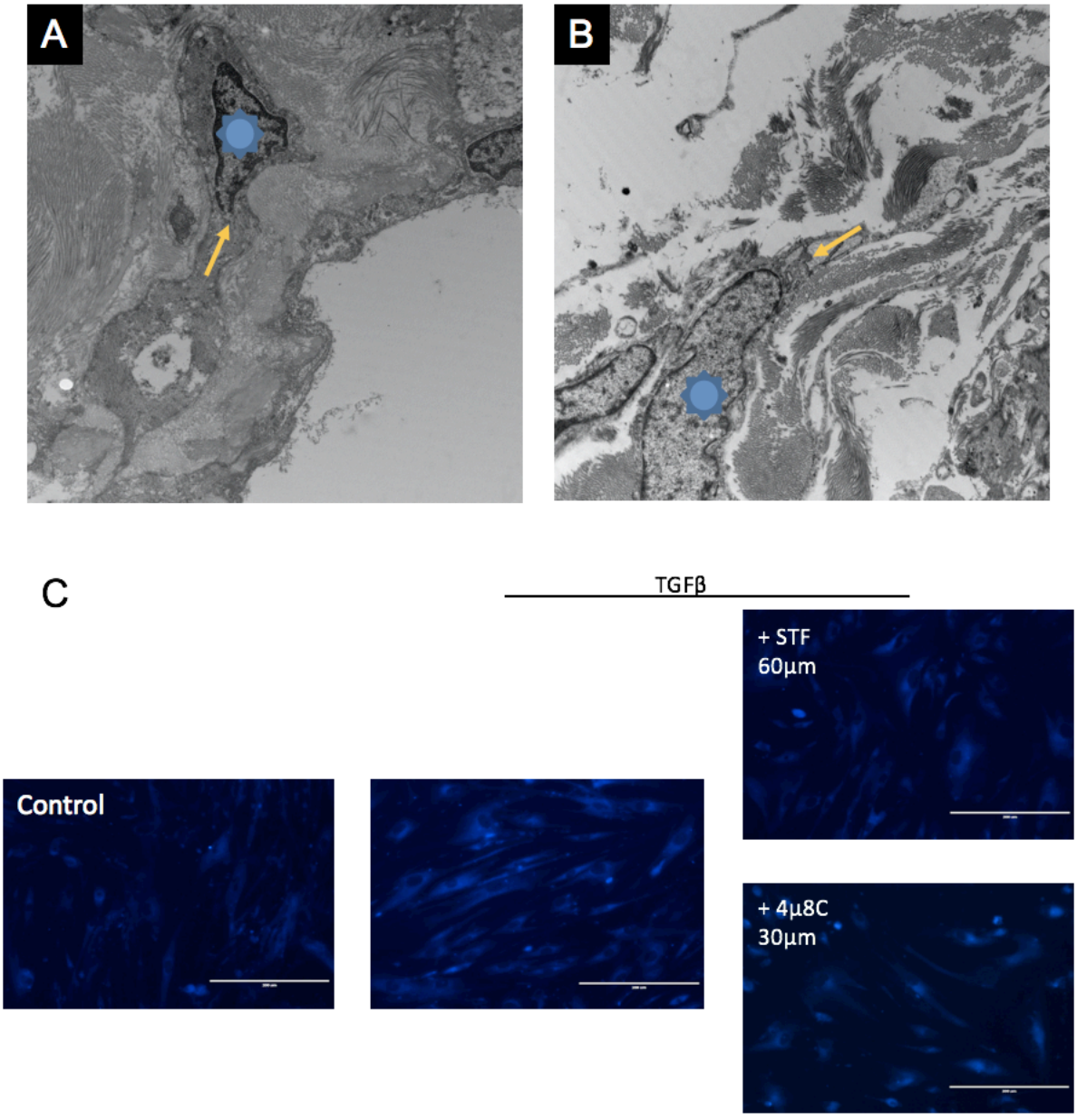

Supplementary Figure A6: Formalin fixed paraffin embedded tissue from IPF patients was rehydrated, and fixed for transmission electron microscopy (TEM), to allow for visualization of endoplasmic reticulum expansion. *A*: Formalin fixed paraffin embedded fibroblast from control patients (n= 3 cells). Endoplasmic reticulum (gold arrows). Nucleus (Blue Star). *B*: Formalin fixed paraffin embedded fibroblast from Idiopathic pulmonary fibrosis patients C: ER tracker dye was used to visually stain the endoplasmic reticulum of primary fibroblast cells blue. Fibroblasts were stimulated with TGFβ stimulated macrophages. TGFβ appeared to enlarge the ER versus control fibroblasts. This expansion process is limited through the administration of 4μ8C and STF-083010.

Supplementary Figure A7: Optimization of THP-1 macrophage Fibroblast co-culture system

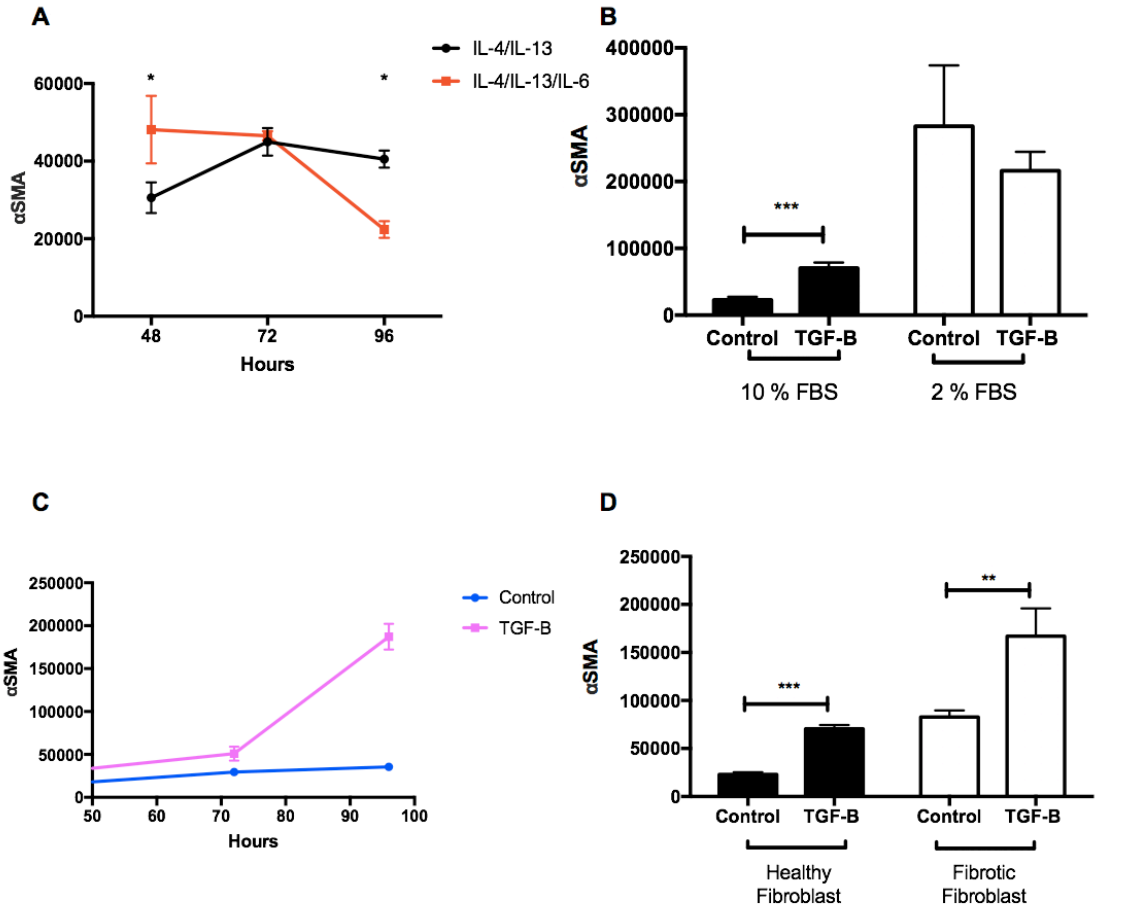

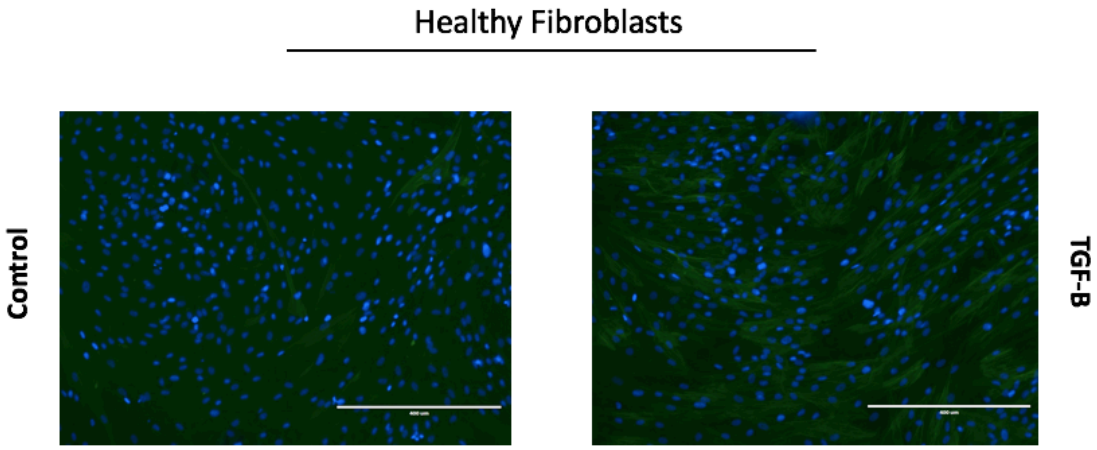

Supplementary Figure A7: *A)* 96-hour time course of how alternatively activated macrophages affect the polarization of fibroblasts as assessed through alpha-SMA staining**.** *B)* Shows how fibroblasts are affected by a lower concentration of FBS at 24-hours, the graph depicts that a low concentration of FBS causes fibroblasts to completely transition to myofibroblasts. *C)* Shows a 96-hour time course of how fibroblasts are affected by either control media or TGFβ supplemented media at 2.5ng/mL**.** *D)* Healthy and fibrotic fibroblasts were stimulated for 48-hours with either control or TGFβ supplemented MEM F15 media (10% FBS) to determine their responsiveness. Fibrotic fibroblasts were more responsive to TGFβ, a representative images of cell staining in the TGFβ and control stimulated fibroblasts is shown. All data was presented as means ± SEM. Statistical analysis used a ANOVA test with a post hoc Bonferroni comparison.

Supplementary Figure A8: Collagen secretion from in healthy fibroblasts stimulated with TGFβ or co-cultured with macrophages

A

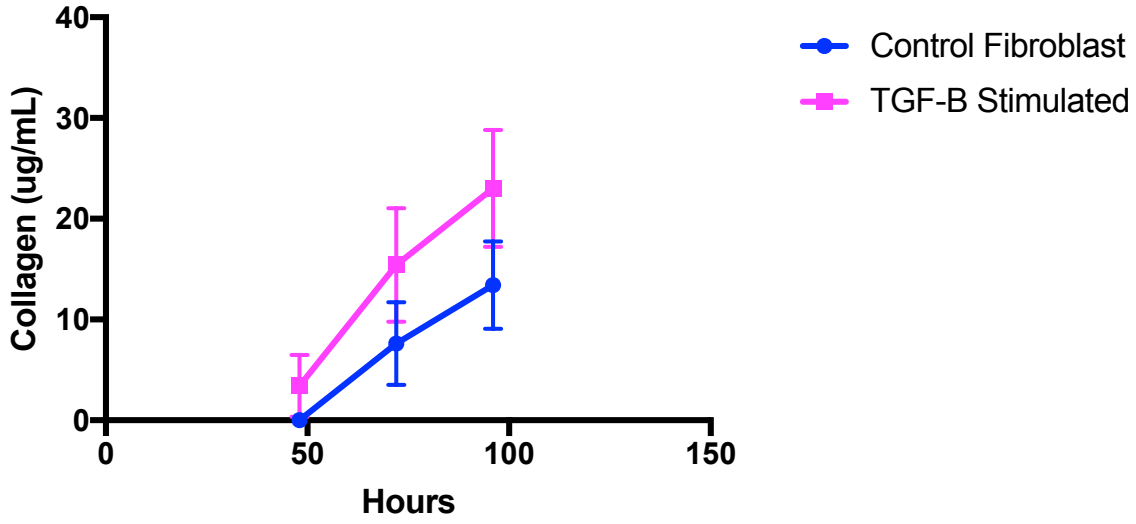

B

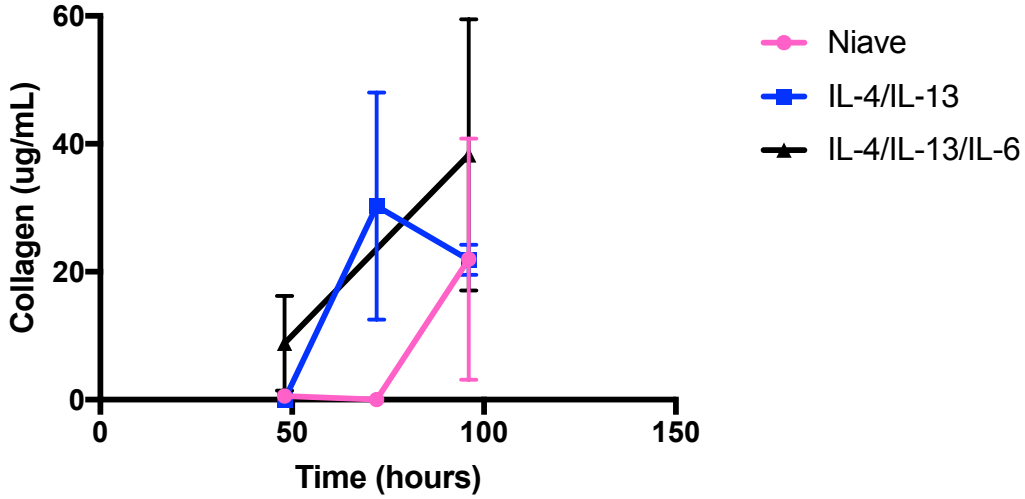

Supplementary Figure A8: *A)* To characterize whether collagen secretion from healthy and fibrotic fibroblasts was affected by media supplemented with TGFβ, cells were stained with PicroSirius Red. Fibrotic fibroblasts show an increased secretion of collagen when stimulated with TGFβ however not significant. *B)* Fibroblasts were co-cultured with naïve, IL-4/IL-13 or IL-4/IL-13/IL-6 supplemented macrophages and collagen secretion was assessed. No significance was determined. All data was presented as means ± SEM. Statistical analysis used a ANOVA test with a post hoc Dunnet's comparison.